ATS-05600

NASA CR-144893

EFFECTS OF NACELLE SHAPE ON DRAG AND WEIGHT OF A SUPERSONIC CRUISING AIRCRAFT

Prepared by:

ELLWOOD BONNER
RONALD Y. MAIRS
RAY M. TYSON

Pages 5, 31 & 39 missing from reproducible copy 12.29.75 Tillery

October 1975

PREPARED UNDER CONTRACT NAS 1-13906
BY LOS ANGELES AIRCRAFT DIVISION
ROCKWELL INTERNATIONAL CORPORATION
LOS ANGELES, CALIFORNIA
FOR
LANGLEY RESEARCH CENTER
NATIONAL AERONAUTICS AND SPACE ADMINISTRATION

FOREWORD

This document presents results of the study "Parametric Analysis of the Effects of Nacelle Shape on Drag and Weight of Supersonic Cruising Aircraft." The NASA Technical Representative was Russell B. Sorrells, III. In addition to the authors noted, significant contributions to this study and report were made by Bruce E. Moore, aerodynamics; David Chaloff, mass properties; Henry K. Chin and Louis C. Young, propulsion; and Lester D. Hendrix, configuration design.

TABLE OF CONTENTS

LIST OF ILLUSTRATIONS

LIST OF ILLUSTRATIONS (Continued)

LIST OF ILLUSTRATIONS (Continued)

LIST OF ILLUSTRATIONS (Continued)

LIST OF ILLUSTRATIONS (Concluded)

LIST OF TABLES

EFFECTS OF NACELLE SHAPE ON DRAG AND WEIGHT OF A SUPERSONIC CRUISING AIRCRAFT

By Ellwood Bonner, Ronald Y. Mairs, and Ray M. Tyson
Los Angeles Aircraft Division, Rockwell International

SUMMARY

The objectives of this study were to develop the quantitive relationship of cruise drag and nacelle shape for a representative advanced supersonic transport configuration and to provide system sensitivity data which could be used to assess the overall value of propulsion system variations. The NASA arrow-wing configuration was used as a baseline airframe. Only those changes that were necessary to install the Pratt and Whitney Aircraft VSCE 502B engine were made to the aircraft.

Nacelle shape parameters were systematically varied, and the effects of these variations on wave and friction drag were determined. The effects of changes in vehicle drag, propulsion weight, and specific fuel consumption on vehicle takeoff gross weight were computed.

Generally, it was found that nacelles shaped such that the maximum cross-sectional area occurred at or near the nozzle exit resulted in the lowest wave drag. In fact, nacelle shapes were found that produce favorable interference effects (drag reduction) of such magnitude as to nearly offset the friction drag of the nacelle. It should be emphasized that these results are valid only for vehicles of this general configuration and nacelle location. Different vehicle configurations or nacelle locations could result in different "best" shapes.

It is recommended that the drag and sensitivity data generated in this program be used in the analysis of future propulsion system trade studies. Further, it is recommended that vectorable, two-dimensional nozzles be studied, and that canting downward of non-vectorable, axisymmetric nozzles be examined.

INTRODUCTION

The National Aeronautics and Space Administration is conducting a continuing program of advanced supersonic technology studies with the objective of developing an adequate technology base to support development of future supersonic cruising aircraft. It is recognized in this program that one of the more sensitive problems in the synthesis of a successful supersonic cruising aircraft is that of airframe/engine integration. This process must investigate and properly manage the interactions between the technical disciplines of external aerodynamics, internal aerodynamics, engine cycle design, acoustics, mass properties, and structural design; and, it must be responsive to the practical considerations of fabrication, maintenance, and operation.

The results of a recently-completed study, reference 1, of the effects of nacelle size and nacelle shape on the drag, weight, and wing camber plane warping of a supersonic transport illustrated the sensitivity of these parameters to relatively small changes in nacelle shape. The resultant shape of a nacelle is dependent on the geometry of the engine (inlet area, mounting provisions, accessory location, nozzle area, etc.) since this establishes certain control points in the design of the nacelle. It is important, therefore, that the engine designer be aware of this sensitivity to engine geometry, and be provided with some guidelines for favorable geometry relationships. It is probable that some engine geometry control can be achieved by the designer with no penalty in engine performance, although on a total system basis some engine performance degradation could be accepted in trade for reduced drag.

Although considerable effort has been expended on the problem of airframe/engine integration, it has been mostly in the nature of point designs. The referenced study produced results for two specific nacelle shapes which resulted from installation of a dry turbojet engine and a duct heating turbofan engine. A comparison of these results shows the superiority of one over the other, but gives no information directly applicable to other installations having differing nacelle shapes. Because of the economy that can be affected in configuration synthesis by having good engine geometry characteristics for use in the first iteration of the engine/airframe integration process, an effort has been made to supply the engine designer with guidelines for favorable geometry that he can apply early in the engine developmental process. Parametric data have been generated on the effects of variations of nacelle shape on cruise drag for a range of shapes that reasonably cover engine designs applicable to supersonic cruising aircraft.

In considering possible trades of reduced drag through design changes in the engine envelope for some penalty in engine weight and specific fuel consumption (SFC), it is necessary to have visibility of the net impact of all three effects on the total airplane system in order to make a comparative evaluation. Therefore, sensitivity data were developed for the effects of changes in drag, propulsion system weight, takeoff thrust, and SFC on the takeoff gross weight as a figure of merit.

The program was of seven months duration, including review and submittal of the final report, and was organized around four tasks. These were: 1 - Baseline Airplane Definition; 2 - Parametric Drag Analysis; 3 - Weight Sensitivity Analyses; and 4 - Reporting.

LIST OF SYMBOLS

A	Area, sq. m. (sq. ft. or sq. in.)
BLB	Boundary layer bleed
BLC	Boundary layer control
B.P.	Basepoint
C	Coefficient or Chord, m. (ft. or in.)
d	Diameter, m. (ft. or in.)
D	Drag, (lb.)

dB	Decibel
K	Drag-due-to-lift factor
ℓ	Length, m. (ft. or in.)
L	Lift, n. (lb.)
M	Mach number
S	Area, sq. m. (sq. ft. or sq. in.)
SFC	Specific fuel consumption, kg./hr./n. (lb./hr./lb.)
T	Thrust, n. (lb.)
TOGW	Takeoff gross weight, kg. (lb.)
V	Velocity, m./sec. (ft./sec.)
W	Weight, kg. (lb.)
X	Nacelle station, m. (ft. or in.)
Δ	Increment

Subscripts

AMAX	Maximum cross-sectional area
c	Capture
D	Drag
F	Friction
i	Inlet throat
K	Indicates lift coefficient at minimum drag
L	Lift
LO	Liftoff
MAX	Maximum
n	Nozzle exit
P	Maximum protrusion
REF	Reference
R	Root
W	Wave
0	Freestream
1	Critical engine failure

STUDY PROCEDURE

Approach

The general approach used in this study was to: 1) define a baseline airplane and determine its performance, 2) parametrically vary nacelle shape and determine nacelle drag increments due to these variations, 3) determine vehicle takeoff gross weight sensitivity to changes in drag, weight, takeoff thrust, and SFC, and 4) report results. In this report, descriptions of the airplane configurations used are as follows:

1) the reference airplane is the NASA modified SCAT 15F arrow-wing, supersonic transport (defined in reference 2)
2) the basepoint vehicle is the reference modified only as required to install the Pratt and Whitney Aircraft (P&WA) VSCE 502B engine
3) the baseline airplane is the basepoint resized to the design requirements on a standard-plus-8°C day

The structure design and operational empty weight of the reference airplane were assumed to meet all design criteria. Weight and aerodynamic characteristics of the study airplanes were derived by increments from the reference configuration.

Baseline Airplane Definition

Basepoint airplane.- The "basepoint" airplane for this study is based on the NASA modified SCAT 15F arrow wing reference configuration as described in reference 2. The propulsion system of this airplane has been replaced with P&WA variable stream control engines (VSCE 502B) having 408 kg./sec. (900 lb./sec.) airflow each and with axisymmetric variable geometry inlets designed for Mach 2.4 cruise conditions. The resulting basepoint vehicle is shown in figure 1. This airplane has a gross weight of 336 973 kg. (742 890 lb.), a range of 7 471 km. (4 034 n.mi.), and a balanced field length of 3 017 m. (9 898 ft.).

All performance and sizing calculations were made using the Rockwell Vehicle Sizing and Performance Evaluation Program (VSPEP). This computer program is a design tool capable of scaling a known basepoint vehicle according to specified values of several different design parameters. These include vehicle gross weight (or fuel weight), thrust-to-weight ratio (or engine size), wing-loading (or wing area), and payload or fixed equipment weight and volume. Performance may be determined at specified gross weight, or alternatively, a search routine permits automatic sizing of the vehicle gross weight such that a specified radius or range of the design mission is satisfied. Vehicle performance is calculated internally from a set of subroutines programmed according to a detailed performance analysis model. The subroutines are general in nature and permit calculation of a wide variety of mission profiles. Several mission profiles may be calculated simultaneously. Takeoff and landing distances and maneuvering capability may also be determined. Figure 2 illustrates the evaluation process.

Typical mission legs which may be calculated include warmup, taxi, takeoff, climb, descent, cruise, and loiter operations. Climb and descent performance are determined by numerical integration of the equations of motion along a specified flight schedule. Internally generated schedules are also available, including minimum time and minimum fuel flight paths as defined by the energy method. Constraints on the allowable flight regime are included. Cruises and loiters may be determined at fixed or optimum speeds and altitudes. Numerical searches are used to determine optimum speeds and altitudes at the beginning and end of each of these legs.

Data input to the VSPEP for the AST basepoint vehicle include:

- Weights broken down by major component, along with scaling information on the wing, tails, fuselage, and engines.
- Drags broken down by major component and by type (e.g., friction drag, wave drag, drag due to lift, base drag).
- Installed propulsion data, including thrust and fuel flow as functions of speed, altitude, and power setting.
- Dimensional data such as lengths, areas, and volumes for major components and the total vehicle.

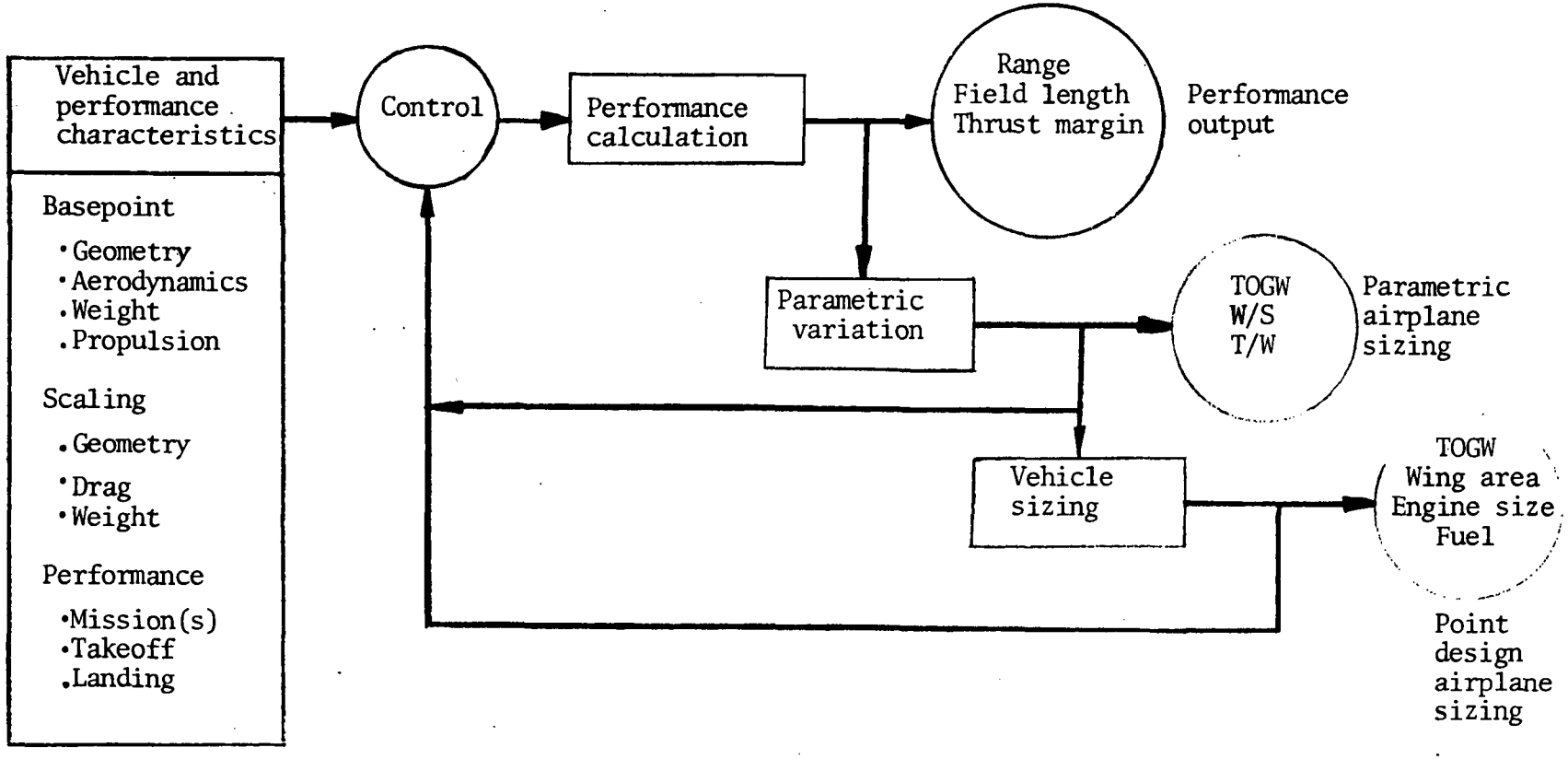

Figure 2.-Vehicle sizing and performance evaluation program.

Performance items calculated by the VSPEP on the basepoint and baseline vehicles for this study consist of the following:

1. Design mission range
2. Alternate mission range
3. Takeoff distance with FAR 36 (Federal Aviation Regulation, part 36) noise requirements.
4. Balanced field takeoff distance
5. Thrust-to-drag ratio at Mach 2.32, 18 300 m. (60 000 ft.)
6. Thrust-to-drag ratio at Mach 1.2 during the climb leg

A description of each of these performance items is given in the following paragraphs. Because engine data were provided for a standard-plus-8°C (14.4°F) day, all airplane performance characteristics were computed for that atmospheric condition.

Design mission.-A profile of the design mission is shown in figure 3. This mission consists mainly of a Mach 2.32 cruise. Fuel reserves as recommended in reference 3 are calculated for an alternate airport located 460 km. (250 n.mi.) from the destination airport.

The design mission consists of:

1. Warmup and takeoff - 10 minutes at idle power plus 1 minute at maximum power.

2. Climb - Maximum power climb and accelerate to cruise altitude and Mach number.

3. Cruise - Cruise at Mach 2.32 at altitude for best cruise range.

4. Descent - Descend and decelerate to Mach 0.5 and 457 m. (1 500 ft.) using idle power.

5. Approach and land - Descend to Mach 0.3 at sea level using idle power.

6. Taxi - 5 minutes at idle power.

7. Reserve allowance - 5 percent of total fuel used in all previous legs.

8. Reserve climb - Climb to subsonic cruise conditions.

9. Reserve cruise - Subsonic cruise at Mach number and altitude for best range.

10. Reserve descent - Descend and decelerate to holding altitude and Mach number using idle power.

11. Reserve hold - Loiter for 30 minutes at 3 048 m. (10 000 ft.) at the Mach number for best endurance.

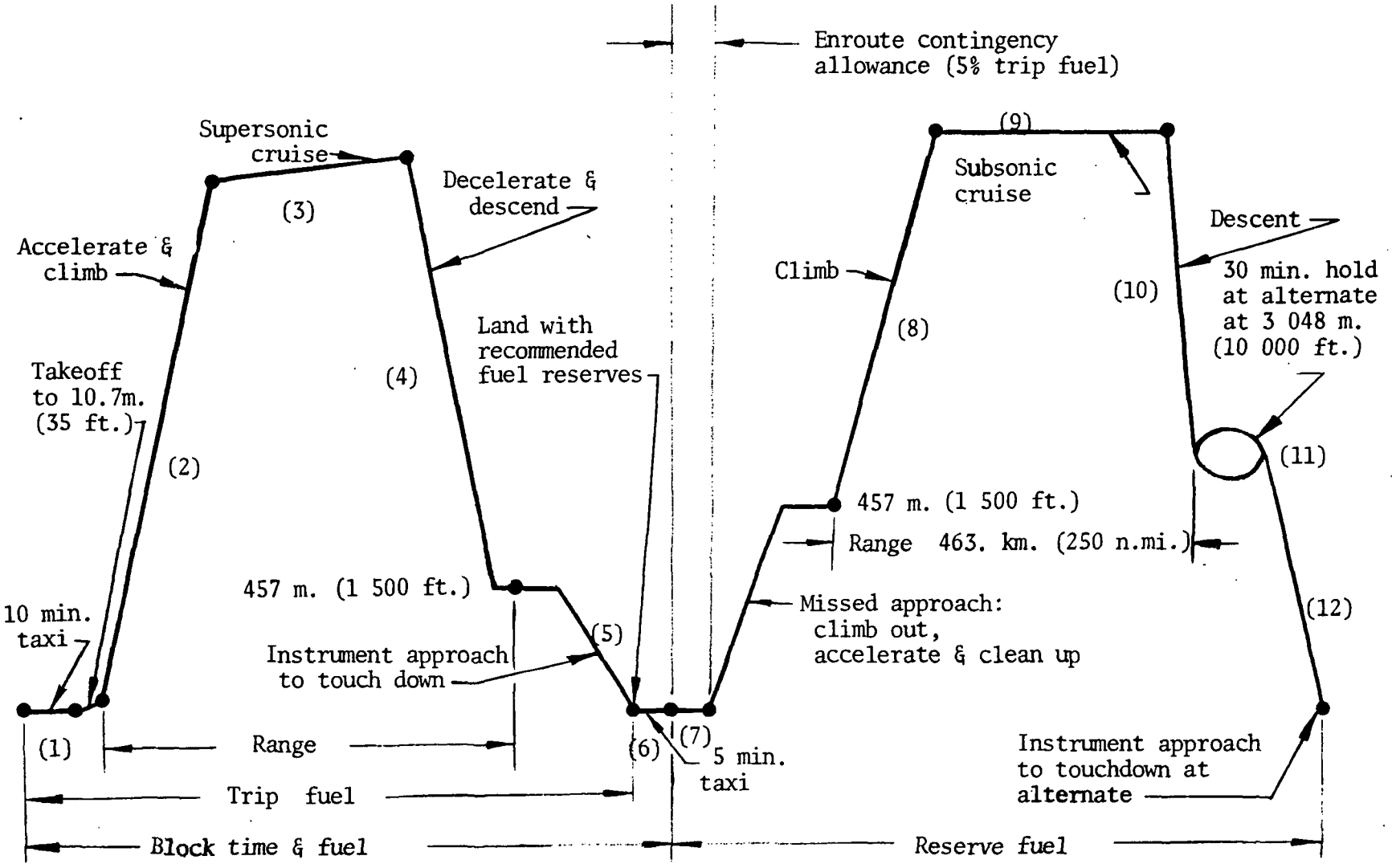

Figure 3.-Reference mission

12. Reserve approach and land - Descend to sea level using idle power.

Alternate mission.-A profile of the alternate mission is shown in figure 4. The first half of the alternate is identical to the first half of the design mission. At the point corresponding to the midpoint of the design mission, a failure is assumed to occur in the most critical engine. At this point, the airplane descends and continues to cruise subsonically with one engine windmilling. The fuel reserve remaining at the end of this mission is equal to the reserve fuel as calculated for the design mission.

The alternate mission consists of:

1. Warmup and takeoff - Same as design mission.
2. Climb - Same as design mission.
3. Cruise - Same as design mission.
4. Descent - Descend and decelerate to subsonic cruise conditions using idle power, following failure of most critical engine.
5. Cruise - Subsonic cruise at Mach number and altitude for best range with one engine inoperative.
6. Descend and land - Descend to sea level using idle power
7. Reserve - Allow total reserve fuel equal to that calculated for design mission legs 7 through 12 .

FAR 36 takeoff.-Takeoff distance is calculated over a 10.7 m. (35 ft.) obstacle using takeoff thrust which has been throttled so that FAR 36 noise requirements are not exceeded. It is assumed that a maximum usable lift coefficient of 0.555 is available for climbout.

Balanced field takeoff.-The balanced field length is defined such that segments B+C = D+E for takeoff over a 10.7 m.(35 ft) obstacle as shown in figure 5. The speed at which the engine failure occurs (i.e., V_1) is varied until this definition is satisfied to a reasonable tolerance. The balanced field length is then taken as the larger of the total takeoff distance or the accelerate-stop distance. For the stop distance calculation, the remaining engines are cut to idle power.

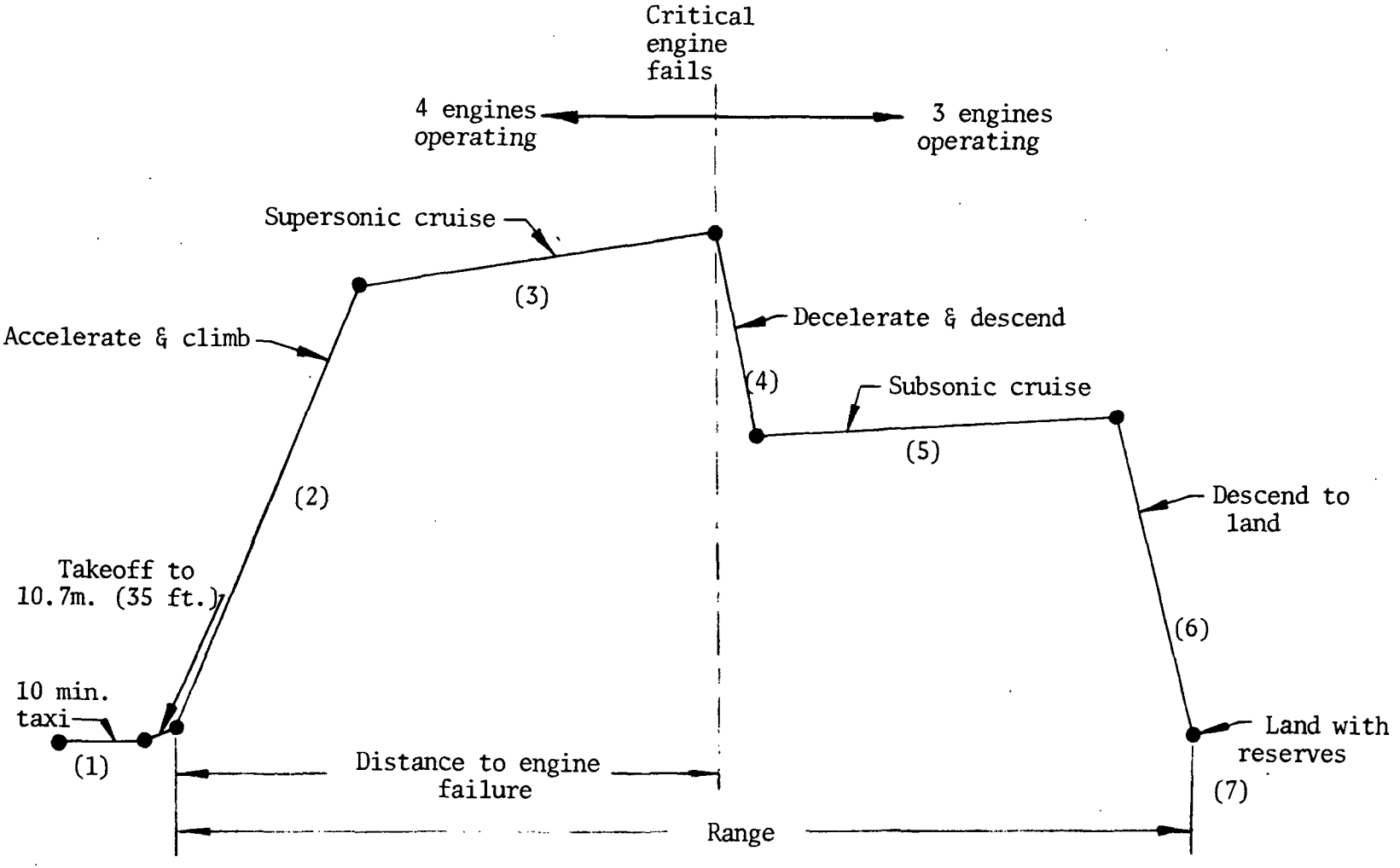

Figure 4.-Alternate mission

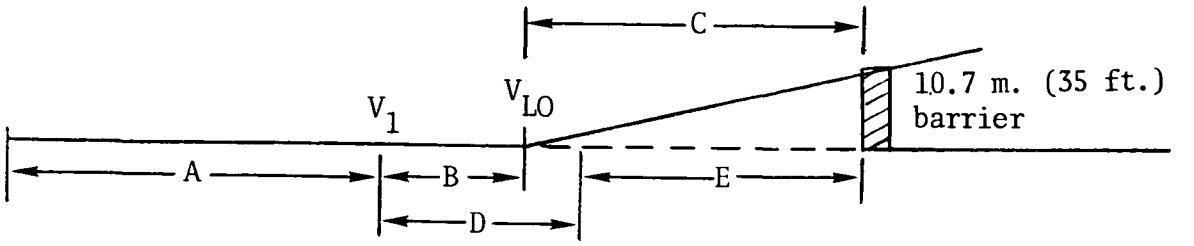

A - Distance up to critical engine failure speed V_1

B - 3-engine acceleration distance from V_1 to V_{LO}

C - 3-engine lift-off to barrier distance

D - Distance gained after engine failure before full brake application

E - Stopping distance

V_1 - Critical engine failure speed

V_{LO} - Lift-off velocity

Figure 5. - Balanced field length definition

Thrust-to-drag ratio.-The thrust-to-drag (T/D) ratio is calculated using maximum available thrust at 2.32 Mach, 18 300 m. (60 000 ft.). Drag is that for level flight at the same conditions. Airplane weight is that at the start of the supersonic cruise as calculated for the design mission. The thrust-to-drag ratio is also calculated for the point in the climb-accelerate leg at which Mach 1.2 is reached. In this case the altitude and vehicle weight are the actual values during the climb at which the Mach number reaches 1.2.

Baseline Airplane.-The "baseline" airplane for this study is a resized version of the above-described "basepoint." Resizing was accomplished by exercising the VSPEP for a matrix of thrust-to-weight and wing loading values, and allowing the program to search for the gross weight, in each case, that satisfies the design mission range requirement of 7 408 km. (4 000 n.mi.). Plots of the results are shown in figures 6 through 8. The parameters shown include vehicle gross weight as well as those performance items for which requirements must be met.

Requirement lines are crossplotted onto the airplane gross weight plot in figure 6. This allows a "baseline" airplane to be chosen which is defined as the minimum gross weight vehicle that meets or exceeds the following performance requirements:

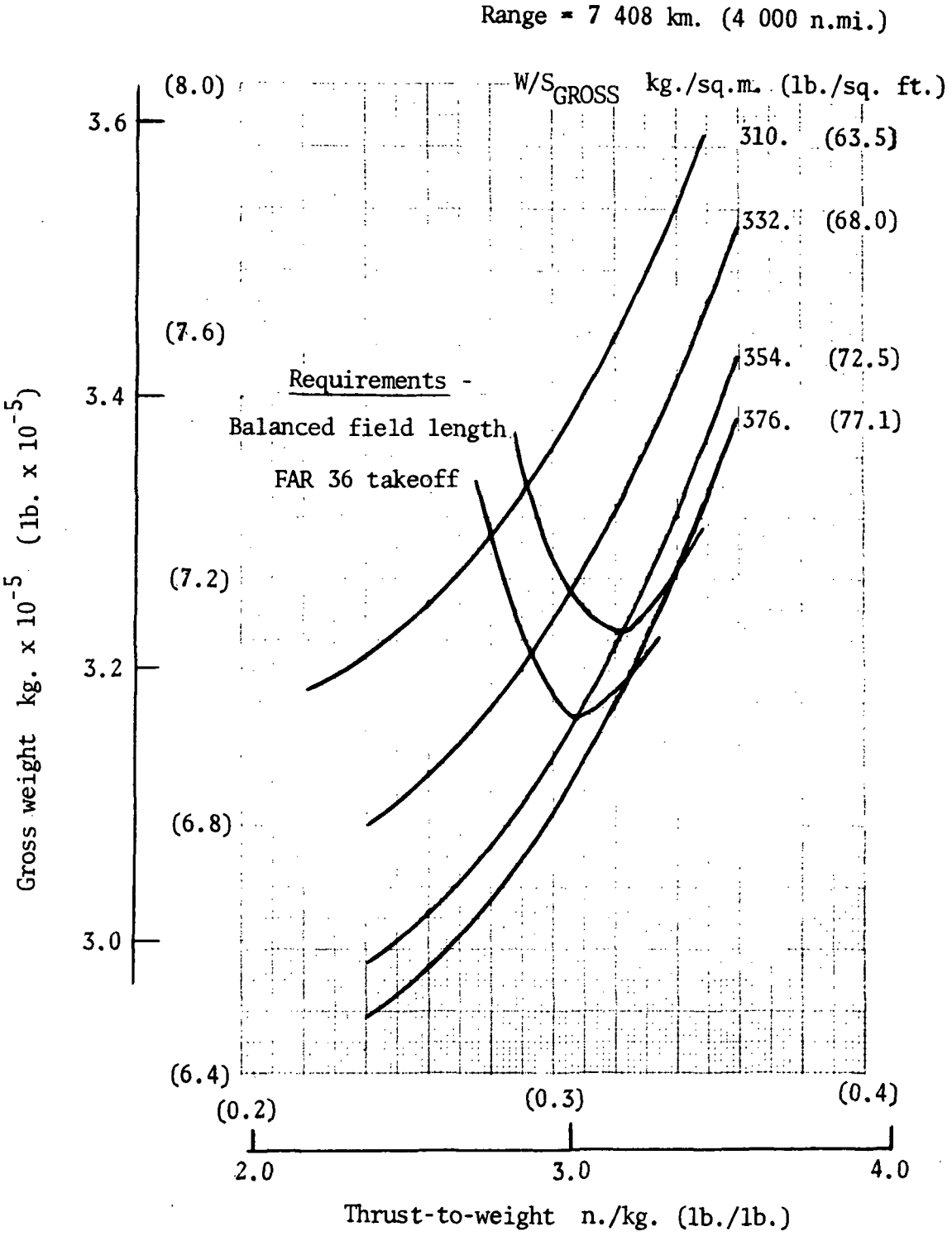

Figure 6.-Gross weight versus thrust-to-weight and wing loading

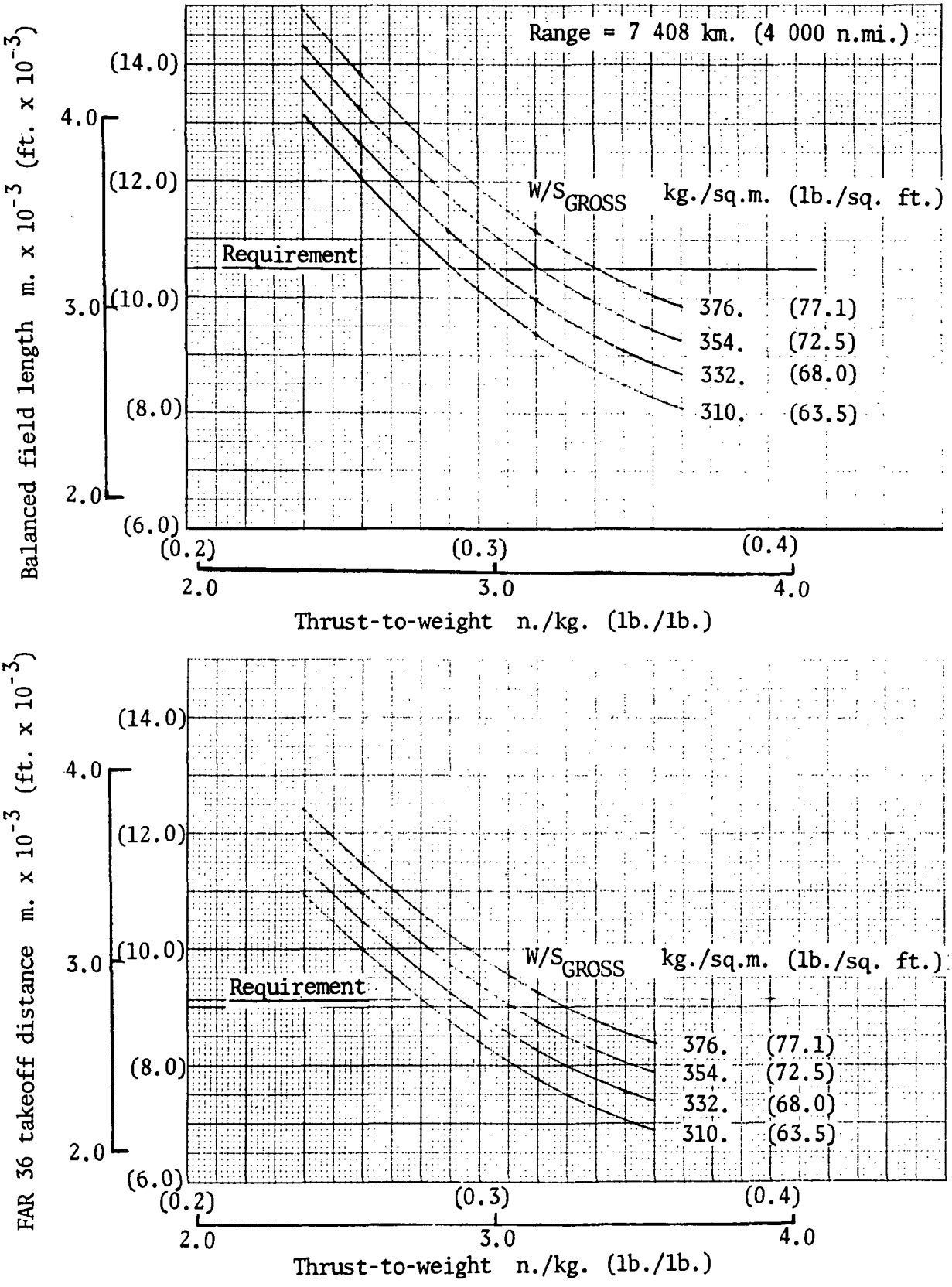

Figure 7 .-Balanced field length versus thrust-to-weight and wing loading

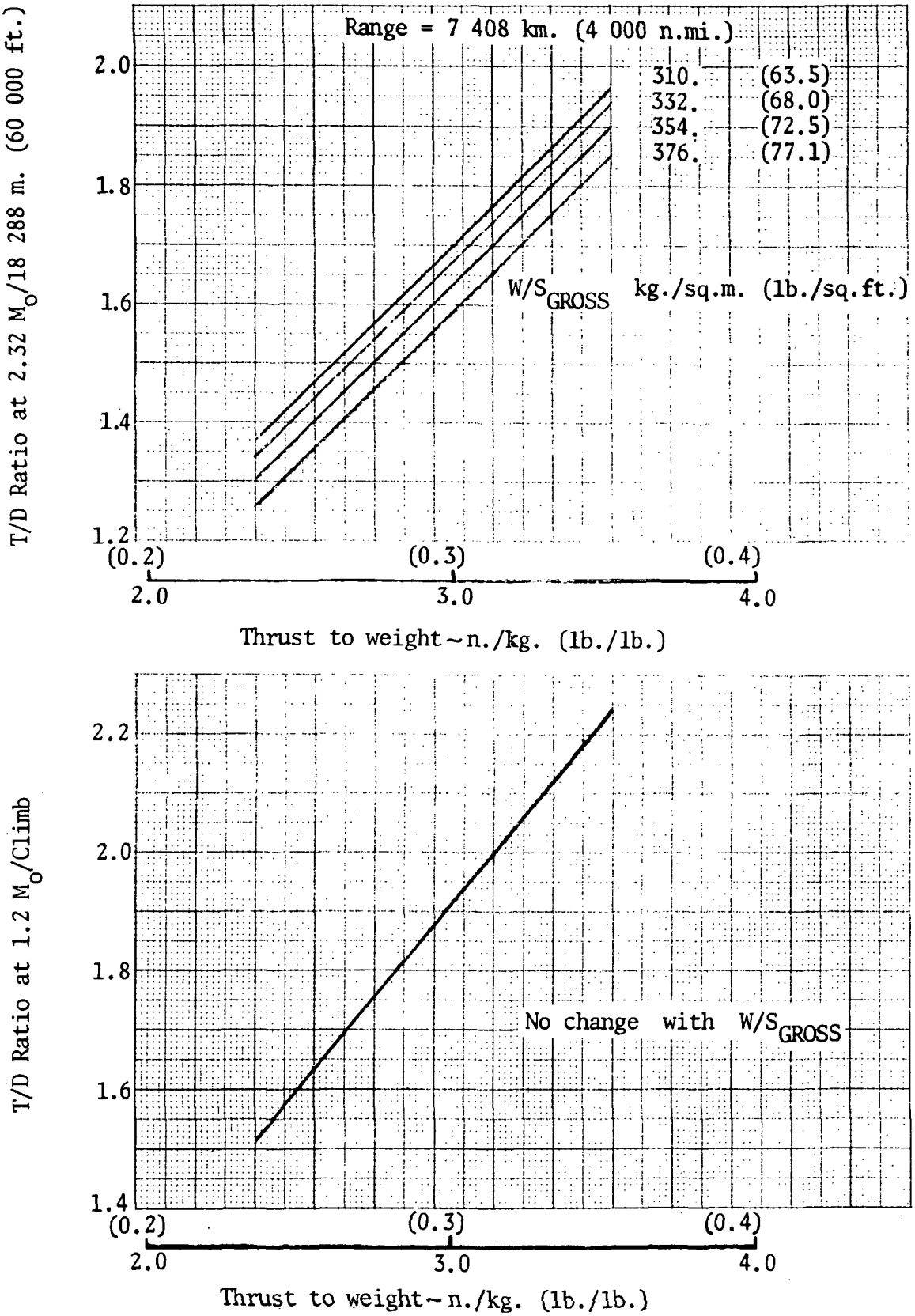

Figure 8 .-Thrust/drag ratio versus thrust-to-weight and wing loading

Design mission range	7 408 km. (4 000 n.mi.) with 292 passengers
Balanced field length	3 200 m. (10 500 ft.)
Minimum T/D during climb or cruise	1.2

Since the thrust-to-drag requirements are exceeded for all cases, only the balanced field length requirements are included in figure 6.

The resulting "baseline" airplane has a gross weight of 323 046 kg. (712 188 lb.); a thrust-to-weight ratio of 3.16 n./kg. (0.323 lb./lb.) based on installed, static takeoff thrust; and a wing loading of 354 kg./sq.m. (72.5 lb./sq. ft.) based on gross wing area.

Further airplane design and performance characteristics for both the "basepoint" and "baseline" airplanes are shown in table I. Design and alternate mission summaries are shown in tables II through V for the baseline airplane. In these tables, the first leg of the alternate mission includes the first four legs of the design mission while leg 5 of the alternate includes reserves for legs 9 through 15 of the design mission. The path followed during the climb-accelerate leg is a minimum fuel path calculated internally by the VSPEP program. This path as calculated for the baseline airplane is shown in figure 9.

Propulsion.-Because many of the current and recently-completed supersonic cruising aircraft studies have used axisymmetric inlets, a mixed-compression, axisymmetric inlet was defined for use in the basepoint aircraft for this study. This inlet is illustrated in figure 10, and the nacelle is shown in figure 11. The inlet diameter is 1.93 meters (76 inches), and capture area is 2.926 square meters (4 536 square inches). The three primary modes of inlet operation are illustrated. Position 1 shows the supersonic cruise geometry. Position 2 shows the centerbody translated forward to the maximum throat area (A_i/A_c of 0.65); the centerbody is translated forward as a single unit. In Position 3, the basic centerbody is held in the transonic position, but the fore and aft conical segments are translated aft to create a centerbody auxiliary inlet. The auxiliary inlet opening in the centerbody is ten percent of capture area. The station cuts on figure 10 show approximate flow passages in the centerbody. In particular, the auxiliary ducting must be divided into four passages around the boundary layer control (BLC) bleed air passages near the centerbody maximum diameter. Inlet pressure recoveries and spillage, bypass, and BLC drags were estimated, and their effects were included in installed propulsion performance.

The engine performance data available for the VSCE 502B engine included the effects of an inlet recovery schedule, nozzle external drags (base plus boattail), 0.45 kilogram-per-second (1.0 pound-per-second) high-pressure compressor air bleed, and 149 kilowatts (200 horsepower) power extraction. Installed performance data were computed by modifying the engine data to include the effects of changes in inlet pressure recovery and inlet drags (spillage, bypass, and boundary layer control). Because the amount of engine data available was not sufficient to compute aircraft mission performance,

TABLE I.-AIRPLANE CHARACTERISTICS

	Basepoint		Baseline	
Engine Airflow, kg./sec. (lb./sec.)	408	(900)	395	(869)
Thrust-to-weight, n./kg. (lb./lb.)	3.14	(0.3208)	3.16	(0.323)
Reference Wing Area, sq.m. (sq. ft.)	926	(9 969)	827	(8 902)
Gross Wing Area, sq.m. (sq. ft.)	1 022	(10 996)	912	(9 819)
Wing Loading (gross area), kg./sq.m. (lb./sq. ft.)	330	(67.56)	354	(72.53)
TOGW, kg. (lb.)	336 529	(742 890)	322 621	(712 188)
Fuel Weight, kg. (lb.)	158 475	(349 834)	151 643	(334 754)
Max. Wing Fuel, kg. (lb.)	207 950	(459 050)	175 484	(387 382)
Design Range, km. (n.mi.)	7 475	(4 034)	7 412	(4 000)
Eng. Out Range, km. (n.mi.)	6 285	(3 392)	6 259	(3 378)
FAR 36 T.O. Dist., m. (ft.)	2 498	(8 194)	2 648	(8 661)
Bal. Field T.O. Dist., m. (ft.)	3 017	(9 898)	3 190	(10 466)
Thrust-to-Drag @ 2.32 M/18 300 m. (60 000 ft.)		1.747		1.716
Thrust-to-Drag @ 1.2M/Climb		2.005		2.019
Initial Cruise L/D		9.649		9.541
Initial Cruise SFC (installed) kg./hr./daN. (lb./hr./lb.)	1.393	(1.366)	1.385	(1.358)

TABLE II.-BASELINE DESIGN MISSION SUMMARY-INTERNATIONAL UNITS

LEG. NO. OPERATION	WEIGHT, kg.	ALTITUDE, m.	MACH	FUEL USED, kg.	TIME, min.	TOTAL TIME min.	RANGE, km.	TOTAL RANGE, km.
INITIAL WEIGHT	323 042						-	
1 WO & TO	319 171	0	0.305	3 871	10.0	10.0	0	0
2 CL TO 1500	317 071	457	0.500	2 100	1.3	11.3	10	10
3 CLB-ACC	292 535	16 746	2.320	24 535	12.8	24.1	288	299
4 CRUISE	239 921	17 910	2.320	52 614	82.9	107.0	3 405	3 704
5 CRUISE	196 262	19 168	2.320	43 659	82.6	189.7	3 395	7 100
6 DESCEND	194 735	457	0.500	1 526	17.3	207.0	296	7 396
7 DES-LAND	194 500	0	0.300	235	1.5	208.6	12	7 409
8 TAXI-ALL	193 853	0	0.0	646	5.0	213.6	0	7 409
9 5PCT ALL	187 394	0	0.0	6 459	0.0	213.6	0	7 409
10 CL 1500	186 826	457	0.500	567	0.7	214.3	5	7 414
11 CLB-ACC	181 460	12 337	0.950	5 366	10.2	224.5	158	7 573
12 CRUISE	179 067	12 427	0.950	2 393	10.8	235.3	181	7 754
13 DESCEND	178 195	3 048	0.470	871	9.5	244.9	123	7 877
14 LOITER	171 744	3 048	0.454	6 450	30.0	274.9	0	7 877
15 DES-LAND	171 207	0	0.300	537	3.7	278.6	33	7 911
TOTAL FUEL USED = 151 834								

TABLE III.-BASELINE DESIGN MISSION SUMMARY - ENGLISH UNITS

LEG. NO. OPERATION	WEIGHT, lbs.	ALTITUDE, ft.	MACH NO.	FUEL USED, lbs.	TIME min.	TOTAL TIME min.	RANGE n.m.	TOTAL RANGE n.m.
INITIAL WEIGHT	712 187							
1 WO & TO	703 653	0	0.305	8 534	10.0	10.0	0	0
2 CL TO 1500	699 022	1 500	0.500	4 631	1.3	11.3	5	5
3 CLB-ACC	644 931	54 943	2.320	54 090	12.8	24.1	155	161
4 CRUISE	528 936	58 761	2.320	115 994	82.9	107.0	1 838	2 000
5 CRUISE	432 684	62 889	2.320	96 252	82.6	189.7	1 833	3 833
6 DESCEND	429 318	1 500	0.500	3 365	17.3	207.0	159	3 993
7 DES-LAND	428 800	0	0.300	518	1.5	208.6	7	4 000
8 TAXI-ALL	427 374	0	0.0	1 425	5.0	213.6	0	4 000
9 5PCT ALL	413 134	0	0.0	14 240	0.0	213.6	0	4 000
10 CL TO 1500	411 882	1 500	0.500	1 251	0.7	214.3	2	4 003
11 CLB-ACC	400 052	40 476	0.950	11 830	10.2	224.5	85	4 089
12 CRUISE	394 775	40 773	0.950	5 276	10.8	235.3	98	4 187
13 DESCEND	392 853	10 000	0.470	1 921	9.5	244.9	66	4 253
14 LOITER	378 632	10 000	0.454	14 221	30.0	274.9	0	4 253
15 DES-LAND	377 448	0	0.300	1 184	3.7	278.6	18	4 271
TOTAL FUEL USED = 334 739								

TABLE IV.-BASELINE ALTERNATE MISSION SUMMARY - INTERNATIONAL UNITS

LEG. NO. OPERATION	WEIGHT, kg.	ALTITUDE, m	MACH NO.	FUEL USED, kg.	TIME min.	TOTAL TIME min.	RANGE km.	TOTAL RANGE km.
INITIAL WEIGHT	323 042							
1 DES LEGS 1-4	239 921	0	0.0	83 121	107.0	107.0	3 704	3 704
2 DES-DEC	239 539	8 212	0.900	381	7.9	115.0	189	3 894
3 CRUISE	194 718	9 461	0.900	44 821	136.7	251.7	2 248	6 142
4 DESCEND	193 850	0	0.300	868	10.2	262.0	113	6 256
5 RESERVE	171 204	0	0.0	22 646	65.0	327.0	502	6 758
Total Fuel Used = 151 838								

TABLE V.- BASELINE ALTERNATE MISSION SUMMARY - ENGLISH UNITS

LEG NO. OPERATION	WEIGHT, lbs.	ALTITUDE, ft.	MACH NO.	FUEL USED lbs.	TIME min.	TOTAL TIME min.	RANGE n.m.	TOTAL RANGE n.m.
INITIAL WEIGHT	712 187							
1 DES LEGS 1-4	528 936	0	0.0	183 251	107.0	107.0	2 000	2 000
2 DES-DEC	528 095	26 944	0.900	841	7.9	115.0	102	2 102
3 CRUISE	429 281	31 040	0.900	98 813	136.7	251.7	1 213	3 316
4 DESCEND	427 368	0	0.300	1 913	10.2	262.0	61	3 378
5 RESERVE	377 441	0	0.0	49 926	65.0	327.0	271	3 649
Total Fuel Used = 334 746								

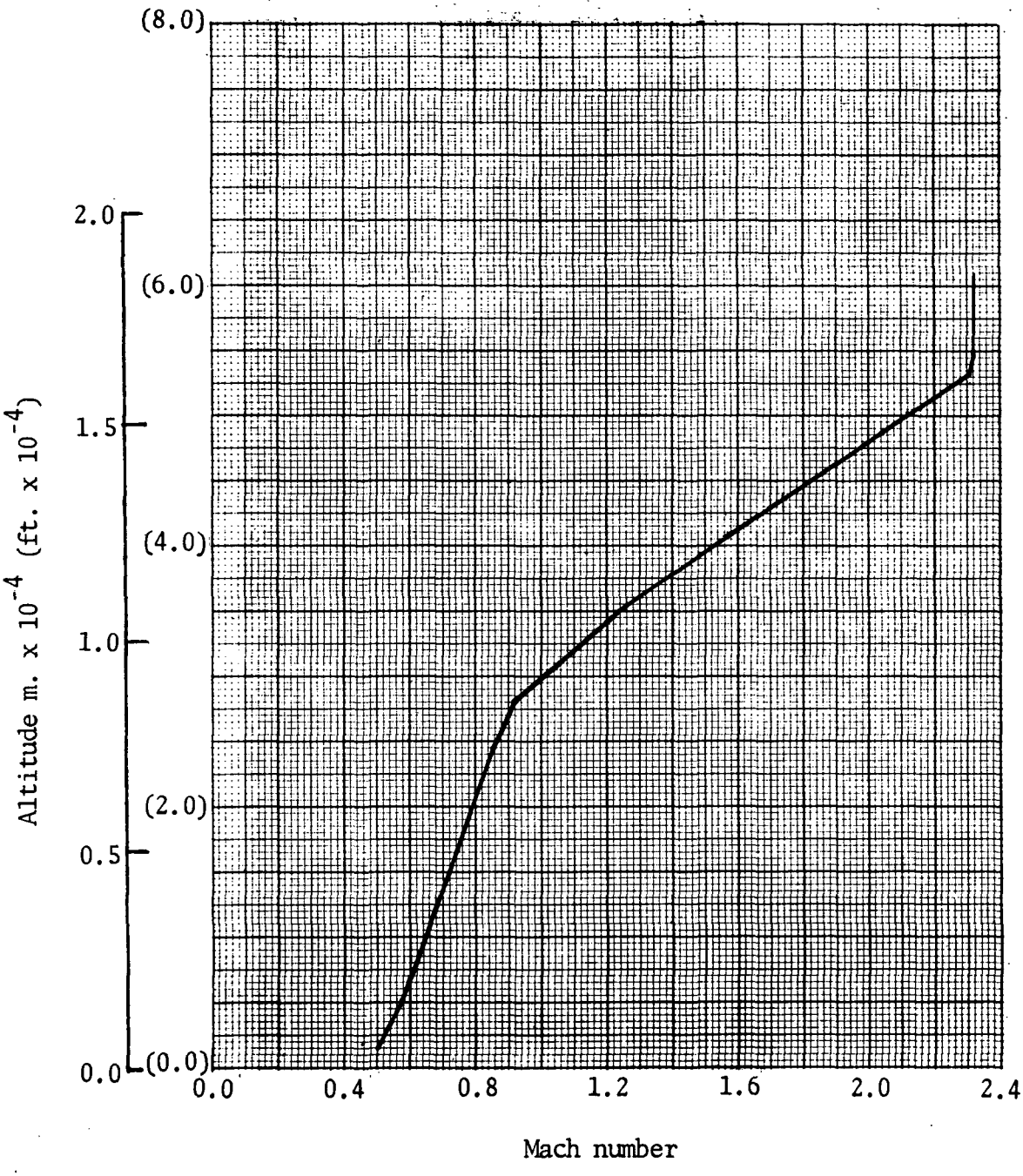

Figure 9.-Baseline airplane climb path

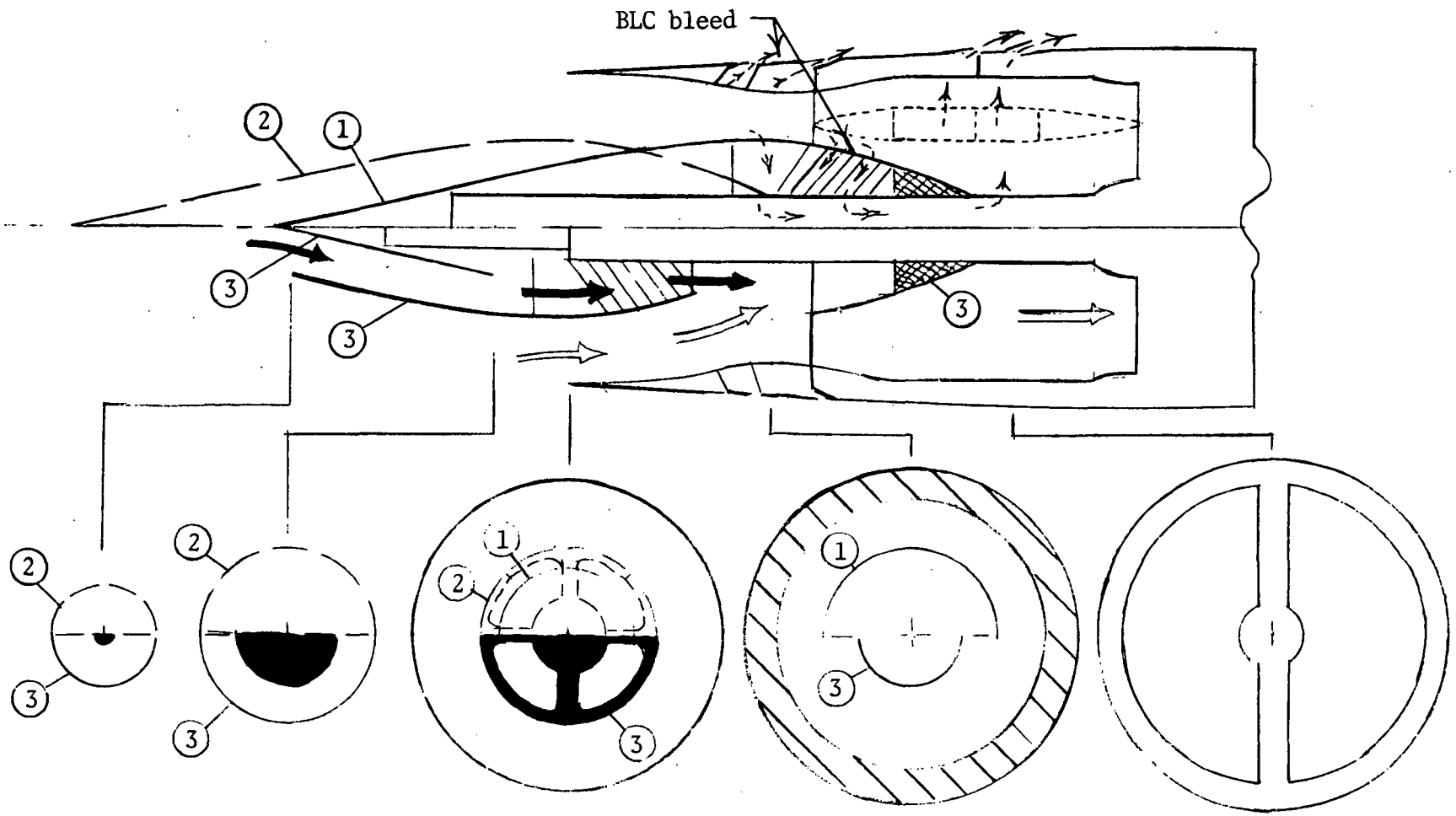

Figure 10.-Mach 2.4 inlet configuration

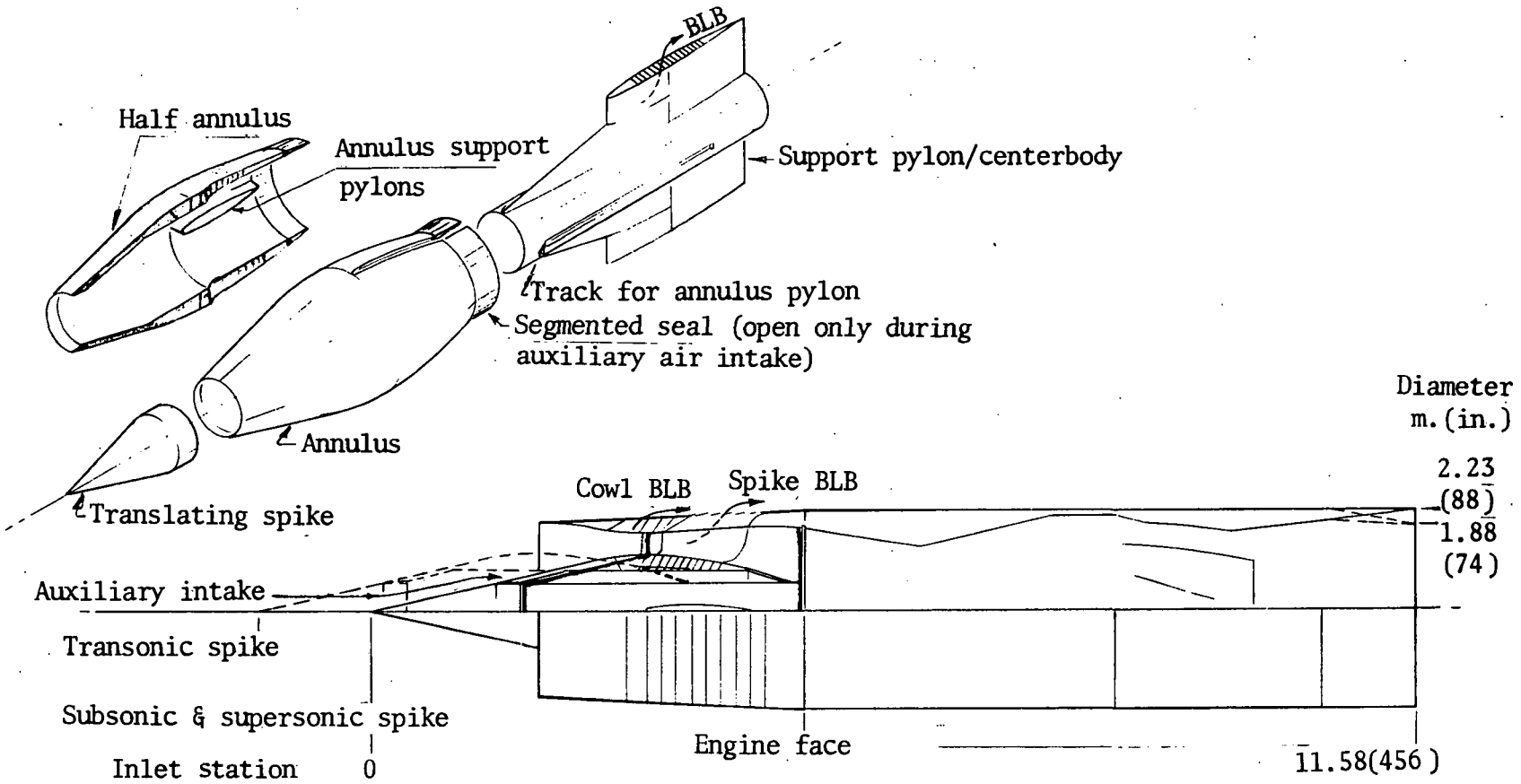

Figure 11.-Basepoint nacelle

additional installed performance data were generated by calculating corrected thrust and fuel flow parameters and by extrapolating based on trends of engines with similar characteristics. Fortunately, these techniques were required only at flight conditions where the airplane flies for a short duration. Thus, any possible errors due to data extrapolation should have minimal effect on airplane performance. All data were for a standard-plus-8°C day.

At takeoff, the engine power setting was scheduled so that the aircraft meets FAR 36-traded noise levels. The SAE exhaust jet noise prediction method was used with the modification to overall sound pressure level recommended by Bushell (reference 4). This modification has no effect on perceived noise level at static condition, but it results in approximately four decibels (dB) higher noise than the standard SAE method at Mach 0.3. A 1.5dB reduction in sideline noise has been assumed due to sideline shielding while the airplane is on the ground. An eight-decibel reduction in noise level due to the coannular nozzle effect has been assumed for all flight conditions and power settings. Information from P&WA indicates that coannular configurations reduce noise by seven to nine decibels when the difference between core velocity and bypass velocity is 152 meters per second (500 feet per second) or more, with the core stream having the lower velocity.

Mass properties.-The basepoint vehicle weight summary is given in table VI. The NASA reference vehicle weight summary (reference 2) from which the basepoint was derived is also shown. The differences between the weights of the two vehicles are in the engines and nacelles. The basepoint vehicle has VSCE 502B 408 kg./sec. (900 lb./sec.) airflow engines in lieu of the 363 kg./sec. (800 lb./sec.) engines in the NASA reference vehicle.

The VSCE 502B bare engine weight including nozzle and thrust reverser was supplied by P&WA. Weight increments of 22.7 kg. (50 lb.) for residual fluids and 22.7 kg. (50 lb.) for miscellaneous engine/airframe interfacing provisions were added to the bare weight to obtain an installed weight. Table VII shows the installed engine weight summary.

The basepoint nacelle weight estimate is based on the nacelle drawing, figure 11. For the weight evaluation the nacelle was divided into three sections: forward of the engine front face (inlet cowl), aft of the front face (engine cowl) and inlet spike. The engine cowl weight was estimated at 34.2 kg./sq.m. (7 lb./sq. ft.) of wetted area. This weight includes all the nacelle structure that supports and surrounds the engine and was derived from prior Rockwell International studies of a similar type. The inlet cowl and spike weights were calculated using statistical weight estimating equations obtained from the Technical Report SEG-TR-67-1, Preliminary Design Methodology for Air-Induction Systems (reference 5). Engine mount weights were calculated statistically at 1.5 percent of the engine weight. The mount weights are included with the nacelle weight.

The weight summary of the basepoint nacelle is presented in table VIII.

TABLE VI.-VEHICLE WEIGHT SUMMARY

ITEM	NASA REFERENCE VEHICLE		BASEPOINT	
	Kg	LB	Kg	LB
Wing	37 805	83 347	37 805	83 347
Horizontal Tail	2 391	5 271	2 391	5 271
Vertical Tail	2 148	4 735	2 148	4 735
Fuselage	24 636	54 314	24 636	54 314
Landing Gear	13 138	28 965	13 138	28 965
Nacelle	8 625	19 015	7 410	16 336
Structure Total	(88 743	(195 647	(87 528	(192 968
Engines	27 139	59 832	24 494	54 000
Thrust Reversers	4 809	10 601		
Miscellaneous Systems	807	1 780	807	1 780
Fuel System-Tanks and Plumbing	2 622	5 781	2 622	5 781
Propulsion Total	(35 377	(77 994	(27 923	(61 561
Surface Controls	4 527	9 981	4 527	9 981
Instruments	1 542	3 400	1 542	3 400
Hydraulics	2 540	5 600	2 540	5 600
Electrical	2 291	5 050	2 291	5 050
Avionics	1 220	2 690	1 220	2 690
Furnishings and Equipment	11 390	25 111	11 390	25 111
Air Conditioning	3 720	8 200	3 720	8 200
Anti-icing	95	210	95	210
Systems and Equipment Total	(27 325	(60 242	(27 325	(60 242
Weight Empty	151 445	333 883	142 776	314 771
Crew and Baggage-Flight,	306	675	306	675
-Cabin,	744	1 640	744	1640
Unusable Fuel	1 059	2 335	1 059	2 335
Engine Oil	361	795	361	795
Passenger Service	4 015	8 852	4 015	8 852
Cargo Containers	1 343	2 960	1 343	2 960
Operating Weight	159 273	351 140	150 604	332 028
Passengers, (292)	21 854	48 180	21 854	48 180
Passenger Baggage	5 828	12 848	5 828	12 848
Zero Fuel Weight	186 955	412 168	178 286	393 056
Mission Fuel	158 680	349 832	158 681	349 834
Design Gross Weight	345 635	762 000	336 967	742 890

TABLE VII.-BASEPOINT ENGINE WEIGHT

ITEM	WEIGHT/VEHICLE Kg	LB
ENGINES (INCLUDING NOZZLE & THRUST REVERSER) (4)	24 312	53 600
RESIDUAL FLUIDS	91	200
MISCELLANEOUS PROVISIONS	91	200
ENGINES AS INSTALLED	24 494	54 000

TABLE VIII.-BASEPOINT NACELLE WEIGHT

ITEM	WEIGHT/VEHICLE Kg	LB
NACELLES		
ENGINE COWL	2 782	6 132
INLET COWL	1 299	2 864
SPIKE	2 961	6 528
ENGINE MOUNTS	368	812
TOTAL NACELLE	7 410	16 336

Aerodynamics.-Friction drag estimates were made for a fully turbulent, hydraulically smooth condition using the incompressible Von-Karman-Schoenherr method (reference 6) in conjunction with the adiabatic compressibility correction of Sommer and Short (reference 7). Component characteristic lengths (e.g. the distance from the inlet lip to the exhaust nozzle exit, the exposed mean aerodynamic chord of planar surfaces, etc.) and the altitude along the mission climb profile were used to evaluate length Reynolds numbers. Flat plate values were increased by three percent to account for form losses.

The wave drag due to thickness was estimated as a function of Mach number using supersonic area rule theory (reference 8 and 9) in conjunction with a transparent wing simulation, an inlet mass flow ratio of one, and the nozzle exit area held fixed at its supersonic cruise position. The effect of inlet spillage and nozzle position is included in the installed thrust. All results reported here are based on the use of a 50-Mach-plane (ΔX = .02 L (Θ)), 13-roll-angle ($\Delta\Theta$ = 15°) analysis. Basepoint configuration results for increased solution mesh density did not indicate any appreciable change.

Supersonic cruise trimmed drag-due-to-lift characteristics are assumed to be equal to the reference configuration of reference 2 and consequently independent of wing and engine size and nacelle shape. A different design wing twist and camber is required for each case to realize this performance. The lifting efficiency may be conservative for some of the more favorably-shaped nacelles of the parametric drag study in that any increased benefit that may be realized from favorable nacelle thickness/wing lift interference over and above that of the reference configuration is neglected. Conversely, for the less favorably-shaped nacelles, the analysis may be somewhat optimistic. At off design conditions, the above assumption is necessary because the required analysis is beyond the scope of the contract effort.

A comparison of the VSCE 502B (408 kg./sec., 900 lb./sec. airflow) nacelle of figure 11 to that of the reference configuration non-afterburning single spool turbojet with variable geometry turbine (363 kg./sec., 800 lb./sec. airflow) of reference 2 is presented on figure 12. The basepoint nacelle is 1.95 meters (6.4 feet) shorter and has a 0.14 meter (0.46 feet) smaller maximum diameter. The relative cross-sectional shape of the two nacelles is presented on figure 13. The basepoint total configuration normal cross-sectional area distribution is shown on figure 14.

Estimated total and nacelle incremental skin friction and wave drag characteristics (relative to nacelles off) for the basepoint configuration are presented on table IX. The wave drag results are for the case in which the nozzle exit planes are the same as the reference configuration. A slightly higher drag results (ΔC_{D_W} = 0.00006 at Mach 2.7) if the inlet planes are matched.

The friction, wave, and total drag increments of the basepoint nacelle are compared to those of the reference nacelle on figure 15. The basepoint

TABLE IX.-BASEPOINT CONFIGURATION ESTIMATED SKIN FRICTION AND WAVE DRAG CHARACTERISTICS

S_{REF} = 929 sq.m. (10 000 sq.ft.)

M_o	ALTITUDE		AIRCRAFT		NACELLE	
	m.	ft.	C_{D_P}	C_{D_W}	ΔC_{D_P}	ΔC_{D_W}
.4	457	1 500	0.0061	----	0.00065	----
.8	6 400	21 000	0.00572	----	0.00062	----
1.2	10 455	34 300	0.00545	0.00365	0.00060	-0.00017
1.4	11 521	37 800	0.00522	0.00316	0.00058	-0.00018
1.8	13 594	44 600	0.00490	0.00254	0.00055	-0.00019
2.32	16 764	55 000	0.00450	0.00222	0.00050	-0.00018
2.7	18 288	60 000	0.00418	0.00217	0.00046	-0.00014

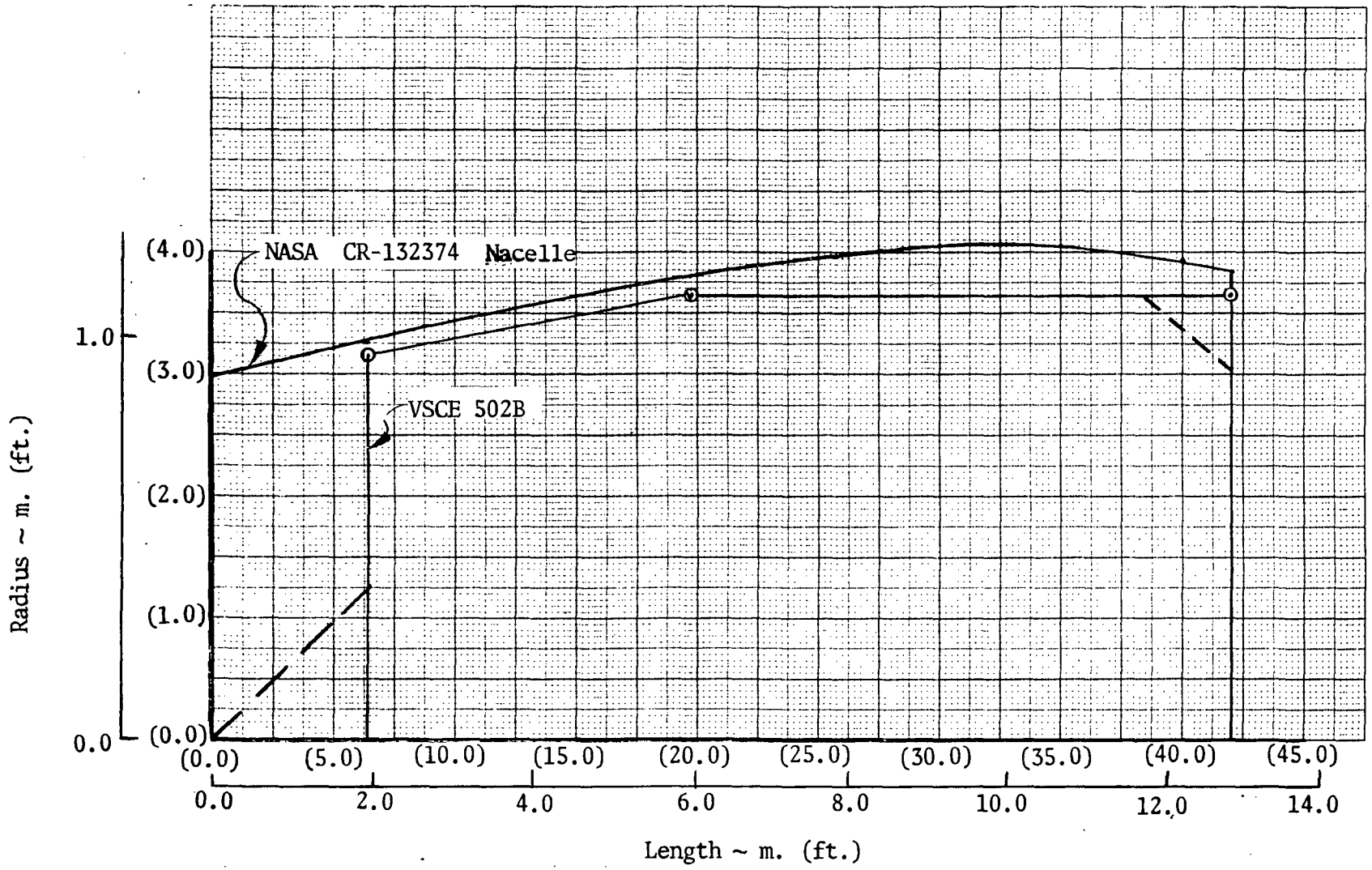

Figure 12.- Comparison of reference and basepoint nacelles

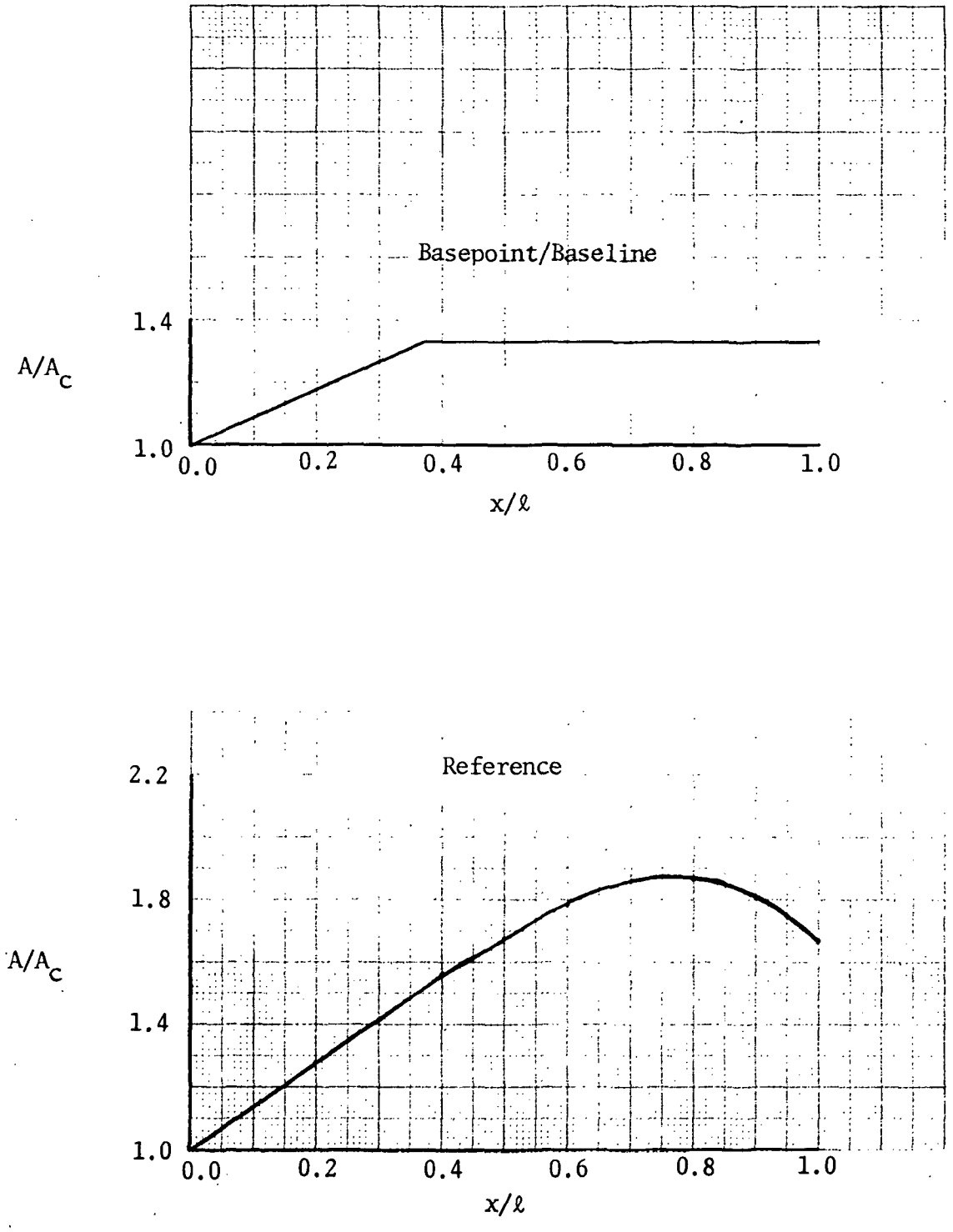

Figure 13.-Nacelle cross sectional area variation

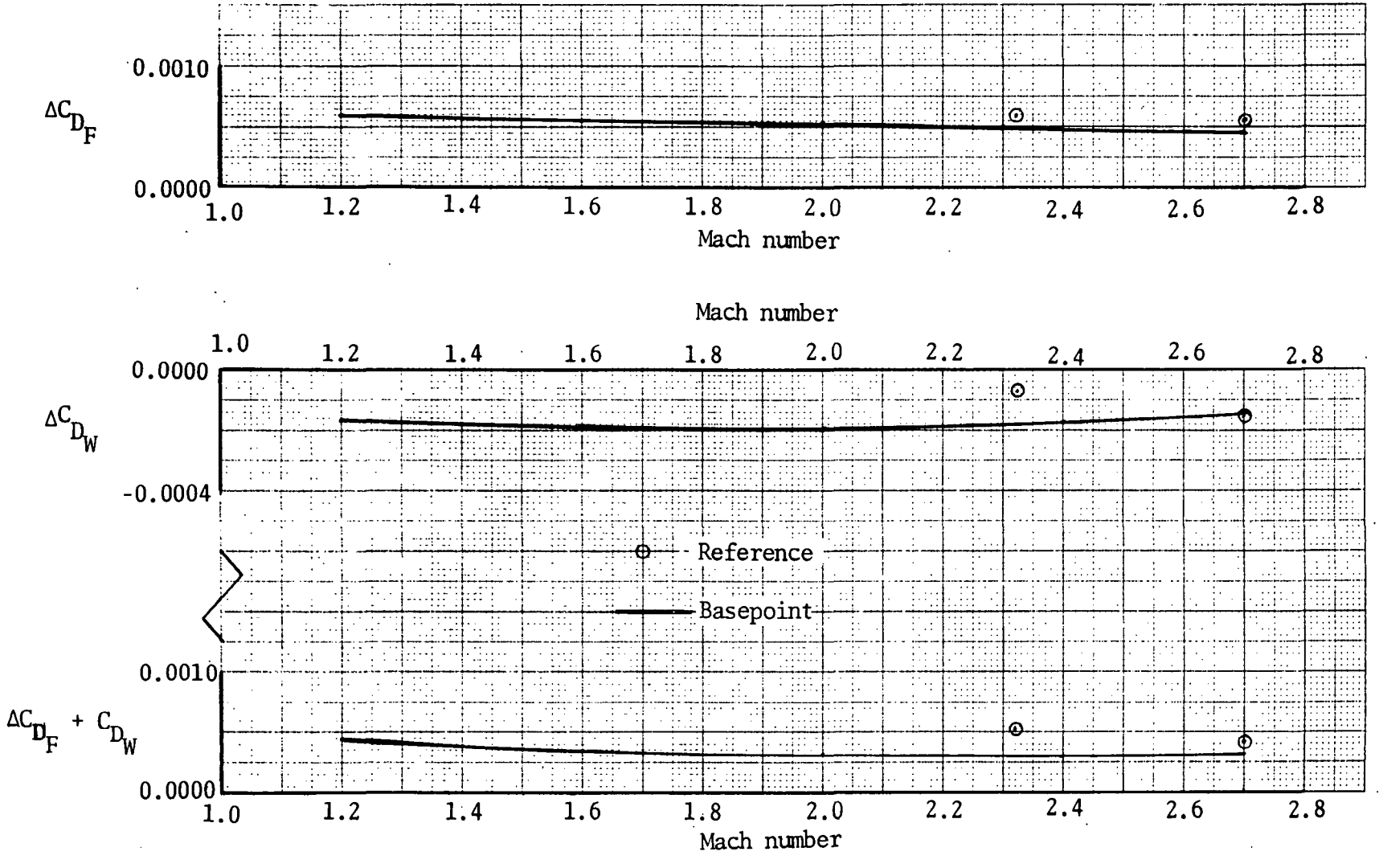

Figure 15.-Basepoint incremental nacelle drag versus Mach number

configuration has a slightly smaller installation drag in spite of 12.5 percent greater airflow. It was subsequently determined that a further reduction of 0.5 count could be realized by meridial contour optimization.

The aerodynamic characteristics used in resizing the basepoint wing and engine size to produce the baseline configuration used for all parametric nacelle drag studies were established as follows:

Fully turbulent friction levels were adjusted for difference in surface area and length Reynolds number of the wing and nacelle. The wave drag variation of the basepoint configuration as a function of wing and engine size were parametrically evaluated for input to the sizing program. The results are presented on figure 16. The effect of engine size was essentially nil at this scale for the nacelle shape under consideration.

The trimmed drag due to lift characteristics were assumed to be independent of wing size and equal to the reference configuration. The specific levels used are presented on figures 17 through 19 and were taken directly from reference 2.

Sizing of the basepoint configuration produced the study baseline (table I) which had a 12 percent smaller wing size and a 3.5 percent smaller engine size. The associated normal cross-sectional area distribution is presented on figure 20. A summary of the component surface areas and reference lengths is presented on table X, and table XI presents baseline drags.

Parametric Drag Analysis

The parametric nacelle wave drag analysis utilized the baseline configuration described in the previous section. The installation of the propulsion system followed several general ground rules in order to preserve the basic arrangement concepts and provide consistent comparisons concerning the effect of nacelle size variations. They are:

1. Nacelle overhang of the wing trailing edge and vertical nacelle-wing separation was limited to the reference configuration values for structural reasons.

2. The longitudinal and lateral separation distance between the inboard and outboard nacelles was preserved in order to maintain inlet flow quality.

3. The reference configuration philosophy of locating the nacelle volume in a region of decreasing wing thickness was maintained.

The impact of these considerations in the propulsion system location for the largest and smallest nacelles of the study are presented on figure 21. The reference configuration is superimposed on these results for comparison purposes. The outboard nacelle is moved inboard and forward as required along the mid-chord (approximate maximum thickness) line of the wing

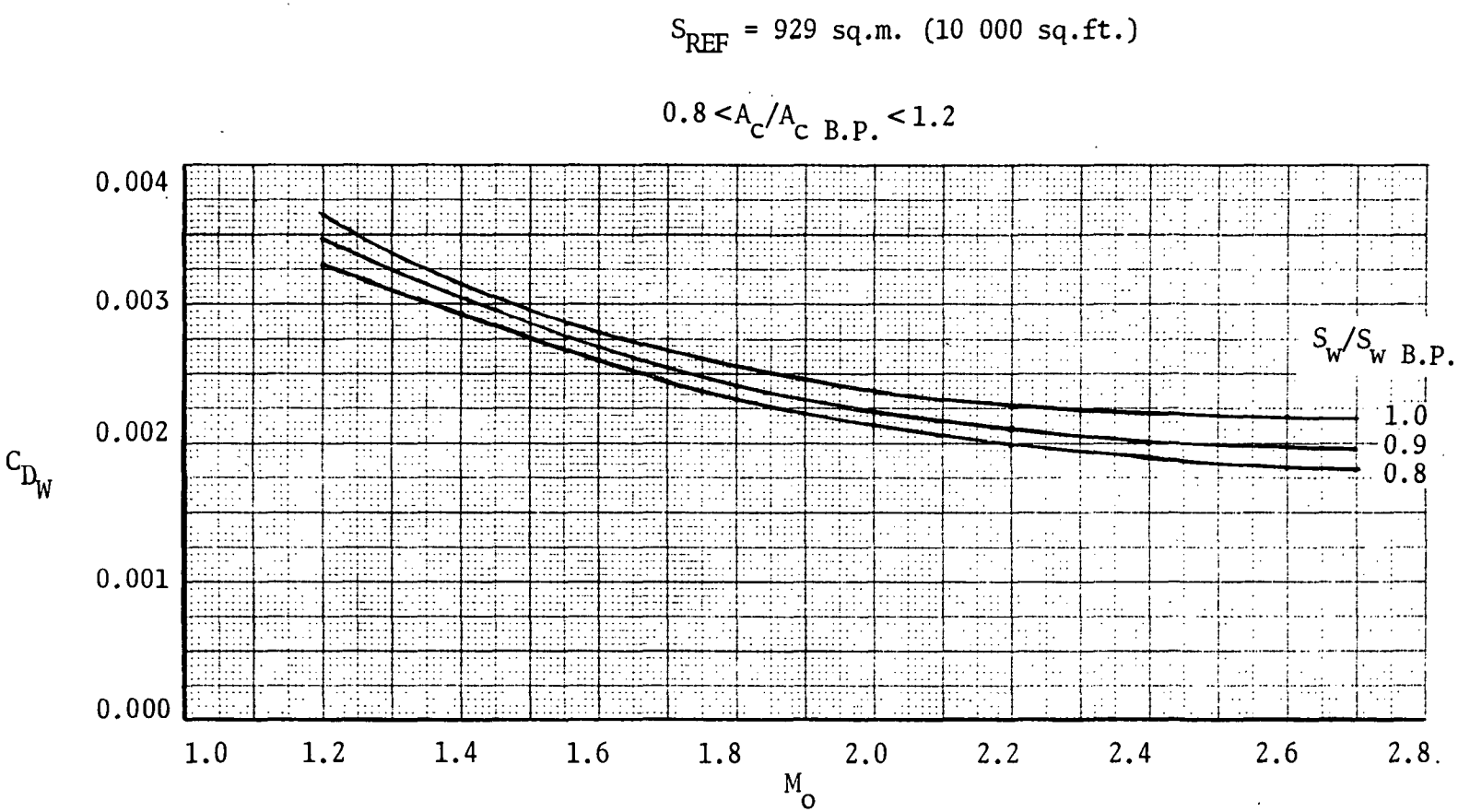

Figure 16.- Basepoint wave drag sizing data

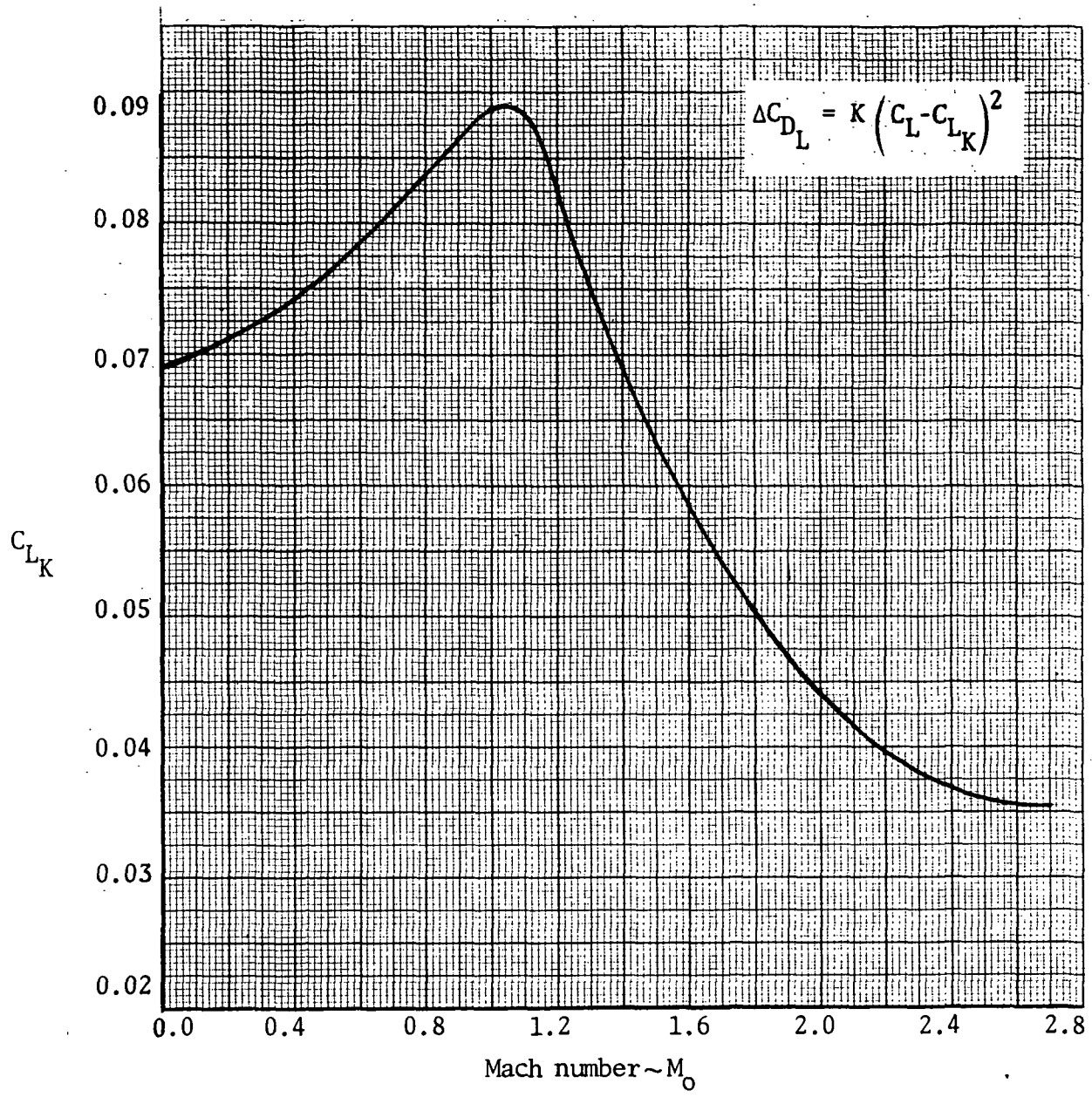

Figure 17. - C_{L_K} versus Mach number

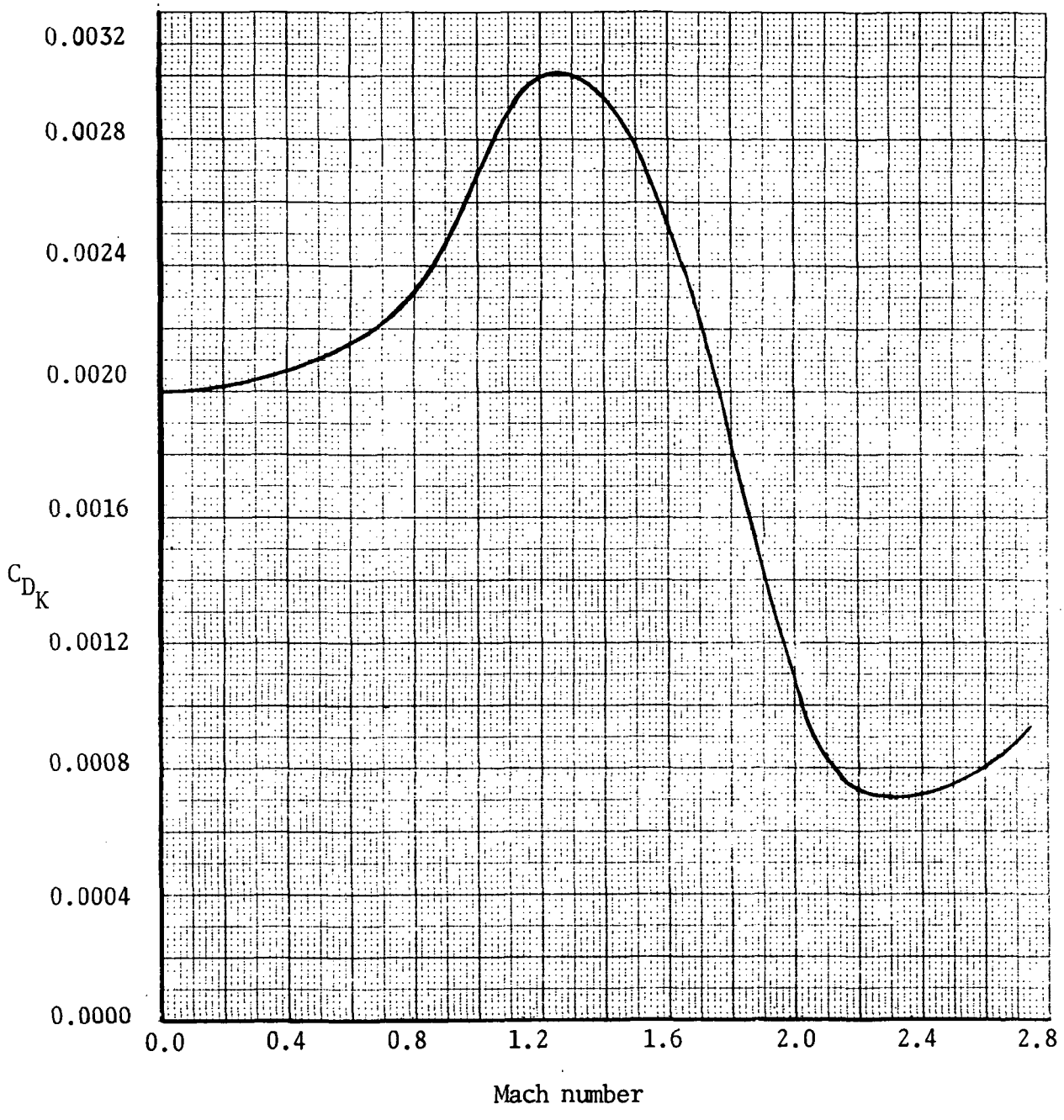

Figure 18.- C_{D_K} versus Mach number

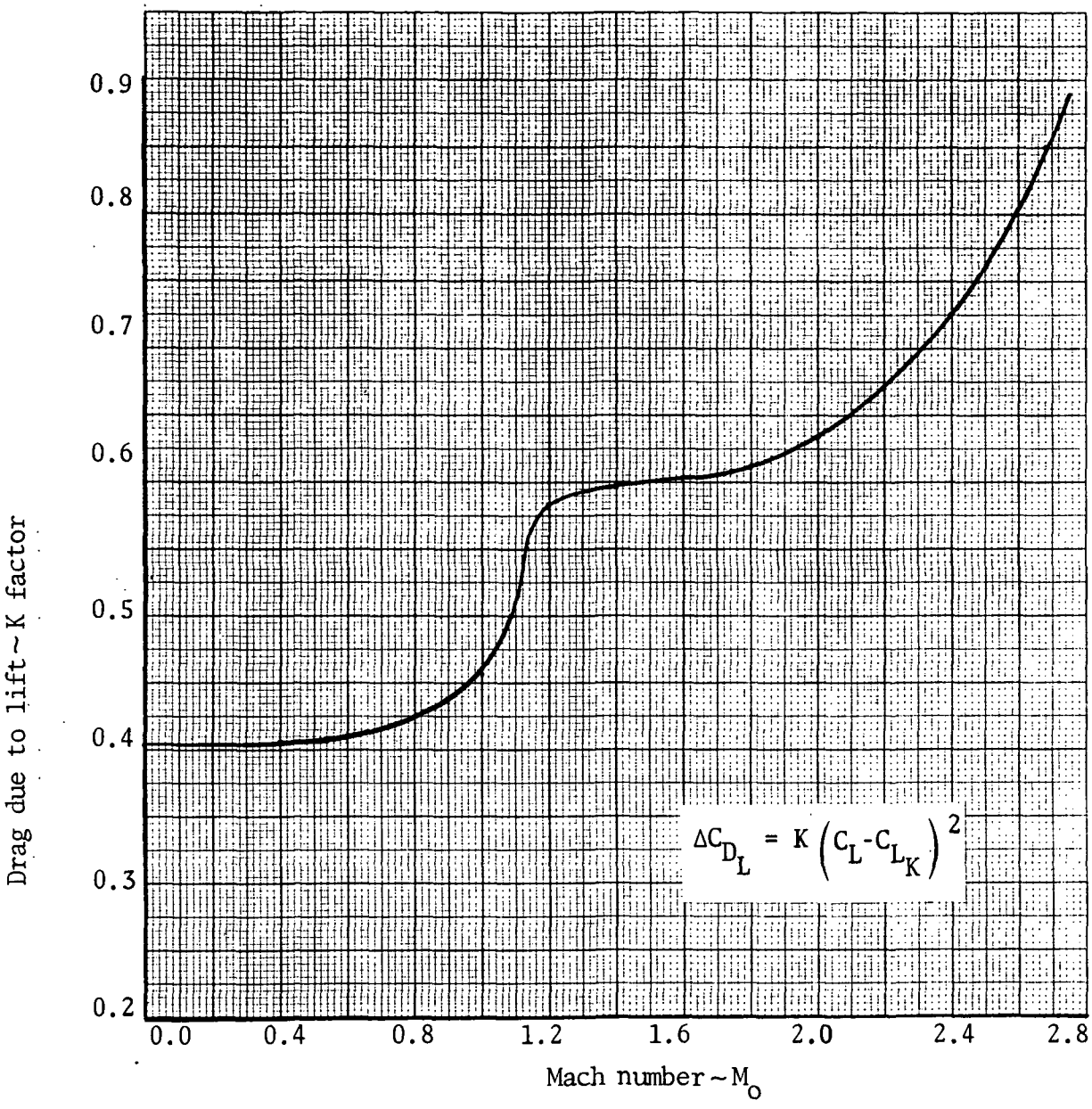

Figure 19. - 'K' factor versus Mach number

TABLE X.-BASELINE CONFIGURATION SURFACE AREA AND LENGTH SUMMARY

COMPONENT	Swet sq.m. (sq.ft.)	Length m. (ft.)
Fuselage	786 (8 450)	96 (315)
Wing	1 505 (16 987)	7.65-39.4 (25.1-129.)
Nacelles (4)	276. (3 088)	12.7 (35.1)
Center Line Vertical	20.1 (219)	4.9 (16.2)
Wing Verticals	91. (992)	7.9 (25.9)
Horizontal	89.5 (921)	5.8 (18.9)

TABLE XI.-BASELINE CONFIGURATION ESTIMATED SKIN FRICTION AND WAVE DRAG CHARACTERISTICS

S_{REF} = 929 sq.m. (10 000 sq. ft.)

M_o	ALTITUDE m.	(ft.)	AIRCRAFT C_{D_F}	C_{D_W}	NACELLE ΔC_{D_F}	ΔC_{D_W}
0.4	457	(1 500)	0.00568	----	0.00065	----
0.8	6 400	(21 000)	0.00537	----	0.00061	----
1.2	10 455	(34 300)	0.00508	0.00339	0.00058	-0.00009
1.4	11 521	(37 800)	0.00489	0.00305	0.00056	0.00003
1.8	13 594	(44 600)	0.00455	0.00237	0.00052	-0.00011
2.32	16 764	(55 000)	0.00420	0.00209	0.00049	-0.00012
2.7	18 288	(60 000)	0.00392	0.00200	0.00045	-0.00011

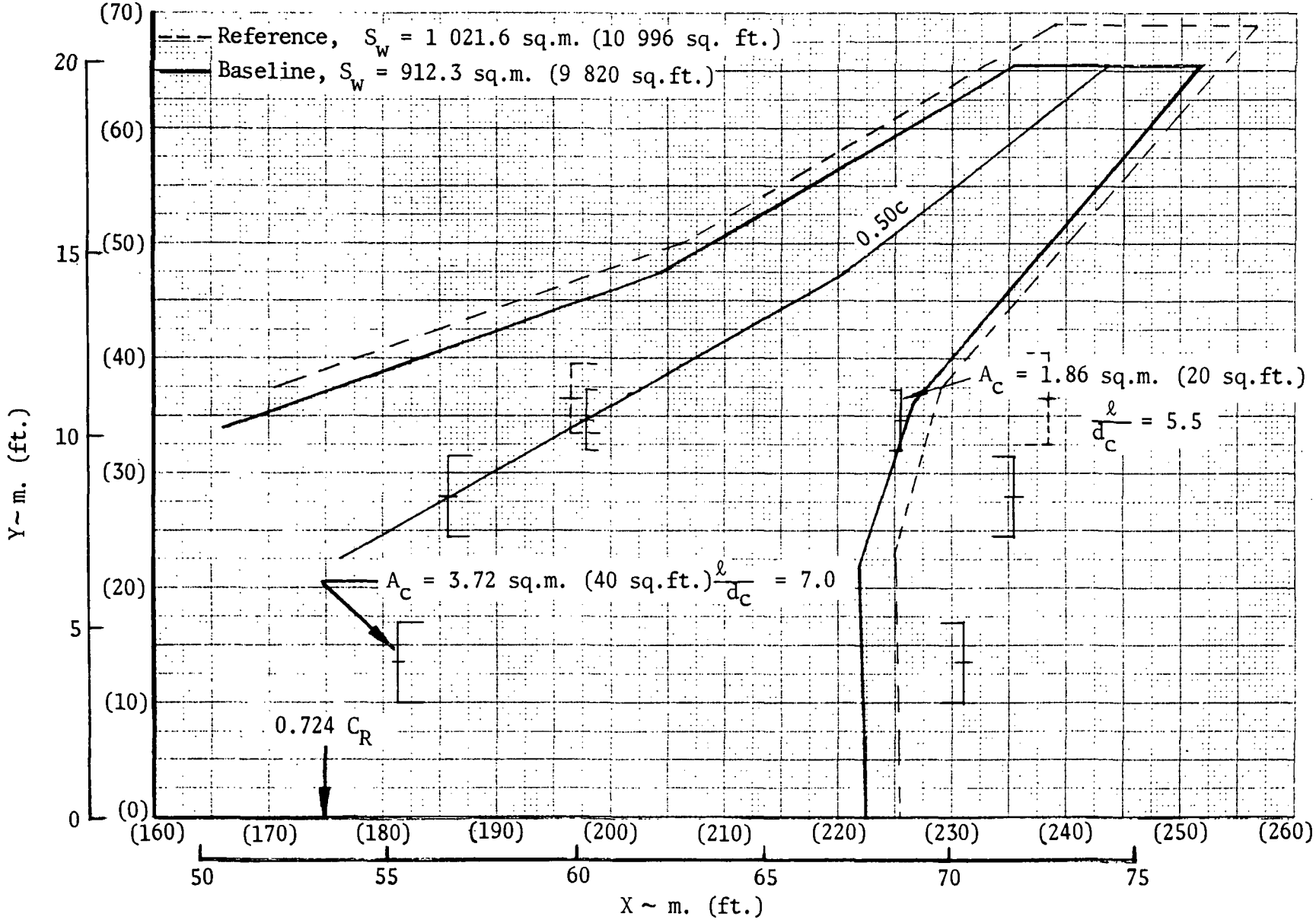

Figure 21.-Effect of nacelle size on nacelle location

until its trailing edge overhang does not exceed 3 meters (10 feet). The inboard nacelle is shifted laterally by the same amount holding the longitudinal distance between the inboard and outboard nacelle inlet planes the same as the reference configuration.

The nacelle parametric variables considered in the present analysis were the ratio of nozzle area to capture area A_n/A_c, the ratio of maximum cross-sectional area to capture area A_{MAX}/A_c, the relative axial position of maximum area X_{AMAX}/ℓ, the ratio of nacelle length to capture diameter, ℓ/d_c, and the nacelle absolute capture area A_c. A summary of the number of variations and variable range analyzed is presented on table XII. For purposes of computation, the nacelles were assumed to be axisymmetric and the inlet, maximum area, and nozzle planes to be connected by straight lines.

The parametric nacelle friction drag analysis is based on the use of fully turbulent flat plate levels in conjunction with the expression for surface areas (for four nacelles):

$$\frac{S_{WET}}{S_{ref}} = 2 \frac{A_c}{S_{ref}} \frac{\ell}{d_c} \left[\frac{X_{AMAX}}{\ell} + \sqrt{\frac{A_{MAX}}{A_c}} + \left(1 - \frac{X_{AMAX}}{\ell}\right) \sqrt{\frac{A_n}{A_c}} \right]$$

$$\approx 2 \frac{A_c}{S_{ref}} \frac{\ell}{d_c} \left[1 + \sqrt{\frac{A_{MAX}}{A_c}} \right]$$

The largest deviation between the exact and approximate expression occurs for X_{AMAX}/ℓ approaching 0.4 and A_n/A_c approaching 2.0 with the former resulting in 10 percent greater area. It will be subsequently found that these differences are negligible in terms of the total installation drag for such cases. A summary of the parametric nacelle friction analyses based on the approximate surface area is presented on table XIII; the table shows friction drag increments relative to nacelles off. As would be expected, progressive penalties are associated with the increasing nacelle diameter and length.

Nacelle normalized cross-sectional area parametric extremes of the present study are presented in figure 22. Maximum-to-capture area ratio of 1 to 2 at 40, 60, and 80 percent of the nacelle length are shown for nozzle-to-capture area ratios of 1 and 2. In order to establish a feel for the corresponding physical variations, the results of figure 22 have been applied to a representative nacelle size (A_c = 2.6 sq.m., 28 sq.ft., ℓ/d_c = 6). The results are presented on figure 23 for the same range of variables used for the normalized area distribution. Note that the vertical scale has been expanded by a factor of 2 for clarity in presentation.

An index of the parametric wave drag results is presented on table XIV. Each figure cited presents the wave drag increment relative to nacelles off as a function of the relative axial position of maximum thickness X_{AMAX}/ℓ

TABLE XII.-NACELLE PARAMETER VALUES

PARAMETER	VALUES
Mach number	1.2, 2.32
A_n/A_c	1.0, 1.25, 1.5, 2.0
A_{MAX}/A_c	1.0, 1.25, 1.5, 2.0
X_{AMAX}/ℓ	0.4, 0.6, 0.8, ≤ 1.0 *
A_c	1.86, 2.79, 3.72 sq.m. (20, 30, 40 sq.ft.)
ℓ/d_c	5.5 and 7.0

* Maximum value considered corresponds to a boattail angle of ten degrees.

TABLE XIII.-SUMMARY OF PARAMETRIC FRICTION DRAG RESULTS

A_c = sq.m. (sq. ft.)	$\frac{\ell}{d_c}$	$\frac{A_{MAX}}{A_c}$	ΔC_{D_F} Mo = 1.2	ΔC_{D_F} = 2.32
1.86 (20.0)	5.5	1.0	0.00033	0.00029
		1.25	0.00034	0.00031
		1.5	0.00036	0.00032
		2.0	0.00039	0.00035
	7.0	1.0	0.00040	0.00035
		1.25	0.00042	0.00037
		1.5	0.00044	0.00040
		2.0	0.00048	0.00043
2.79 (30.0)	5.5	1.0	0.00047	0.00042
		1.25	0.00050	0.00044
		1.5	0.00053	0.00047
		2.0	0.00057	0.00051
	7.0	1.0	0.00058	0.00051
		1.25	0.00061	0.00053
		1.5	0.00065	0.00056
		2.0	0.00070	0.00061
3.72 (40.0)	5.5	1.0	0.00062	0.00055
		1.25	0.00066	0.00058
		1.5	0.00069	0.00061
		2.0	0.00075	0.00066
	7.0	1.0	0.00076	0.00067
		1.25	0.00080	0.00071
		1.5	0.00085	0.00075
		2.0	0.00092	0.00081

NOTE: Altitude is 10 455 m. (34 300 ft.) for M_o = 1.2 case and is 18 288 m. (60 000 ft.) for M_o = 2.32 case.

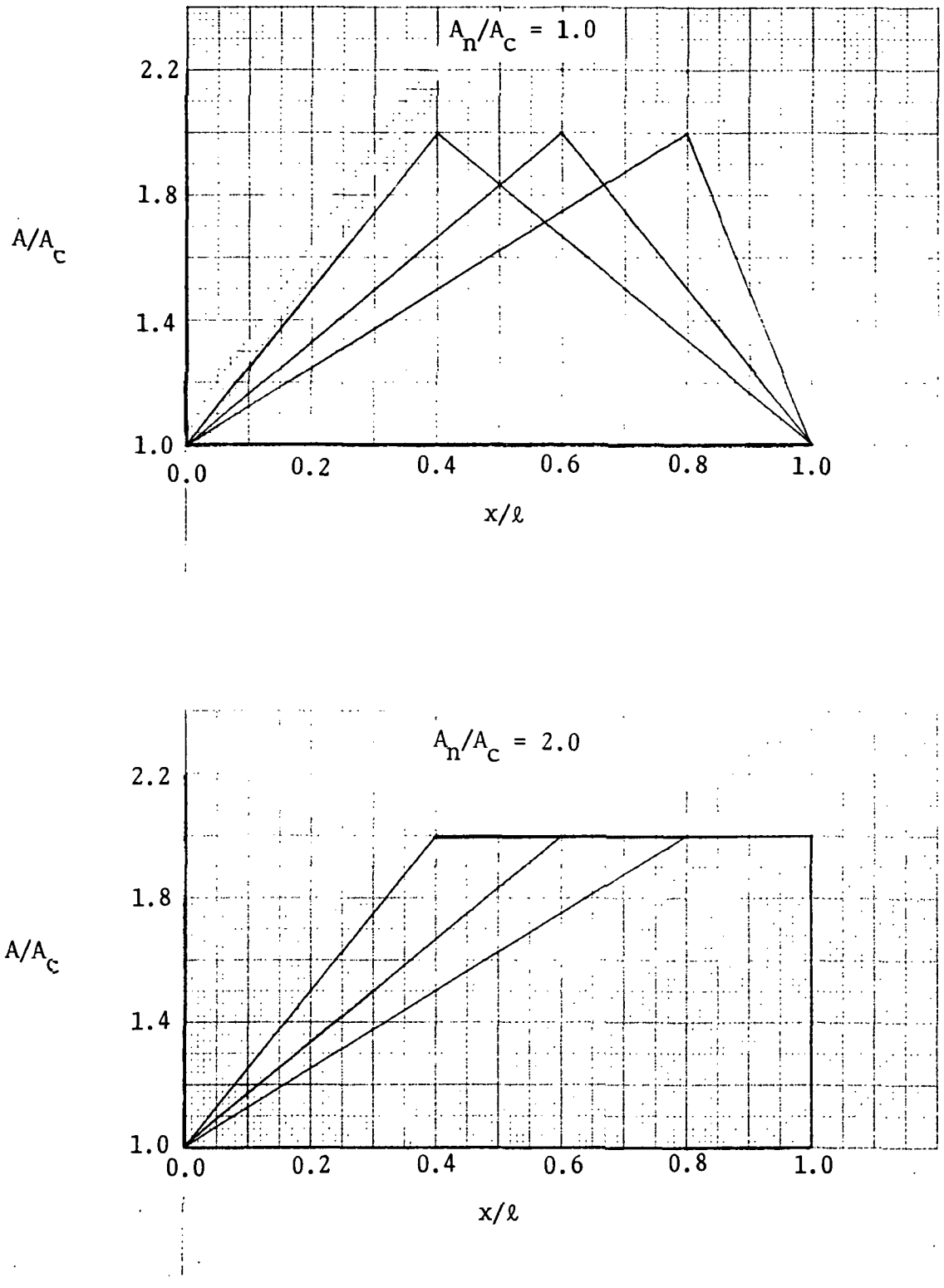

Figure 22.-Nacelle parametric cross-sectional area extremes

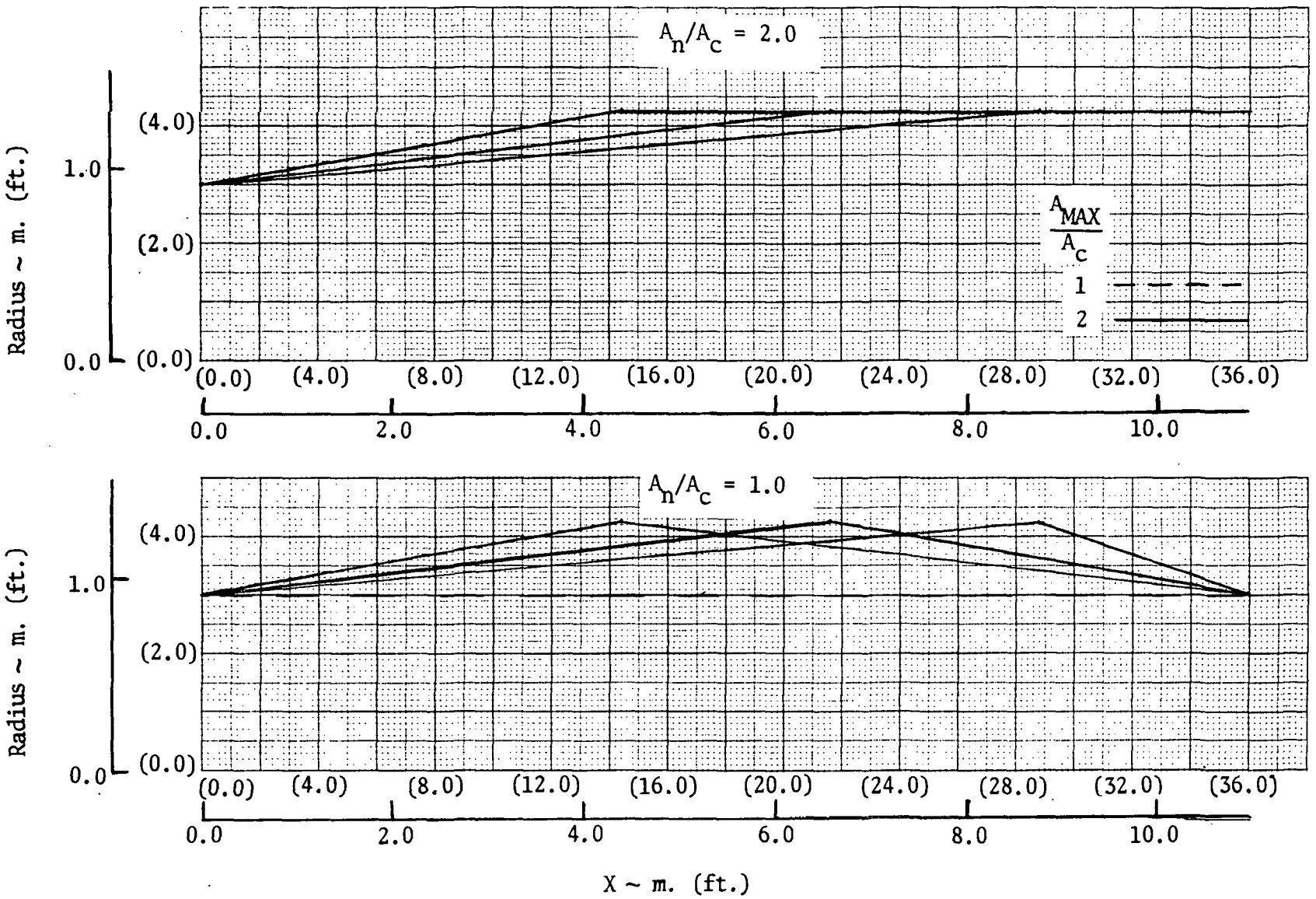

Figure 23. Nominal baseline nacelle shape perturbation extremes, $\ell/d_c = 6$

TABLE XIV.- SUMMARY OF PARAMETRIC WAVE DRAG RESULTS

A_c - sq. m. (sq. ft.)	$\frac{\ell}{d_c}$	$\frac{A_{MAX}}{A_c}$	Figure * Mo	1.2	2.32
1.86 (20.0)	5.5	1.25		24	30
		1.5		25	31
		2.0		26	32
	7.0	1.25		27	33
		1.5		28	34
		2.0		29	35
2.79 (30.0)	5.5	1.25		36	42
		1.5		37	43
		2.0		38	44
	7.0	1.25		39	45
		1.5		40	46
		2.0		41	47
3.72 (40.0)	5.5	1.25		48	54
		1.5		49	55
		2.0		50	56
	7.0	1.25		51	57
		1.5		52	58
		2.0		53	59

* Each figure cited implicitly contains the result for a cylindrical nacelle; this corresponds to the abscissa (i.e. $\Delta C_{D_W} = 0$).

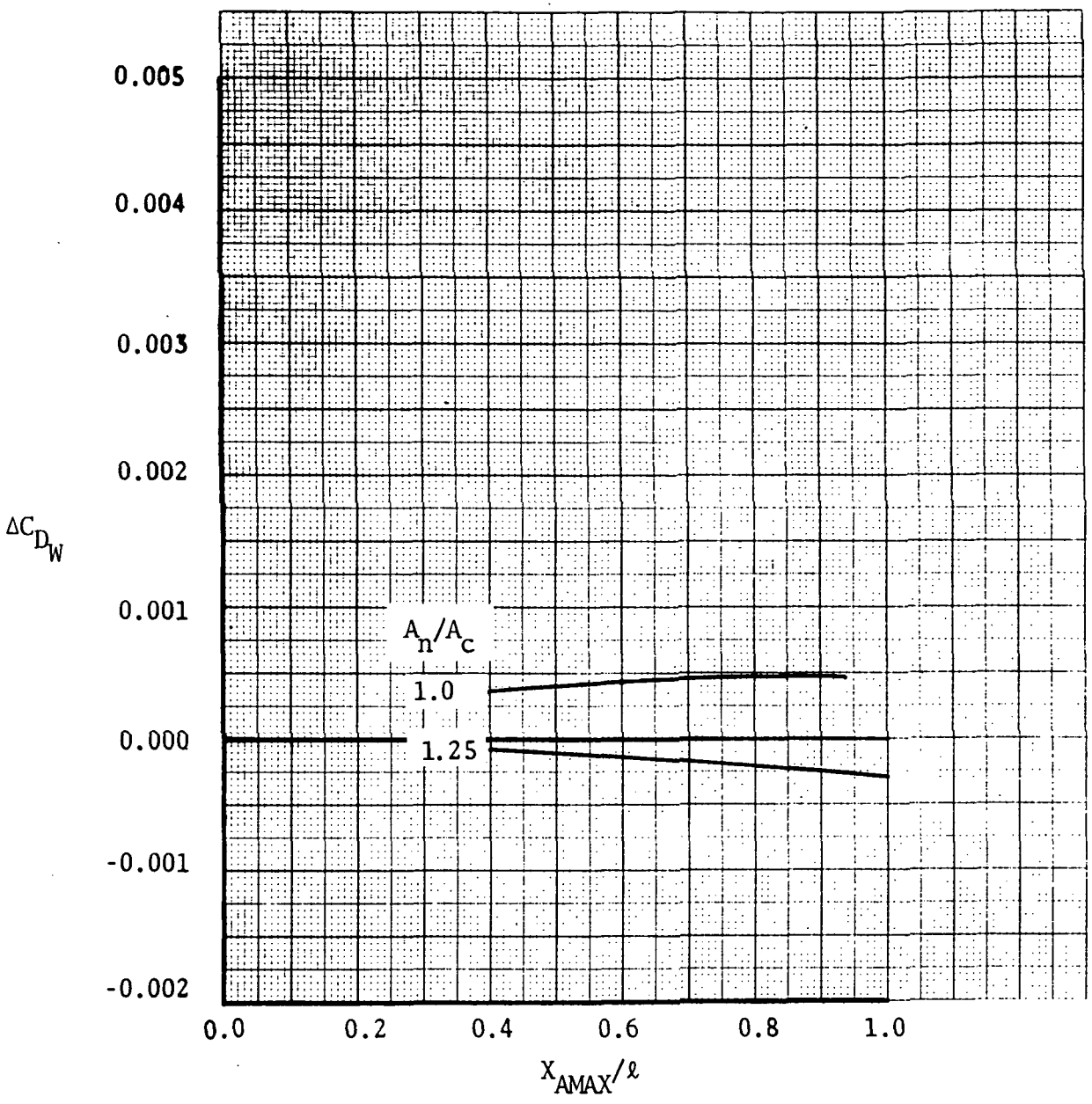

Figure 24.-Effect of geometry perturbations on nacelle incremental wave drag at $M_o = 1.2$

$A_c = 1.86$ sq. m. (20 sq. ft.) $\ell/d_c = 5.5$

$A_{MAX}/A_c = 1.25$

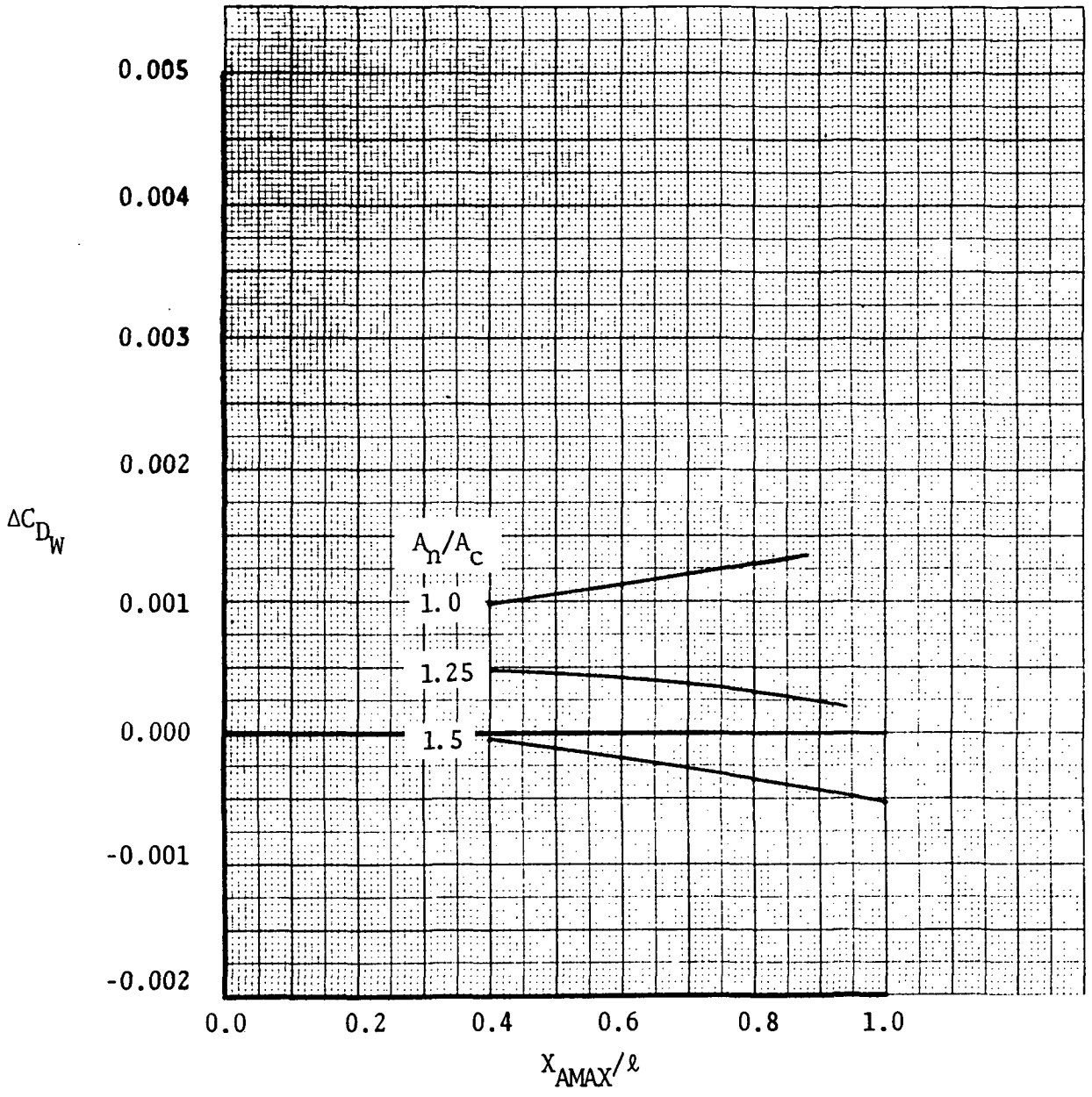

Figure 25.- Effect of geometry perturbations on nacelle incremental wave drag at $M_o = 1.2$

$A_c = 1.86$ sq. m. (20 sq. ft.) $\ell/d_c = 5.5$

$A_{MAX}/A_c = 1.5$

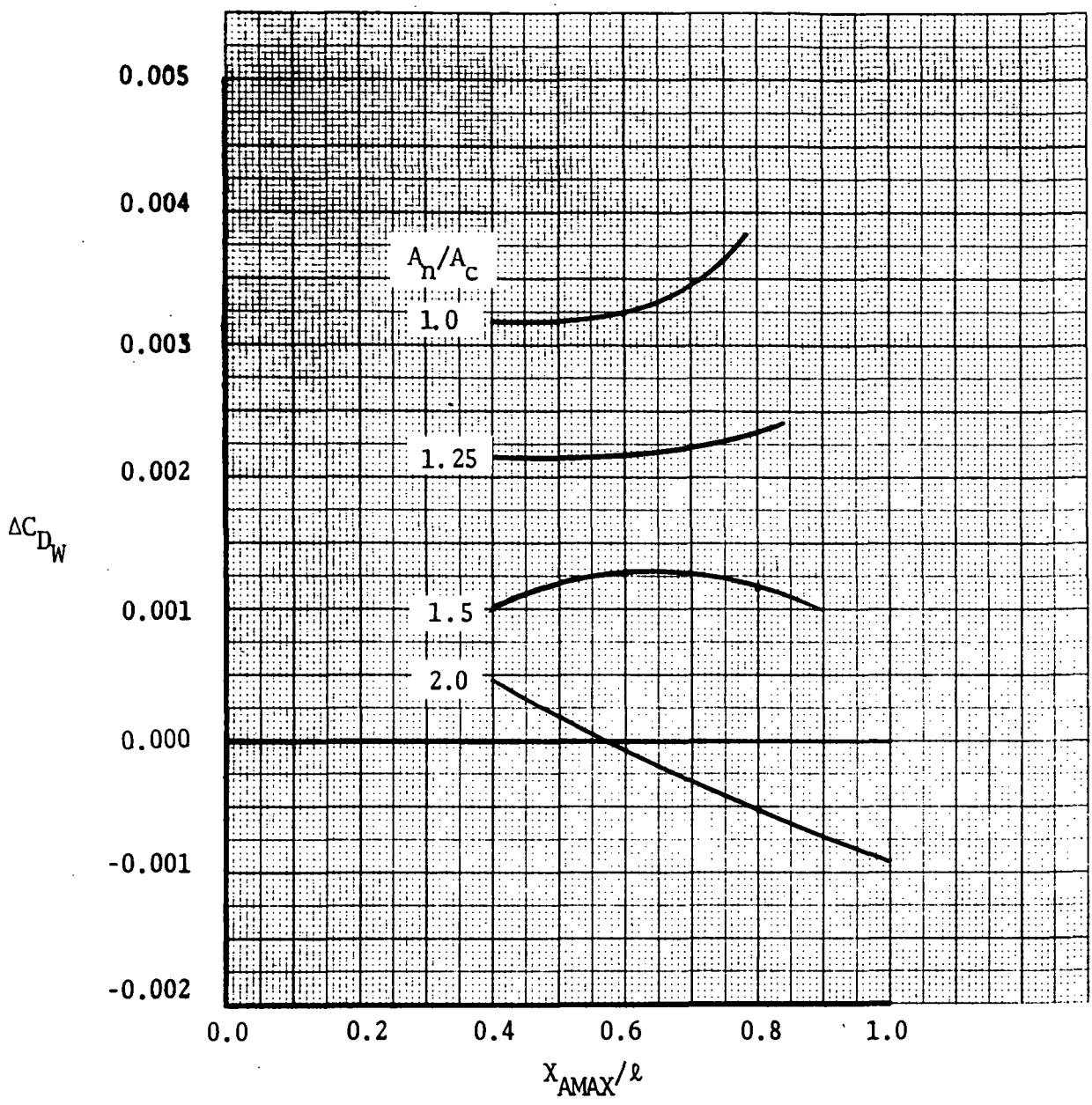

Figure 26.-Effect of geometry perturbations on nacelle incremental wave drag at $M_o = 1.2$

$A_c = 1.86$ sq. m. (20 sq. ft.) $\ell/d_c = 5.5$

$A_{MAX}/A_c = 2.0$

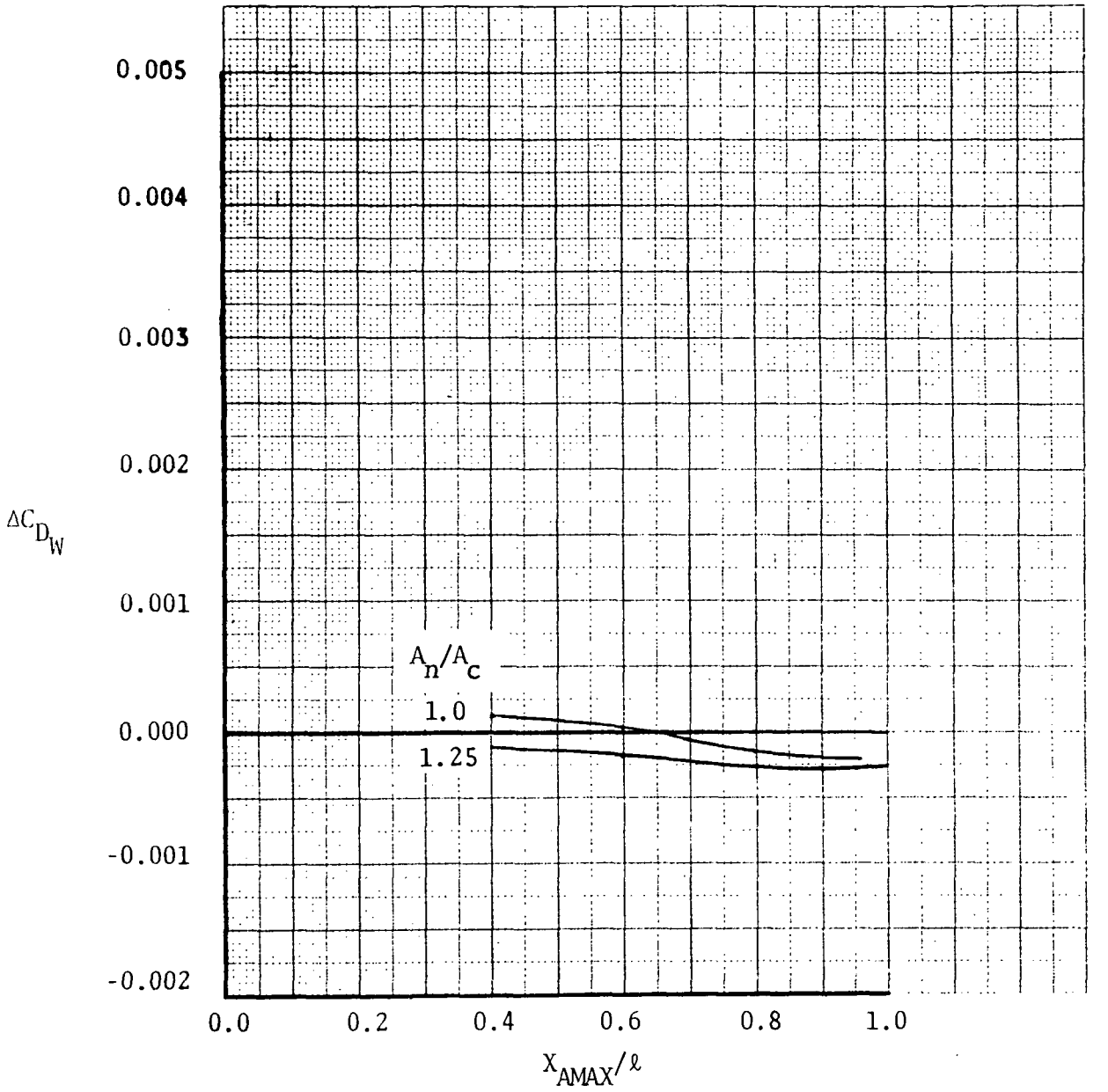

Figure 27.- Effect of geometry perturbations on nacelle incremental wave drag at $M_o = 1.2$

A_c = 1.86 sq. m. (20 sq. ft.) $\ell/d_c = 7.0$

$A_{MAX}/A_c = 1.25$

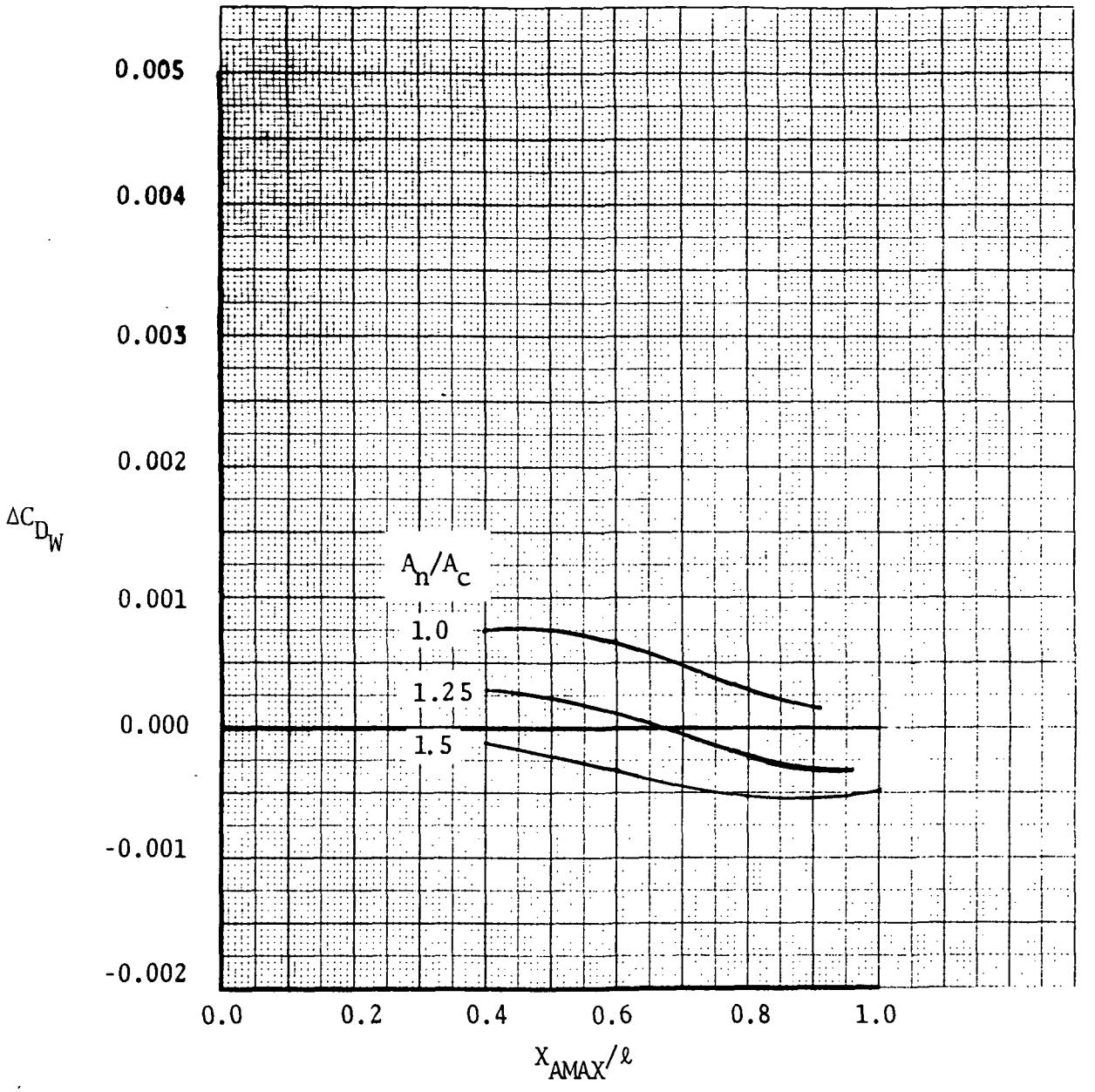

Figure 28.- Effect of geometry perturbations on nacelle incremental wave drag at $M_o = 1.2$

A_c = 1.86 sq. m. (20 sq. ft.) $\ell/d_c = 7.0$

$A_{MAX}/A_c = 1.5$

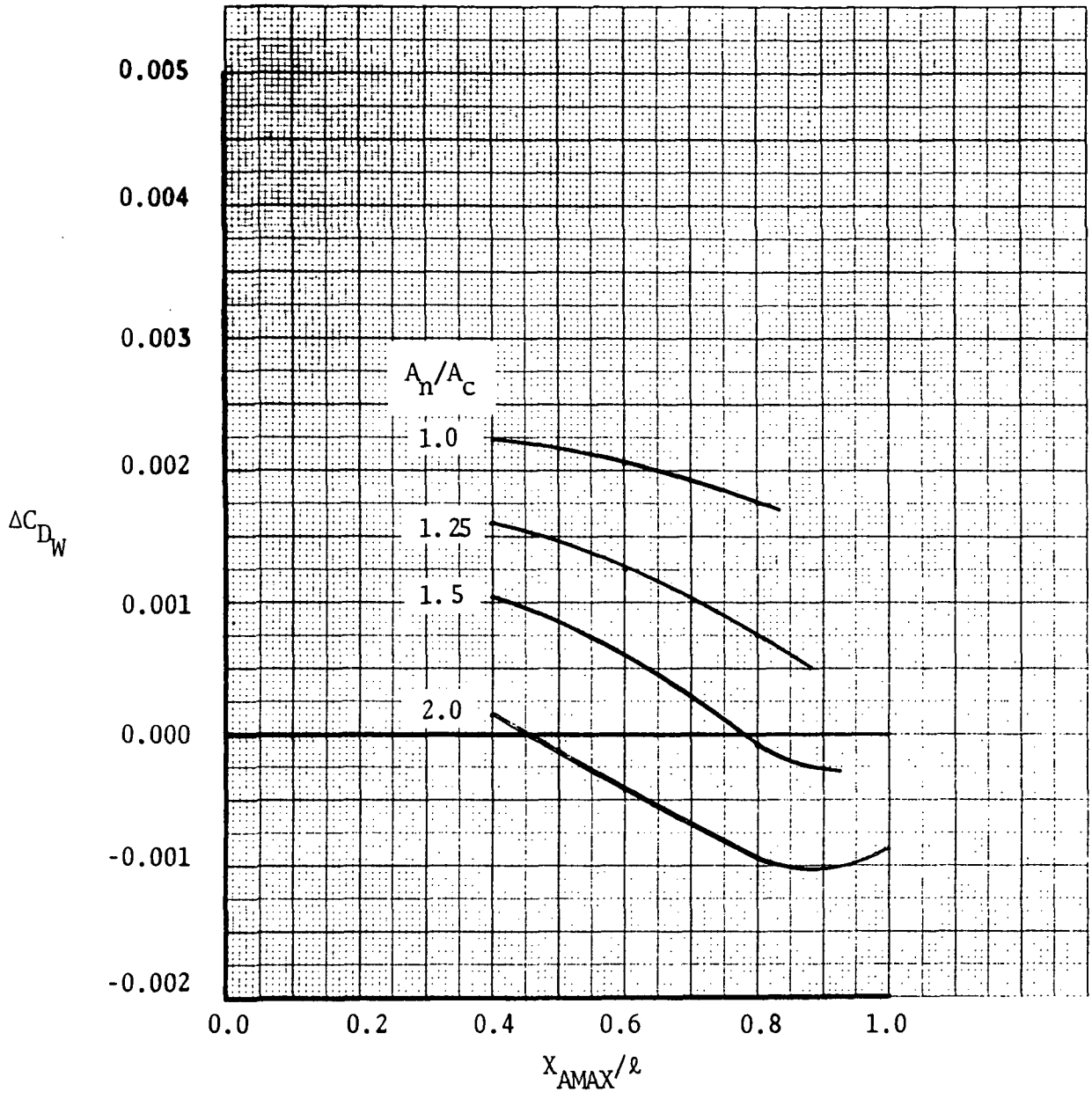

Figure 29.- Effect of geometry perturbations on nacelle incremental wave drag at $M_o = 1.2$

$A_c = 1.86$ sq. m. (20 sq. ft.) $\ell/d_c = 7.0$

$A_{MAX}/A_c = 2.0$

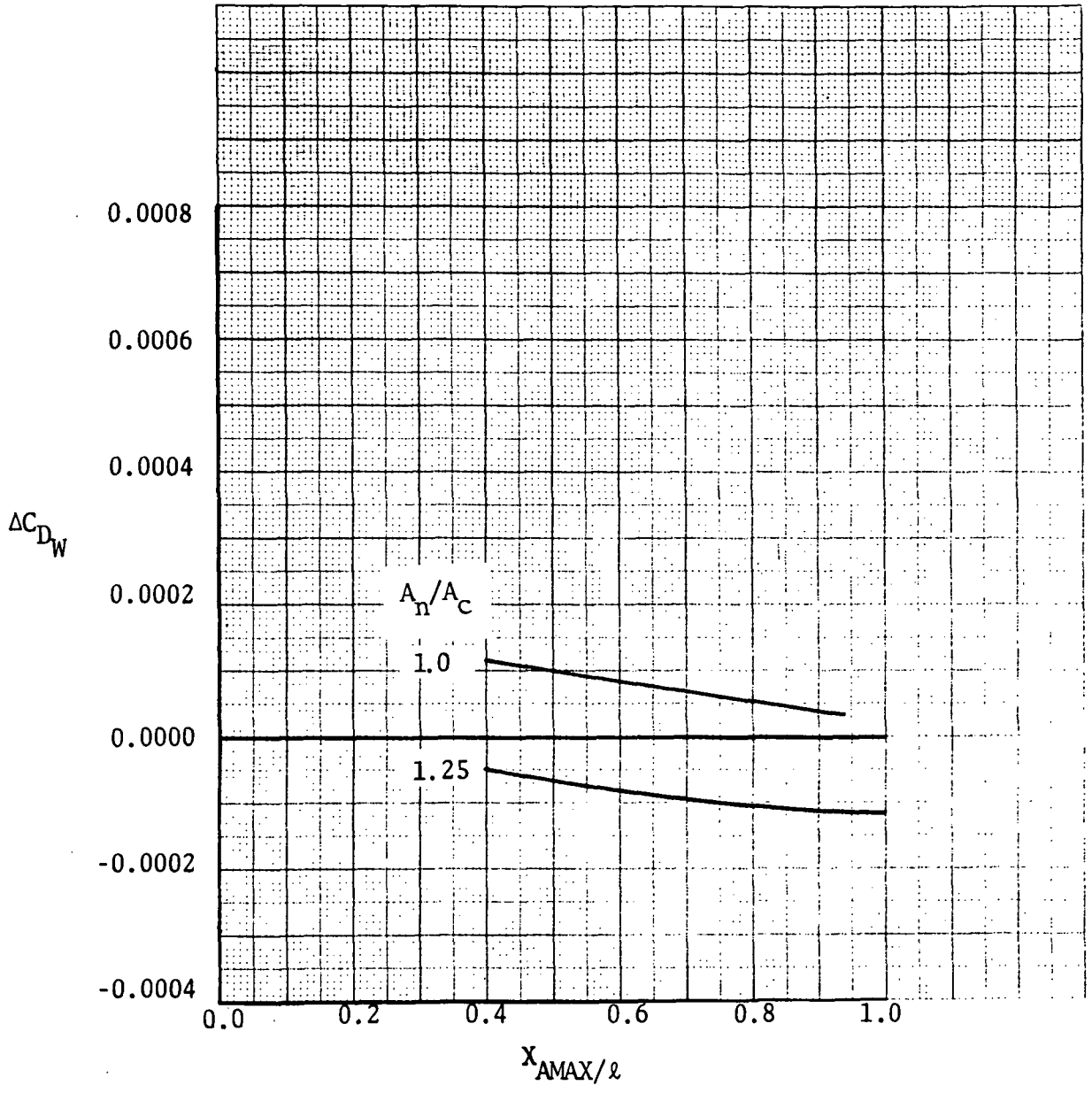

Figure 30.- Effect of geometry perturbations on nacelle incremental wave drag at $M_o = 2.32$

A_c = 1.86 sq. m. (20 sq. ft.) $\ell/d_c = 5.5$

$A_{MAX}/A_c = 1.25$

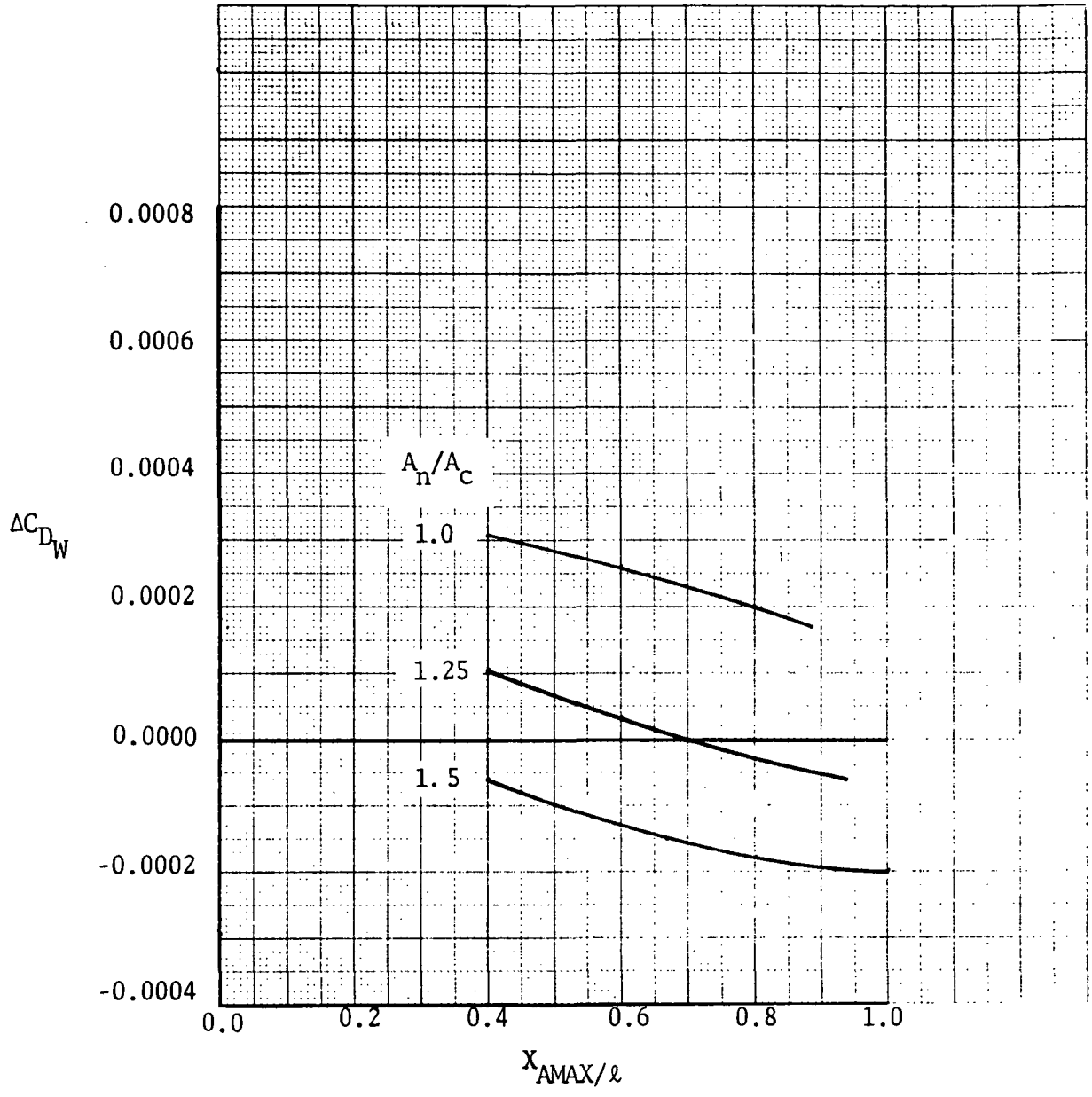

Figure 31.- Effect of geometry perturbations on nacelle incremental wave drag at $M_o = 2.32$

$A_c = 1.86$ sq. m. (20 sq. ft.) $\ell/d_c = 5.5$

$A_{MAX}/A_c = 1.5$

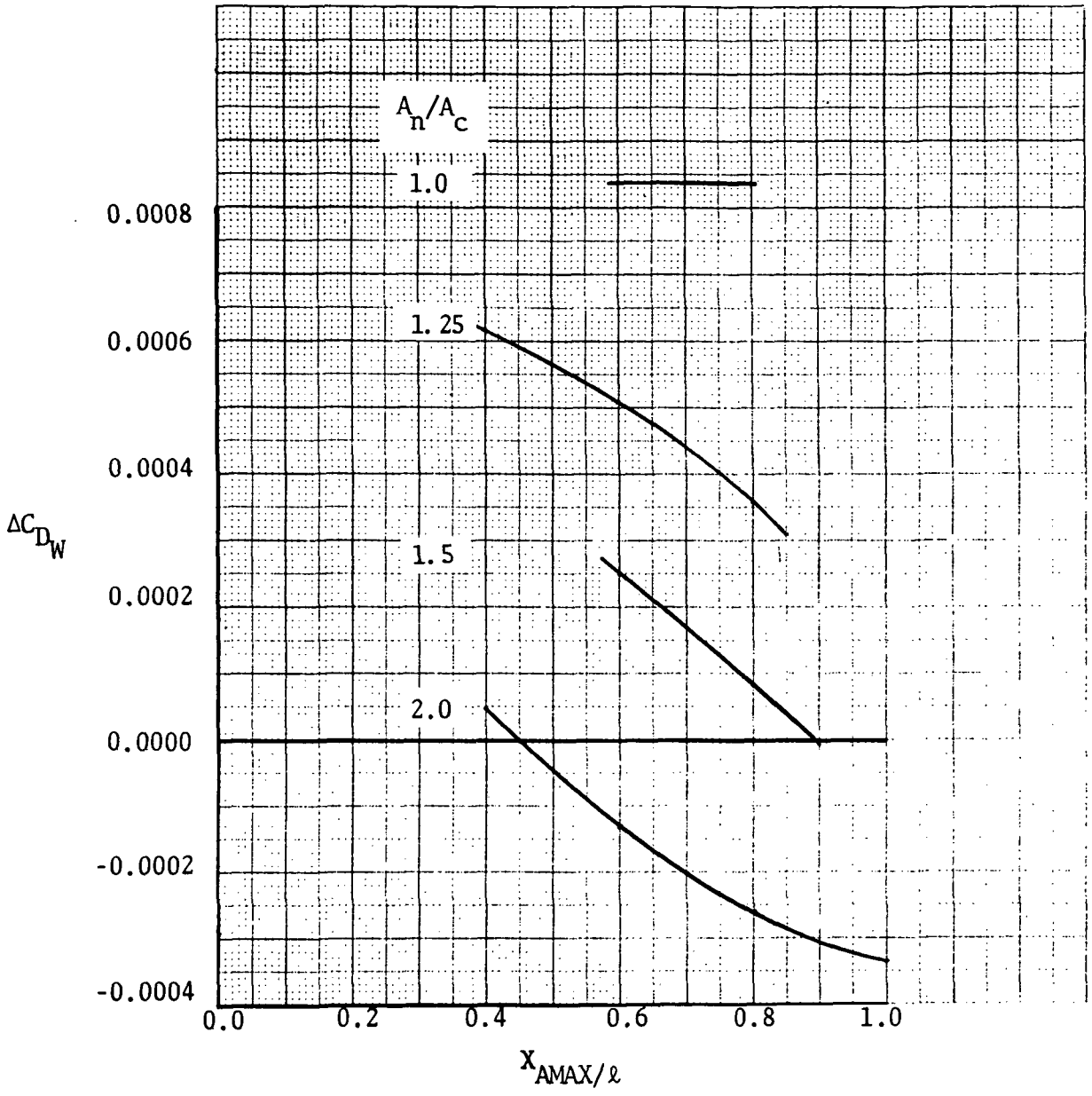

Figure 32.- Effect of geometry perturbations on nacelle incremental wave drag at $M_o = 2.32$

$A_c = 1.86$ sq. m. (20 sq. ft.) $\ell/d_c = 5.5$

$A_{MAX}/A_c = 2.0$

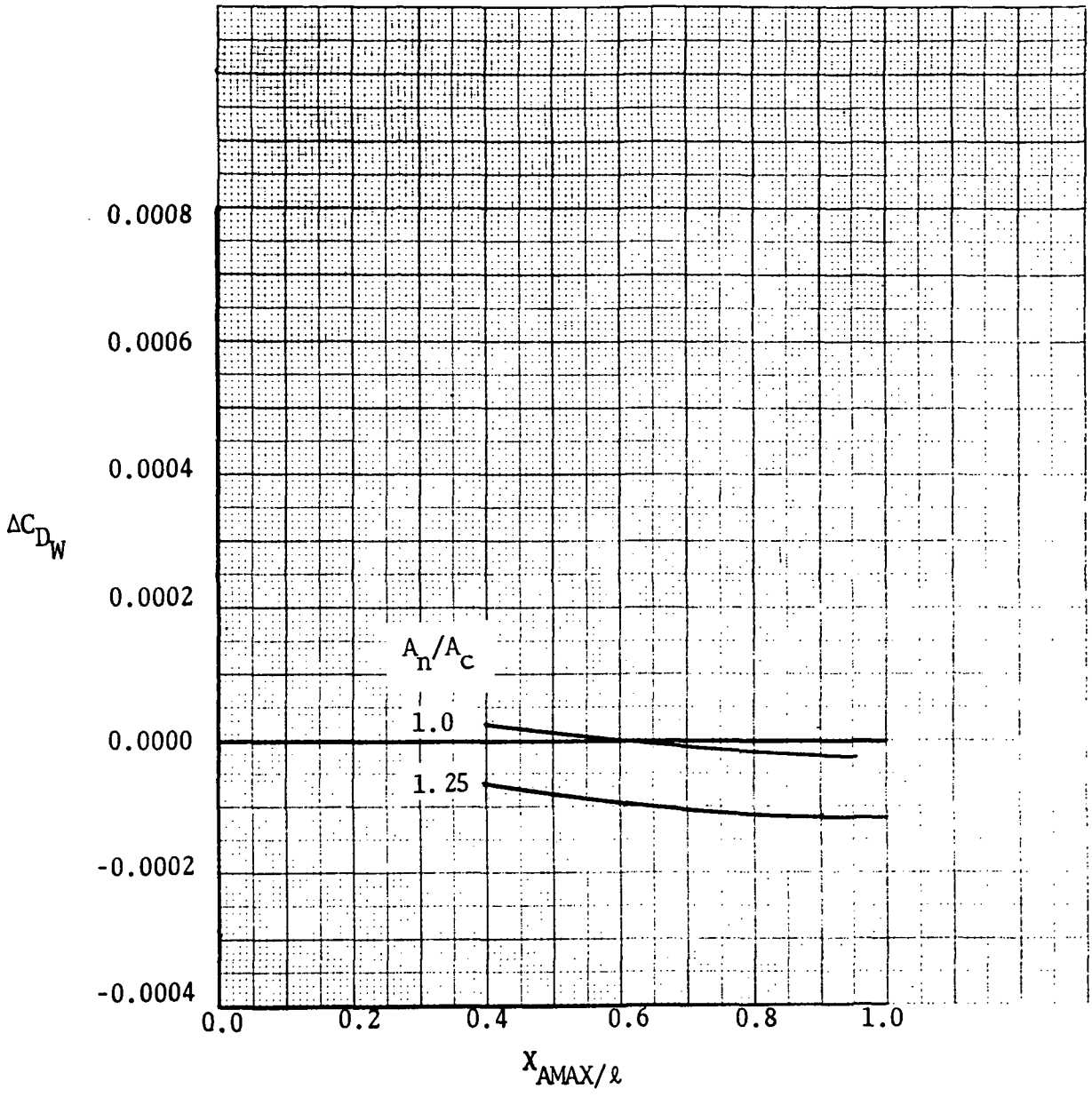

Figure 33.- Effect of geometry perturbations on nacelle incremental wave drag at $M_o = 2.32$

A_c = 1.86 sq. m. (20 sq. ft.) $\ell/d_c = 7.0$

$A_{MAX}/A_c = 1.25$

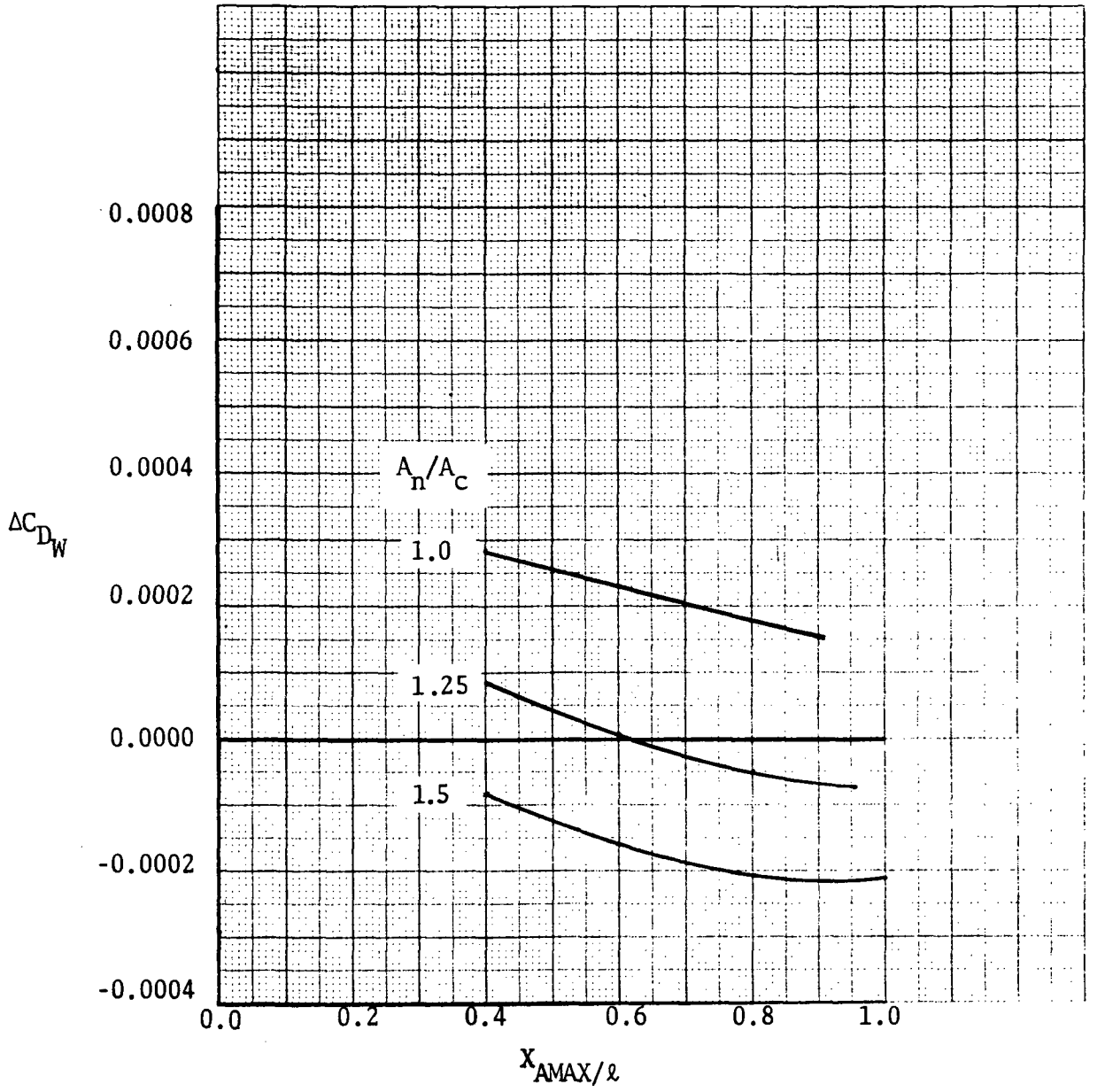

Figure 34.- Effect of geometry perturbations on nacelle incremental wave drag at $M_o = 2.32$

$A_c = 1.86$ sq. m. (20 sq. ft.) $\ell/d_c = 7.0$

$A_{MAX}/A_c = 1.5$

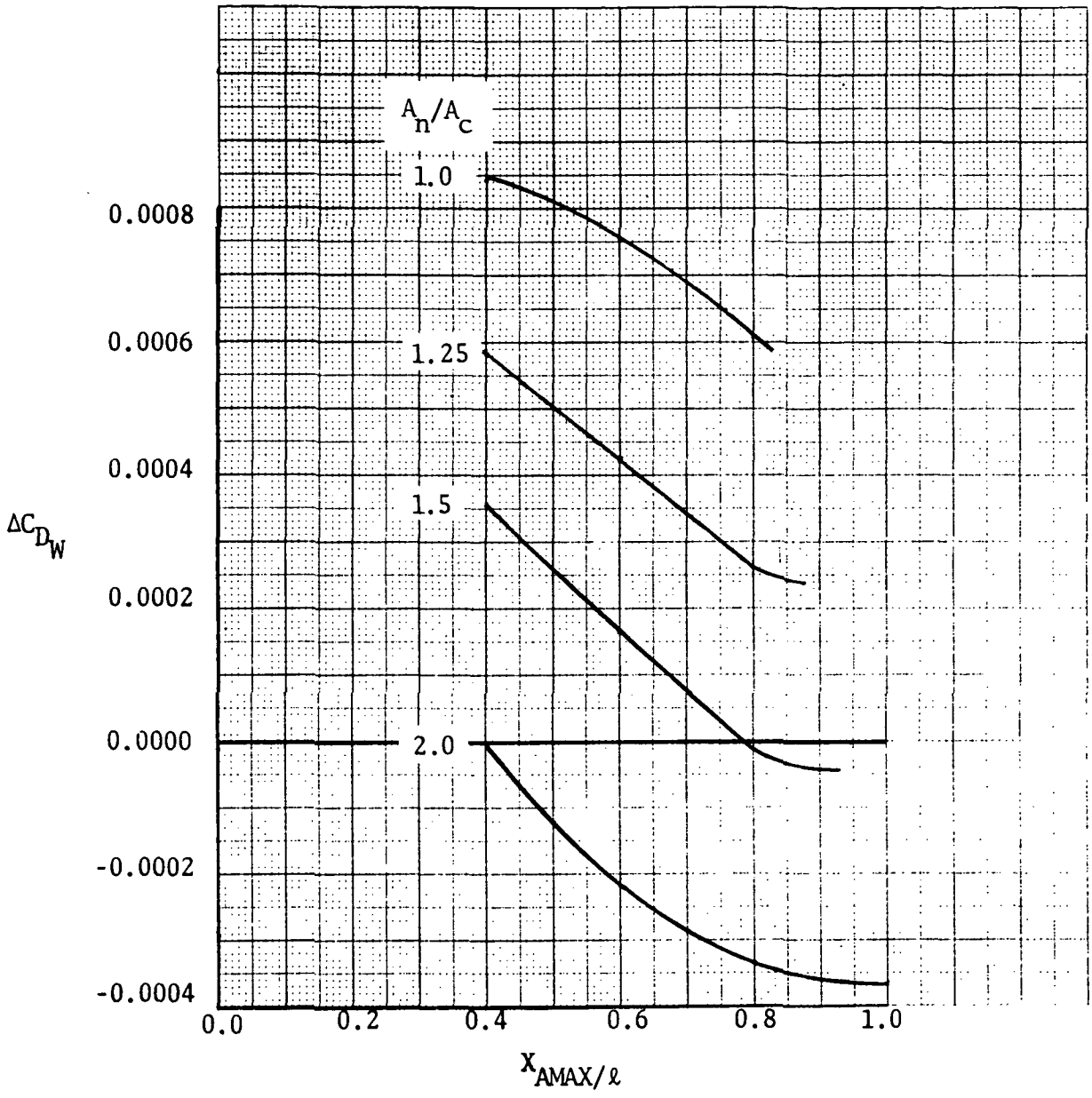

Figure 35.- Effect of geometry perturbations on nacelle incremental wave drag at $M_o = 2.32$

A_c = 1.86 sq. m. (20 sq. ft.) ℓ/d_c = 7.0

A_{MAX}/A_c = 2.0

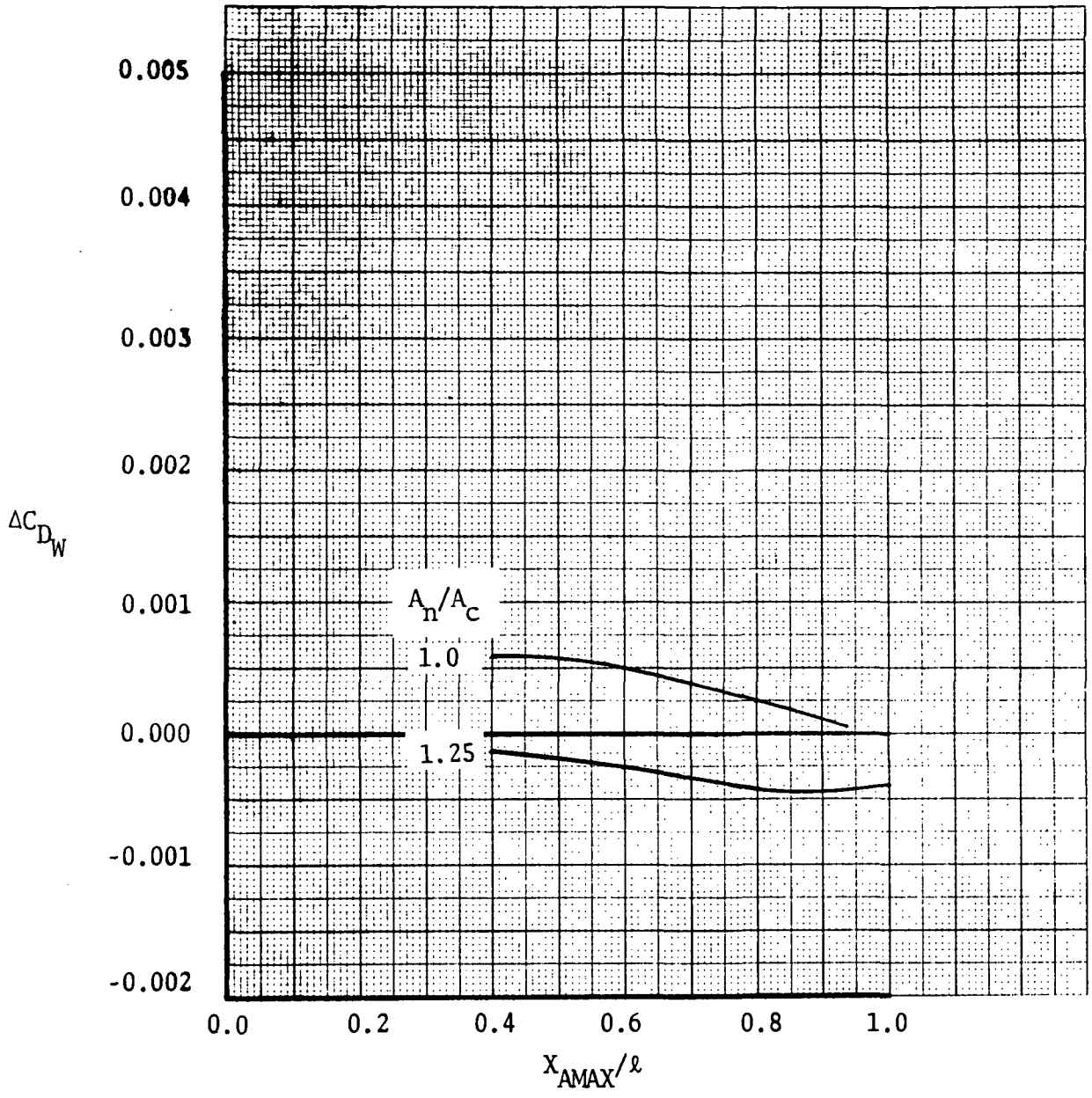

Figure 36.-Effect of geometry perturbations on nacelle incremental wave drag at $M_o = 1.2$

A_c = 2.79 sq. m. (30 sq. ft.) $\ell/d_c = 5.5$

$A_{MAX}/A_c = 1.25$

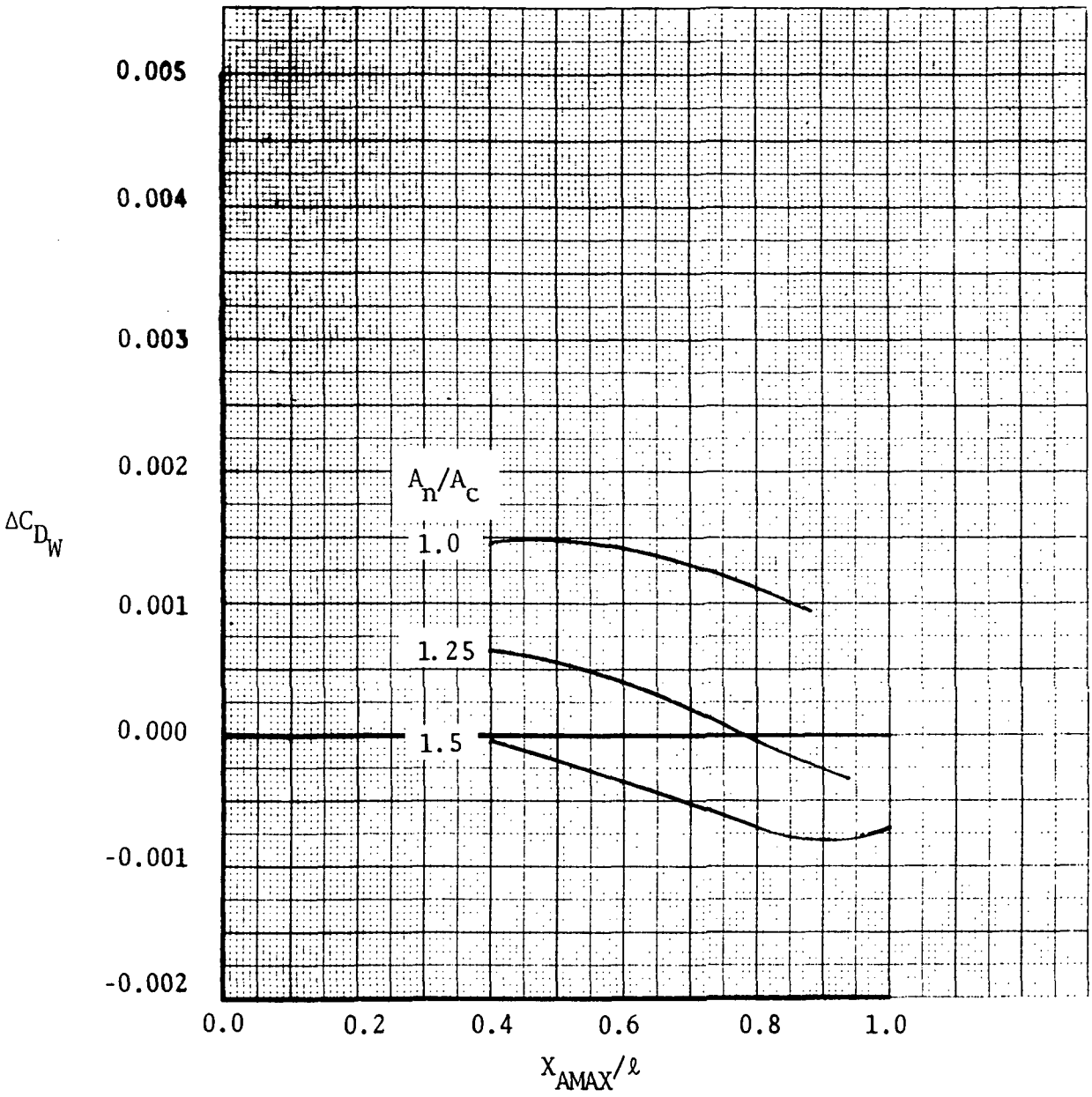

Figure 37.-Effect of geometry perturbations on nacelle incremental wave drag at $M_o = 1.2$

$A_c = 2.79$ sq. m. (30 sq. ft.) $\ell/d_c = 5.5$

$A_{MAX}/A_c = 1.5$

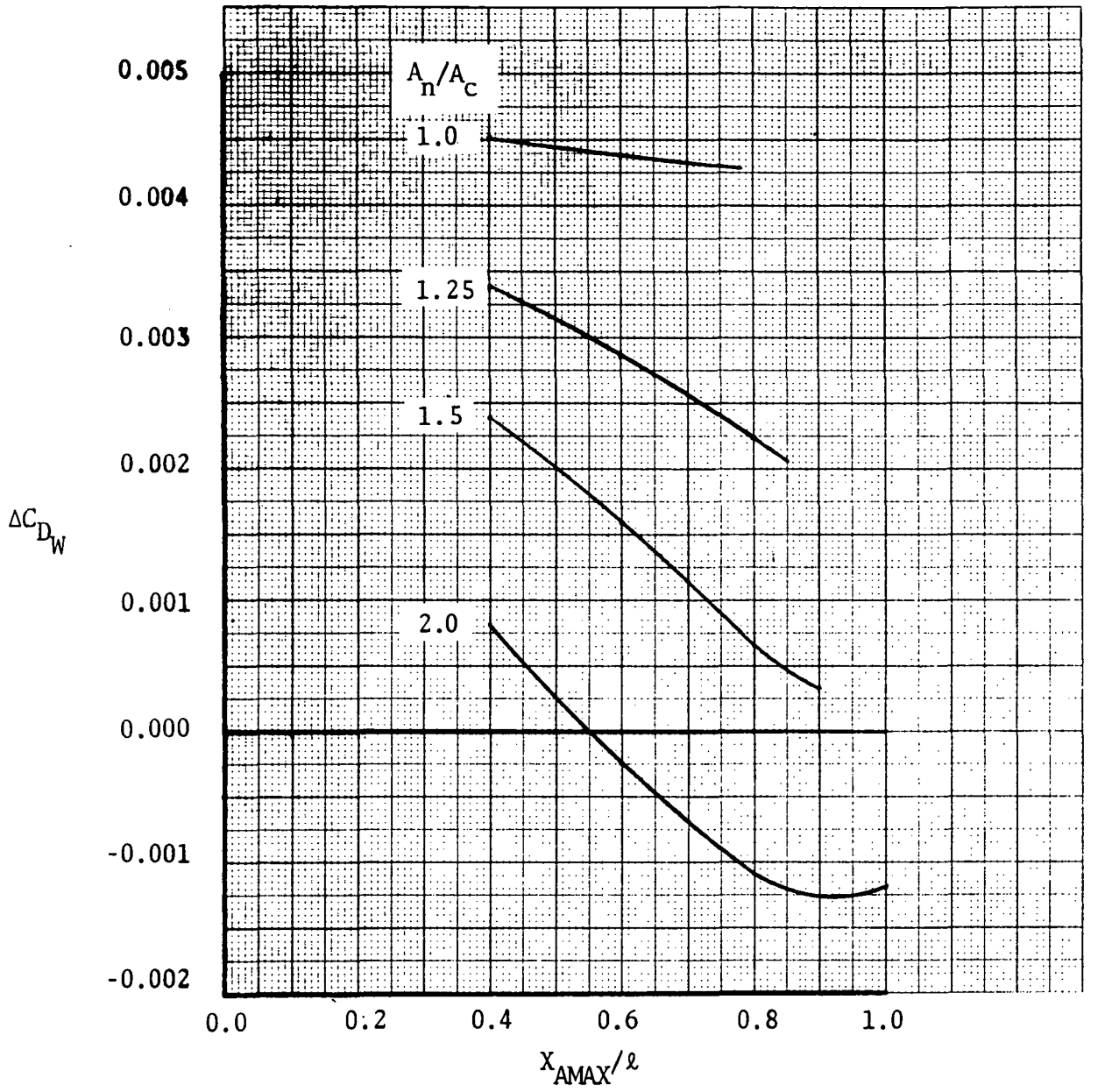

Figure 38.-Effect of geometry perturbations on nacelle incremental wave drag at $M_o = 1.2$

$A_c = 2.79$ sq. m. (30 sq. ft.) $\ell/d_c = 5.5$

$A_{MAX}/A_c = 2.0$

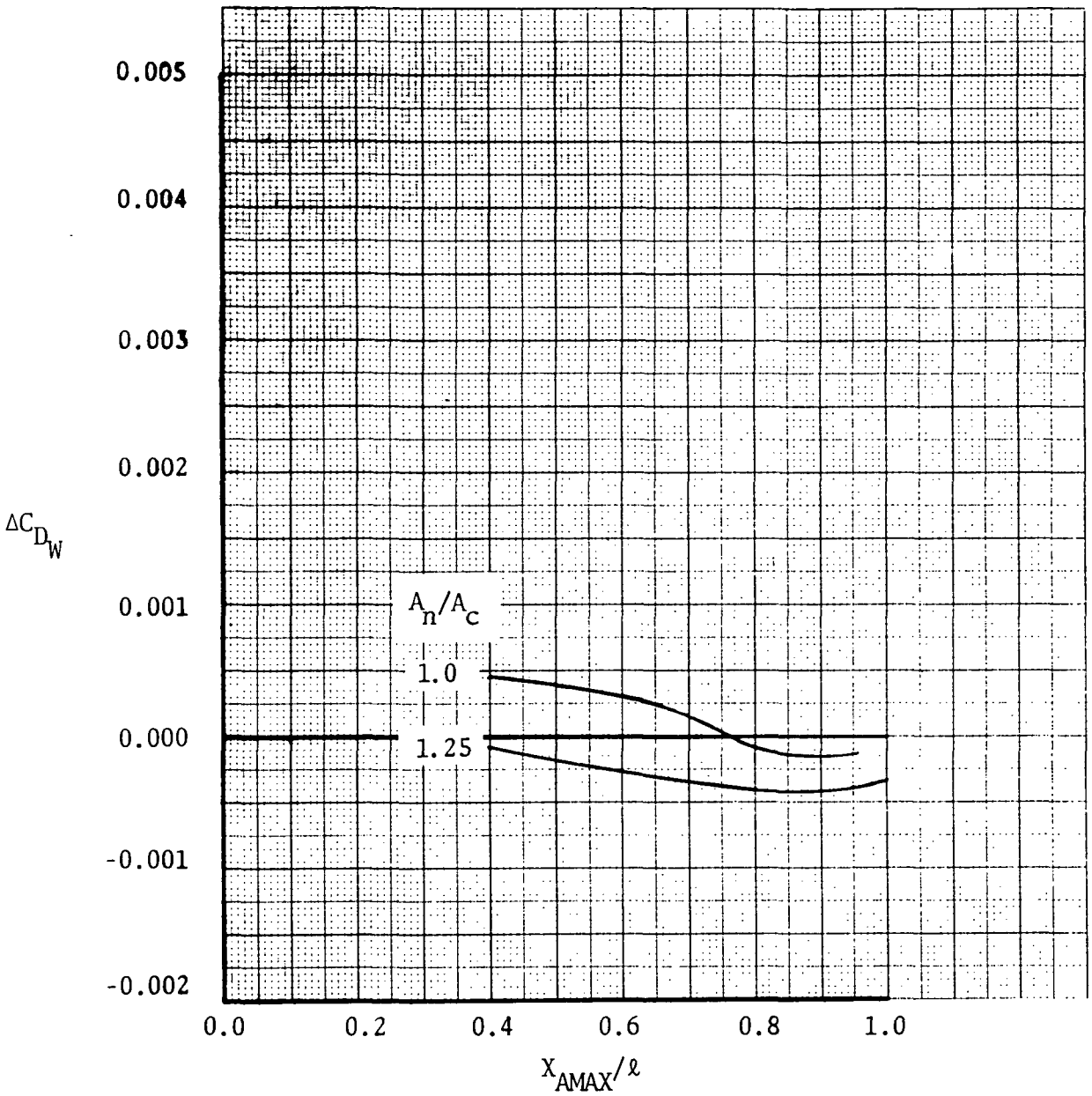

Figure 39.-Effect of geometry perturbations on nacelle incremental wave drag at $M_o = 1.2$

A_c = 2.79 sq. m. (30 sq. ft.) $\ell/d_c = 7.0$

$A_{MAX}/A_c = 1.25$

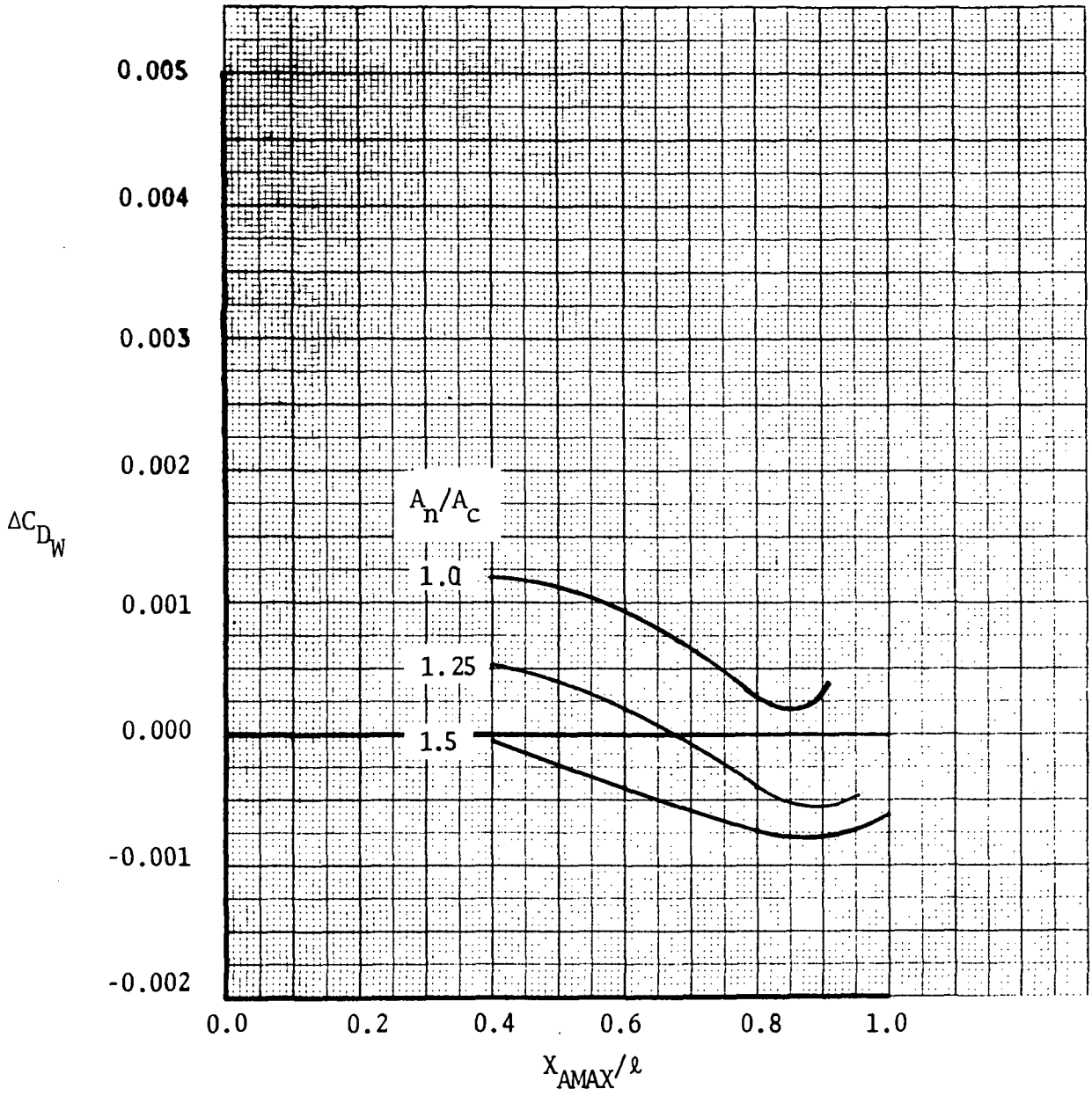

Figure 40.-Effect of geometry perturbations on nacelle incremental wave drag at $M_o = 1.2$

A_c = 2.79 sq. m. (30 sq. ft.) $\ell/d_c = 7.0$

$A_{MAX}/A_c = 1.5$

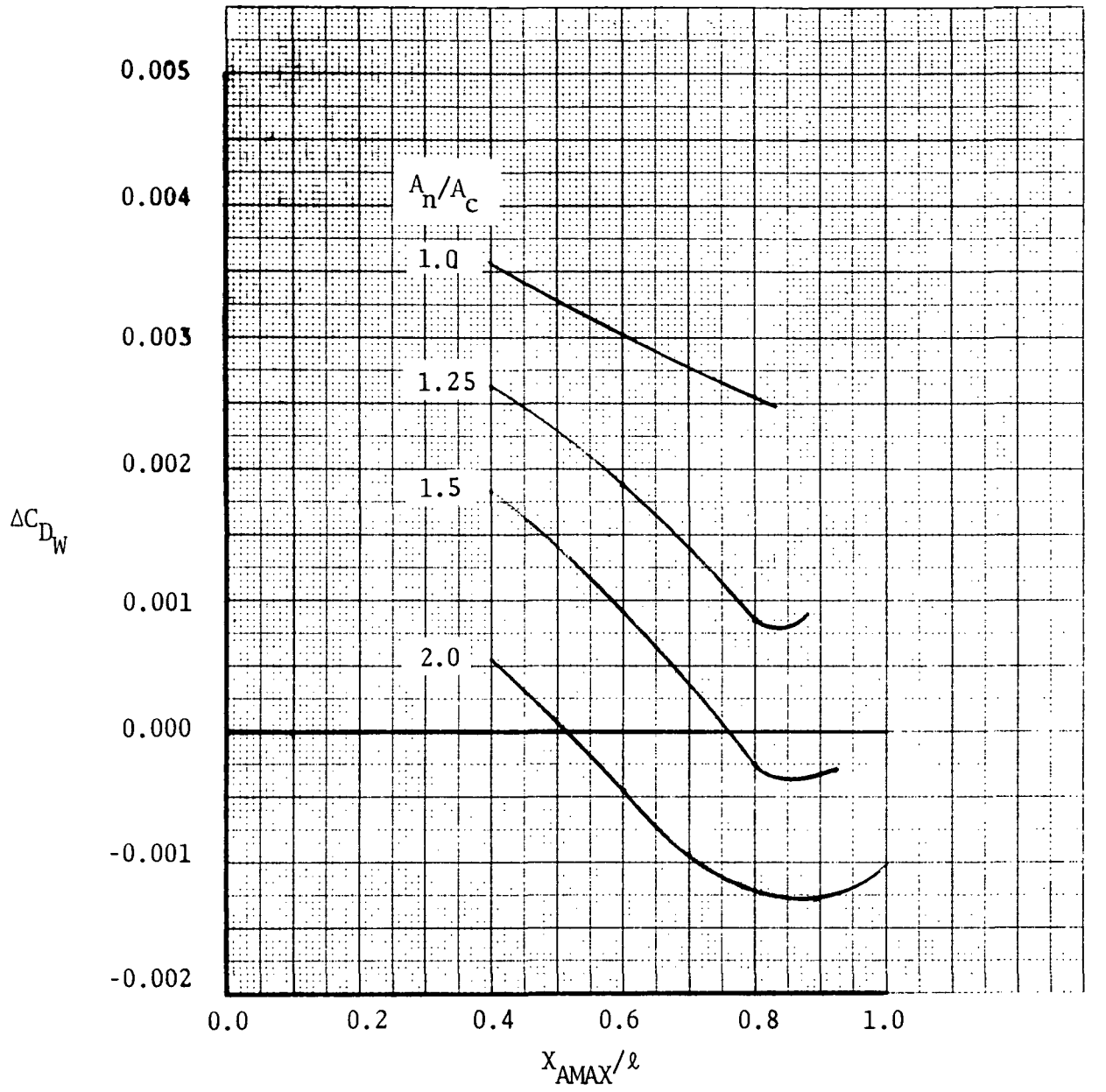

Figure 41.-Effect of geometry perturbations on nacelle incremental wave drag at $M_o = 1.2$

A_c = 2.79 sq. m. (30 sq. ft.) $\ell/d_c = 7.0$

$A_{MAX}/A_c = 2.0$

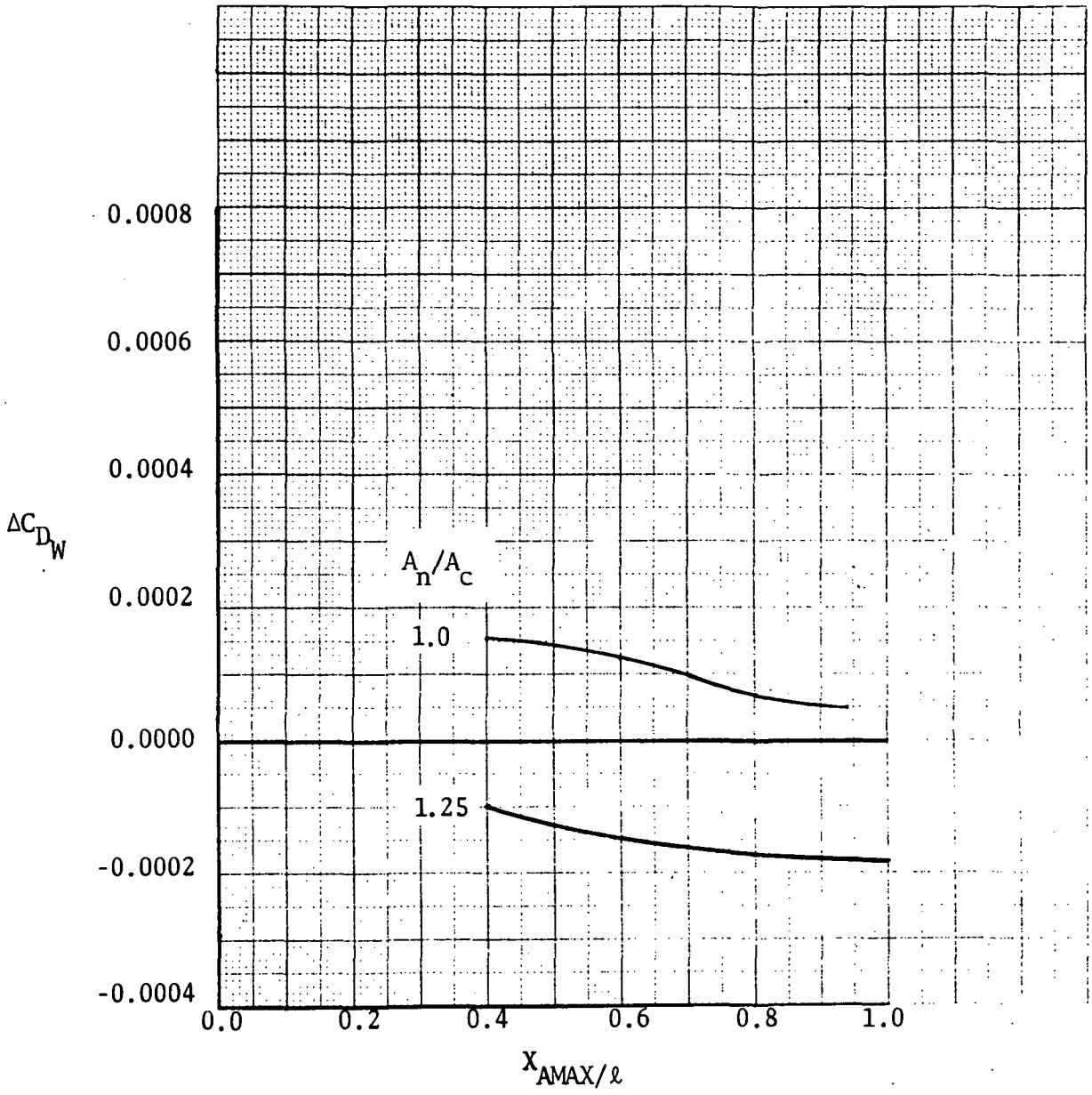

Figure 42.- Effect of geometry perturbations on nacelle incremental wave drag at $M_o = 2.32$

$A_c = 2.79$ sq. m. (30 sq. ft.) $\ell/d_c = 5.5$

$A_{MAX}/A_c = 1.25$

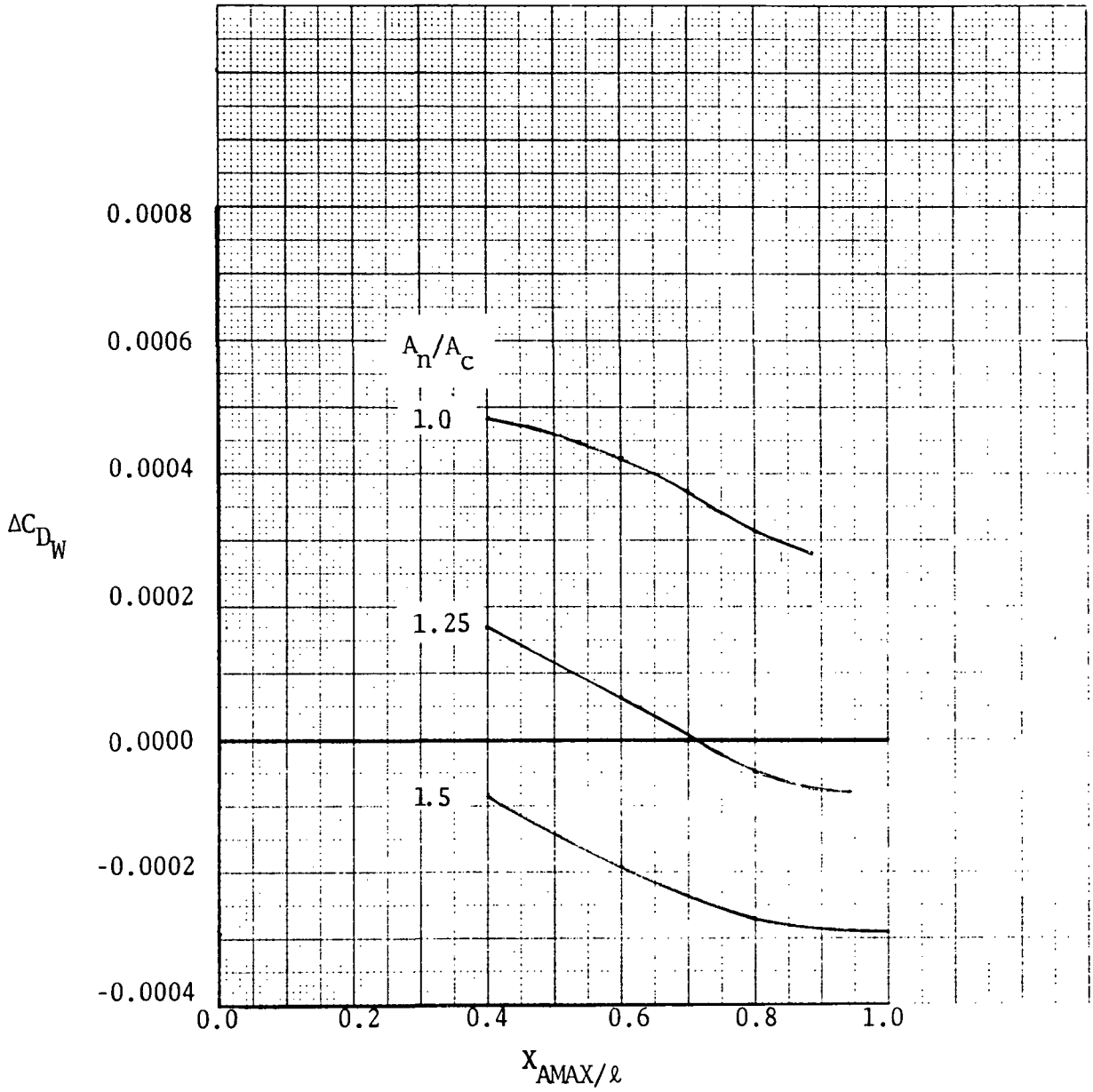

Figure 43. - Effect of geometry perturbations on nacelle incremental wave drag at $M_o = 2.32$

$A_c = 2.79$ sq. m. (30 sq. ft.) $\ell/d_c = 5.5$

$A_{MAX}/A_c = 1.5$

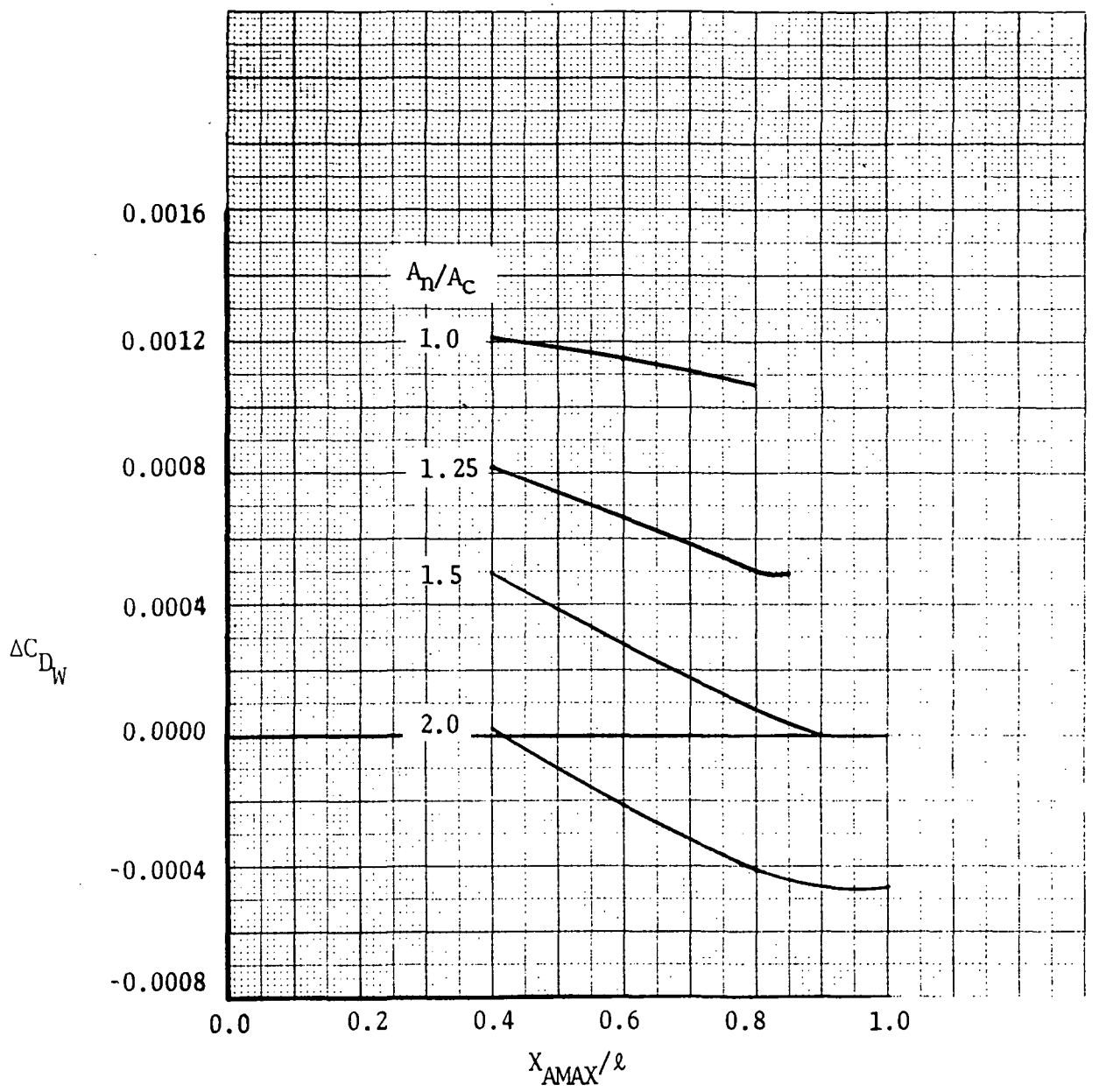

Figure 44.- Effect of geometry perturbations on nacelle incremental wave drag at $M_o = 2.32$

$A_c = 2.79$ sq. m. (30 sq. ft.) $\ell/d_c = 5.5$

$A_{MAX}/A_c = 2.0$

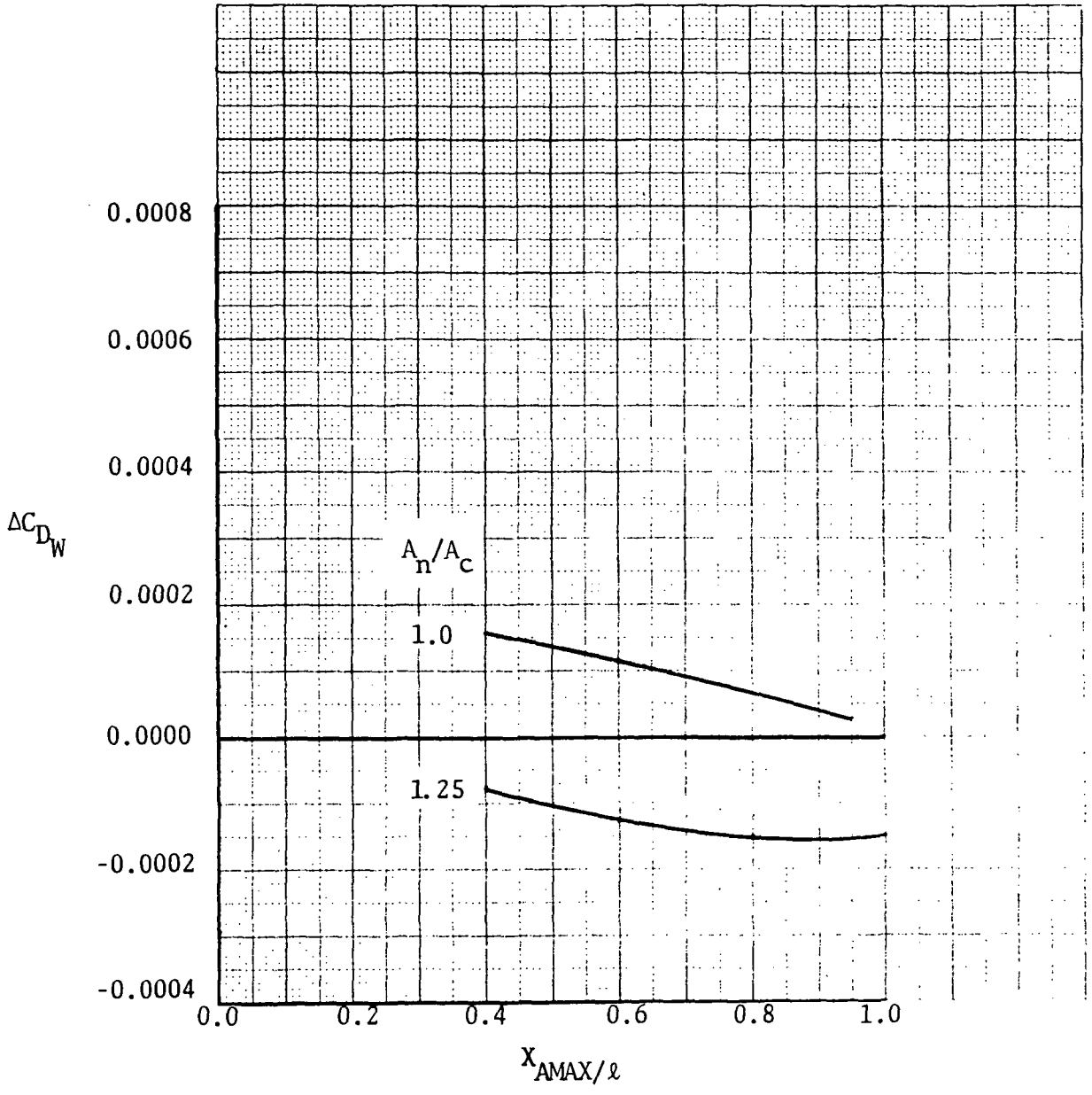

Figure 45.- Effect of geometry perturbations on nacelle incremental wave drag at $M_o = 2.32$

A_c = 2.79 sq. m. (30 sq. ft.) $\ell/d_c = 7.0$

$A_{MAX}/A_c = 1.25$

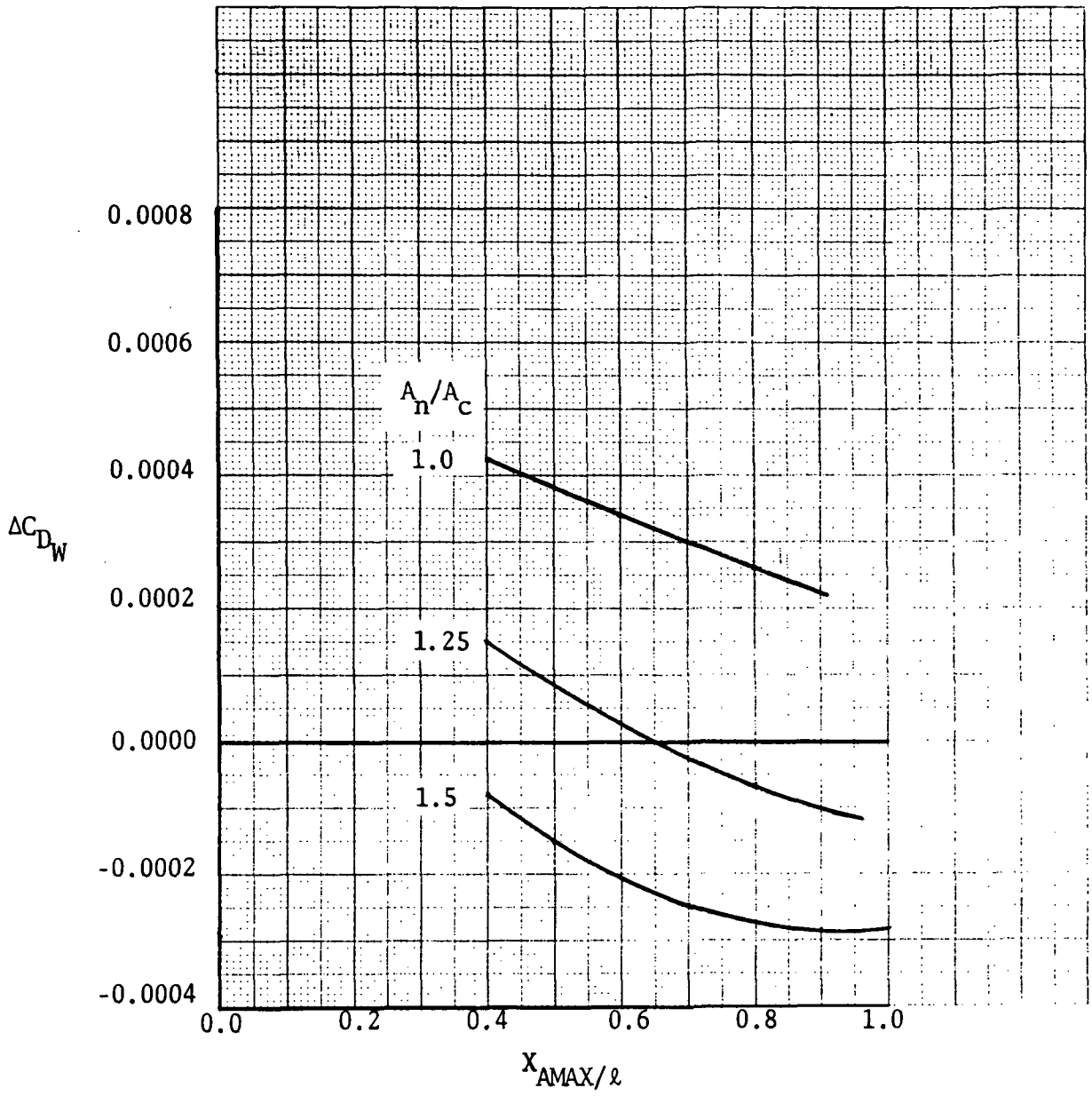

Figure 46.- Effect of geometry perturbations on nacelle incremental wave drag at $M_o = 2.32$

A_c = 2.79 sq. m. (30 sq. ft.) $\ell/d_c = 7.0$

$A_{MAX}/A_c = 1.5$

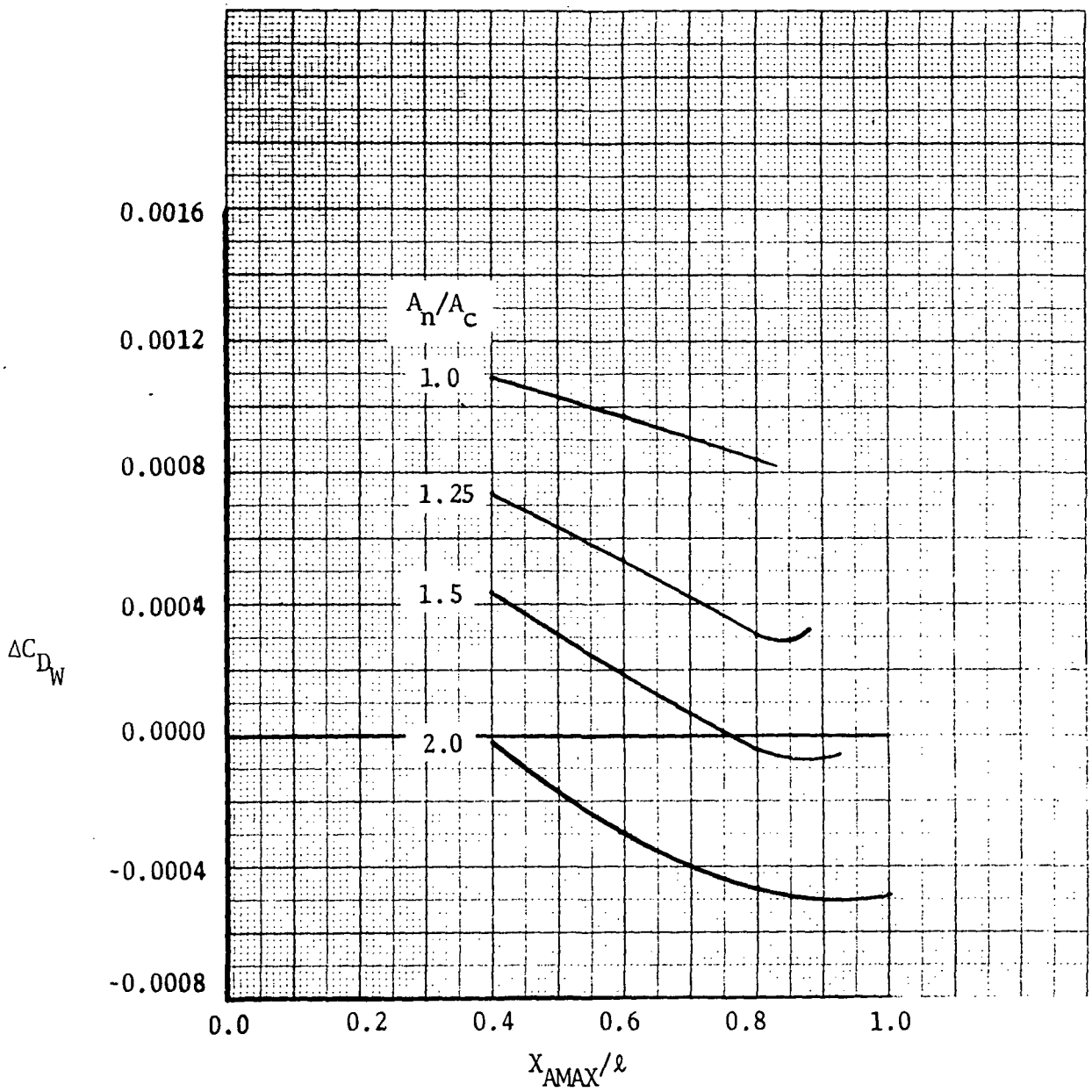

Figure 47.- Effect of geometry perturbations on nacelle incremental wave drag at $M_o = 2.32$

$A_c = 2.79$ sq. m. (30 sq. ft.) $\ell/d_c = 7.0$

$A_{MAX}/A_c = 2.0$

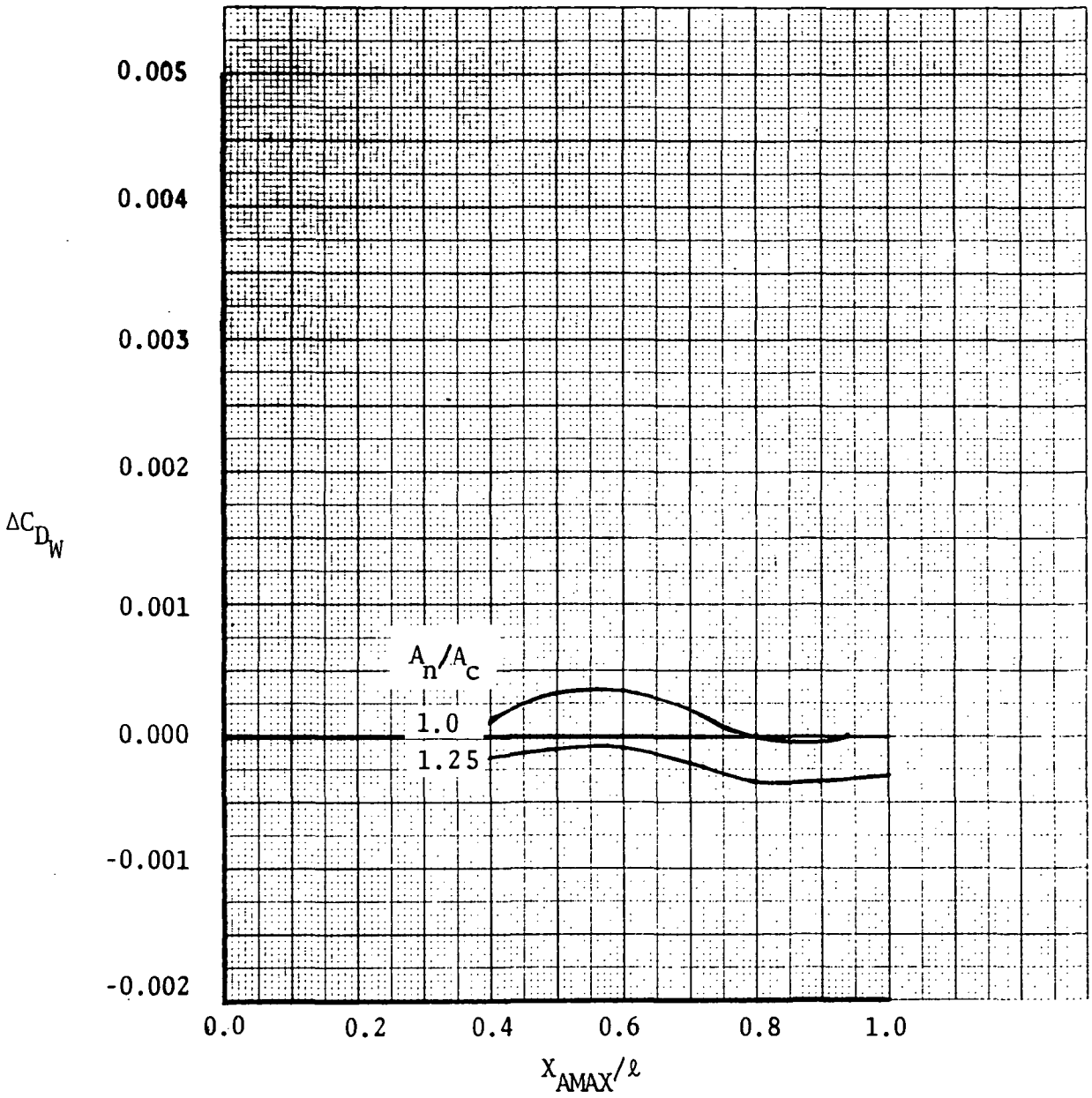

Figure 48. Effect of geometry perturbations on nacelle incremental wave drag at $M_o = 1.2$

$A_c = 3.72$ sq. m. (40 sq. ft.) $\ell/d_c = 5.5$

$A_{MAX}/A_c = 1.25$

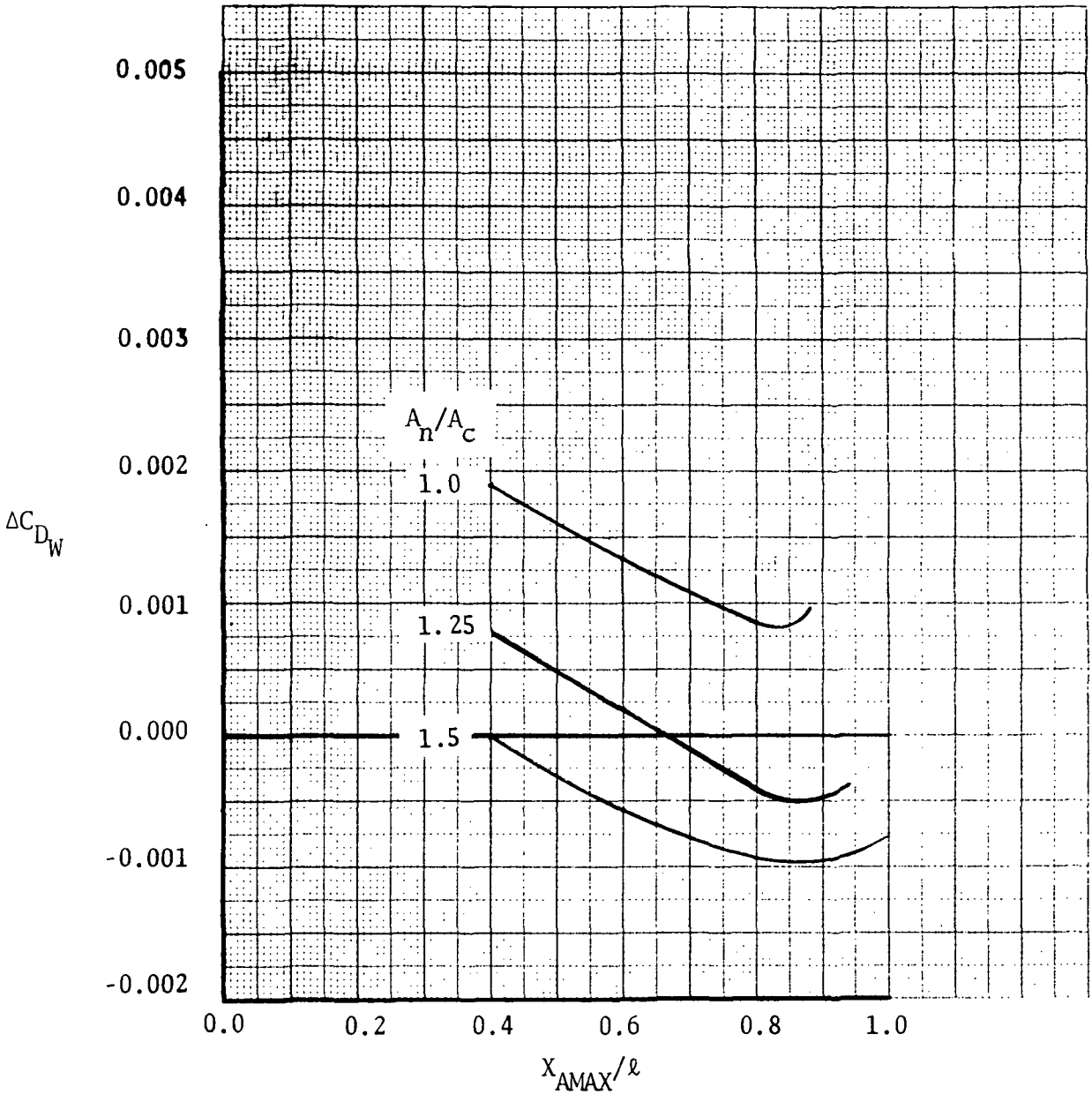

Figure 49.-Effect of geometry perturbations on nacelle incremental wave drag at $M_o = 1.2$

A_c = 3.72 sq. m. (40 sq. ft.) $\ell/d_c = 5.5$

$A_{MAX}/A_c = 1.5$

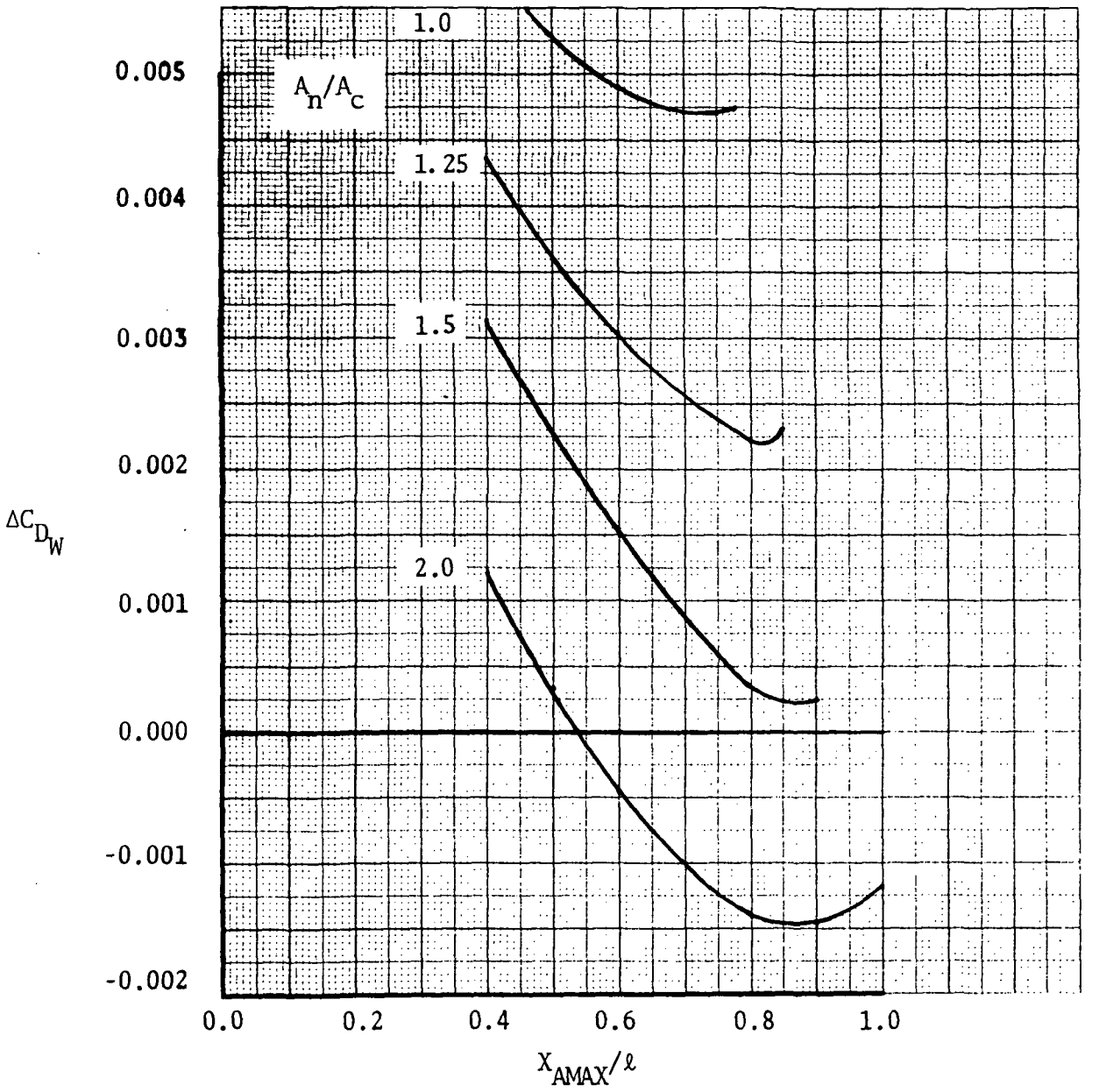

Figure 50.-Effect of geometry perturbations on nacelle incremental wave drag at $M_o = 1.2$

A_c = 3.72 sq. m. (40 sq. ft.) $\ell/d_c = 5.5$

$A_{MAX}/A_c = 2.0$

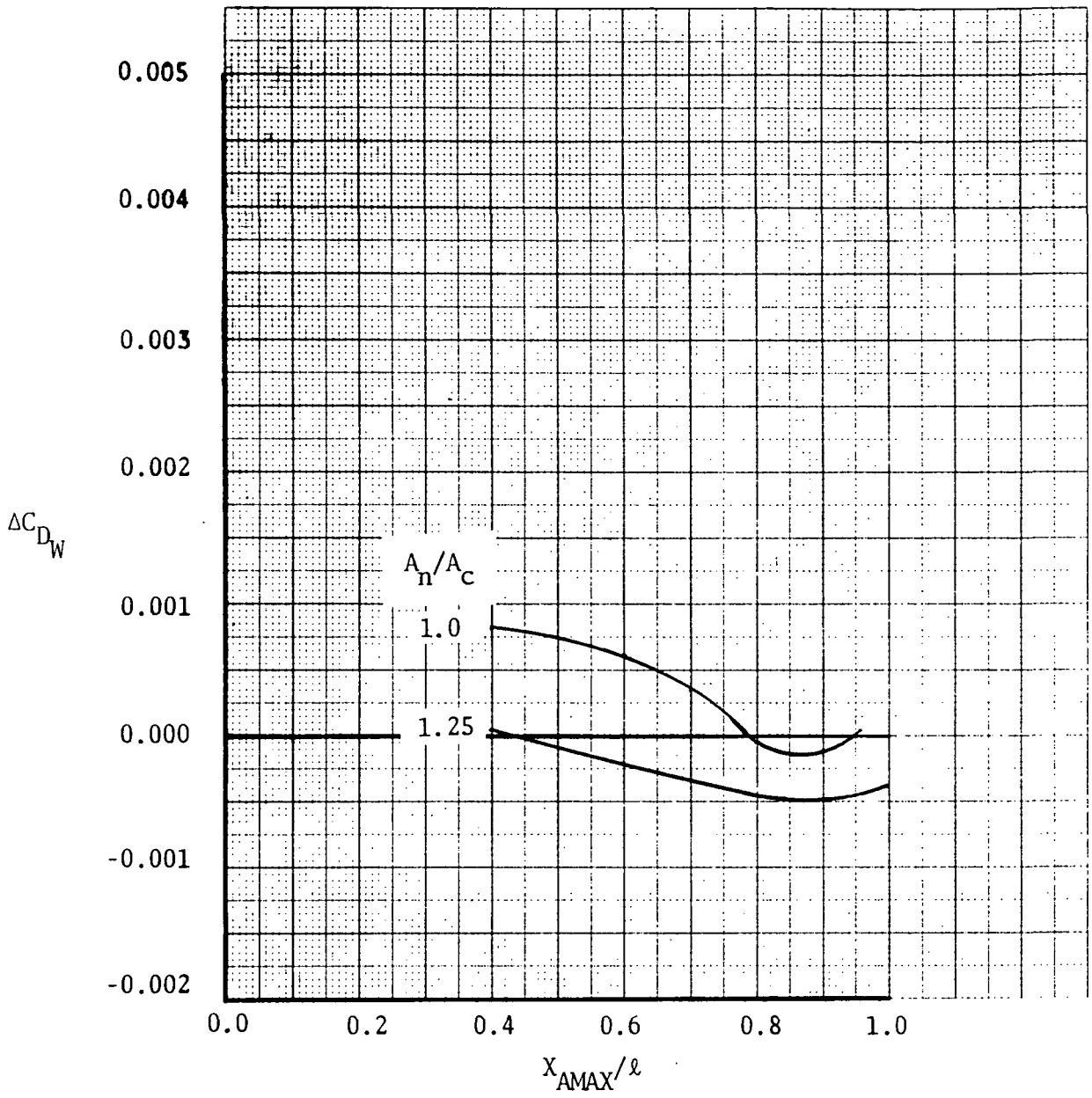

Figure 51.-Effect of geometry perturbations on nacelle incremental wave drag at $M_o = 1.2$

$A_c = 3.72$ sq. m. (40 sq. ft.) $\ell/d_c = 7.0$

$A_{MAX}/A_c = 1.25$

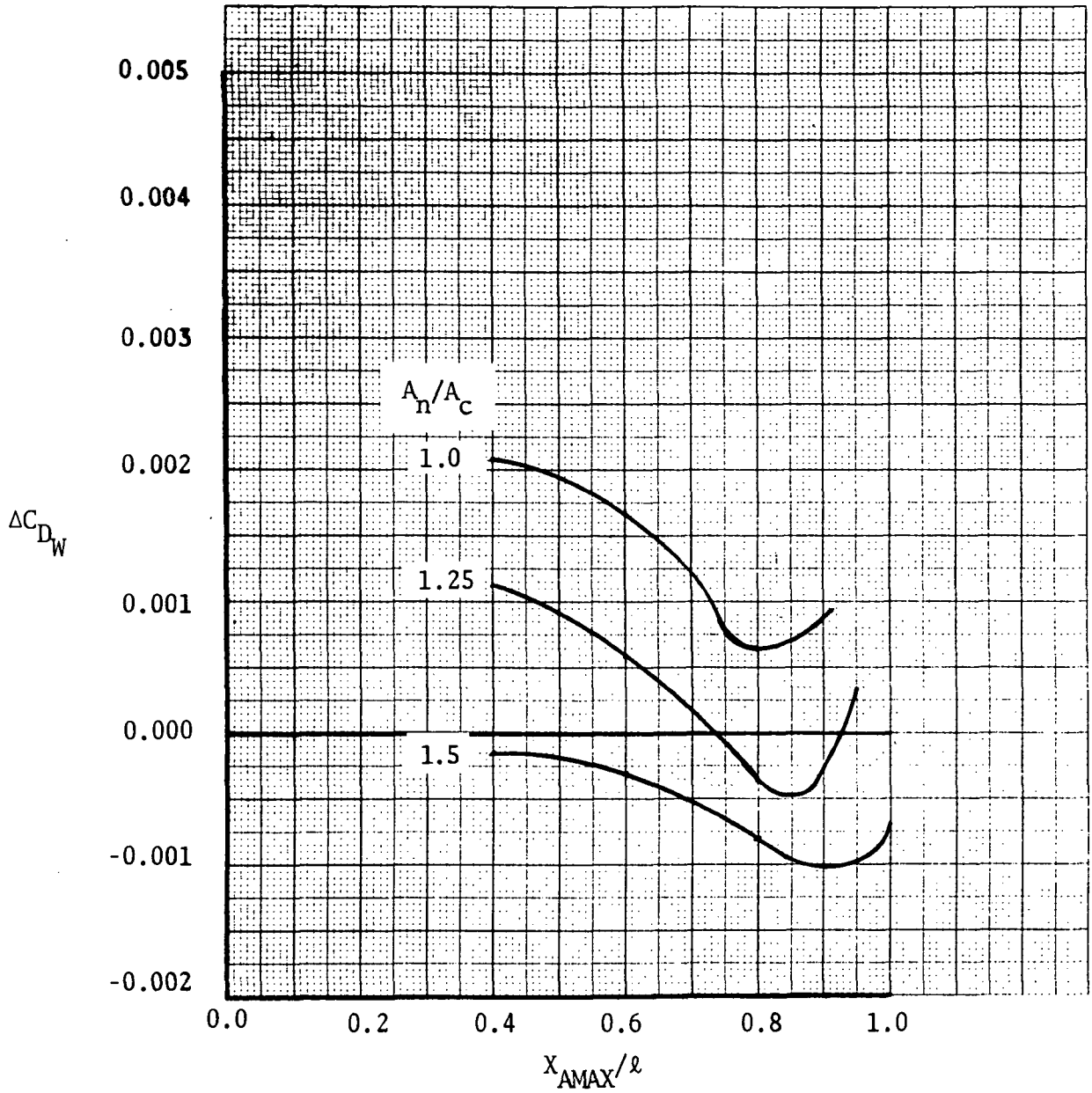

Figure 52.-Effect of geometry perturbations on nacelle incremental wave drag at $M_o = 1.2$

$A_c = 3.72$ sq. m. (40 sq. ft.) $\ell/d_c = 7.0$

$A_{MAX}/A_c = 1.5$

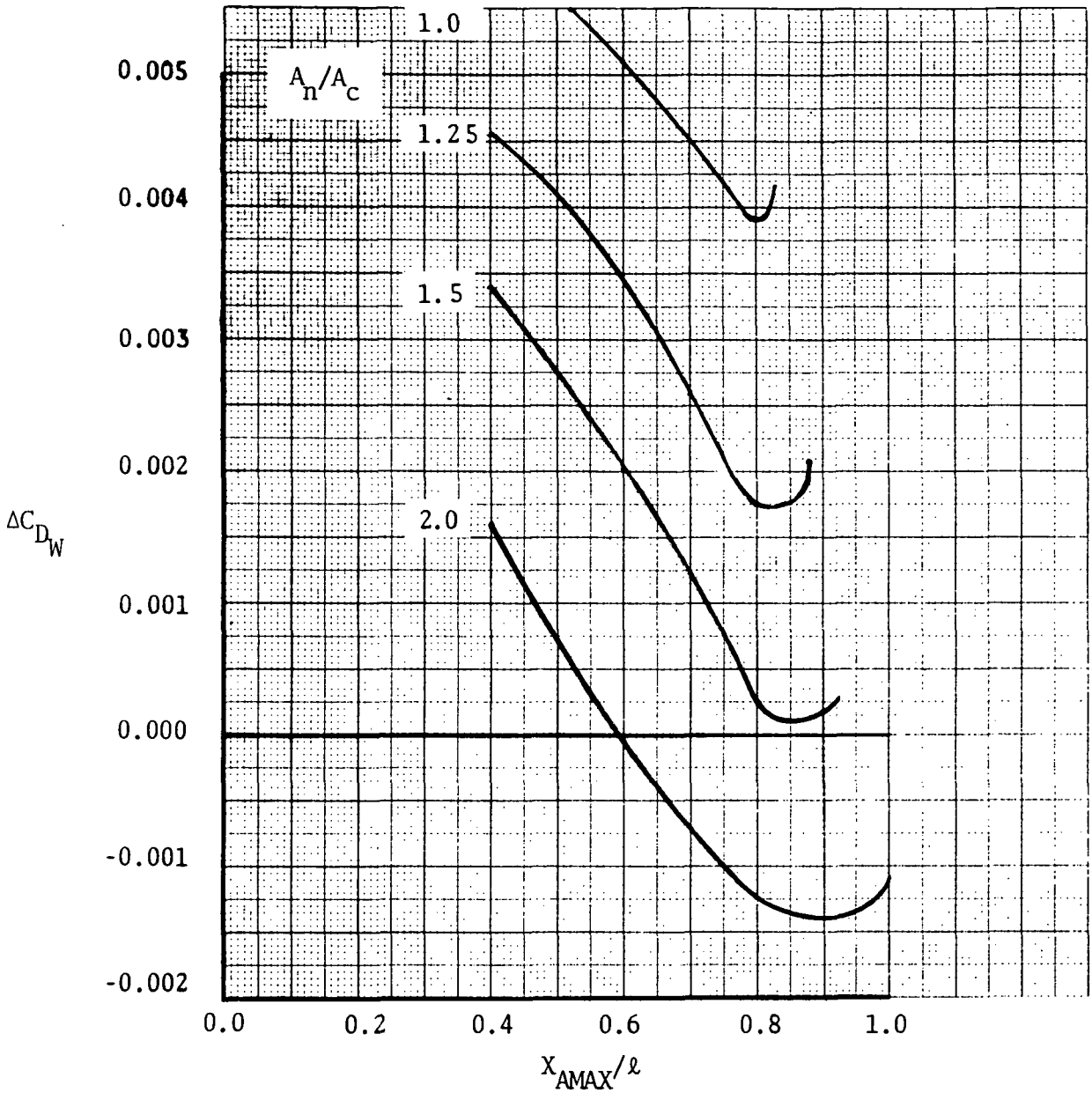

Figure 53.-Effect of geometry perturbations on nacelle incremental wave drag at $M_o = 1.2$

A_c = 3.72 sq. m. (40 sq. ft.) $\ell/d_c = 7.0$

$A_{MAX}/A_c = 2.0$

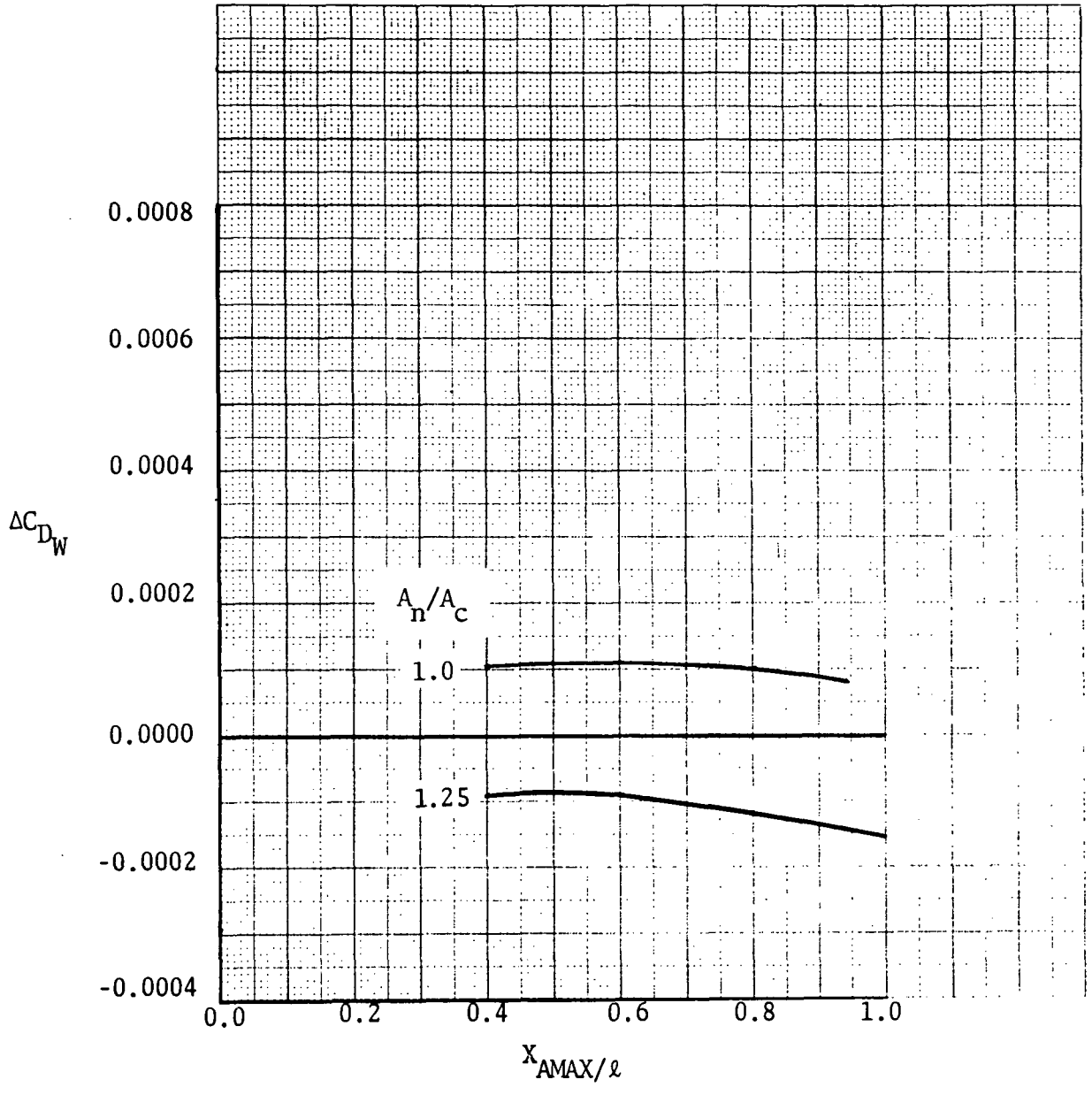

Figure 54.- Effect of geometry perturbations on nacelle incremental wave drag at $M_o = 2.32$

$A_c = 3.72$ sq. m. (40 sq. ft.) $\ell/d_c = 5.5$

$A_{MAX}/A_c = 1.25$

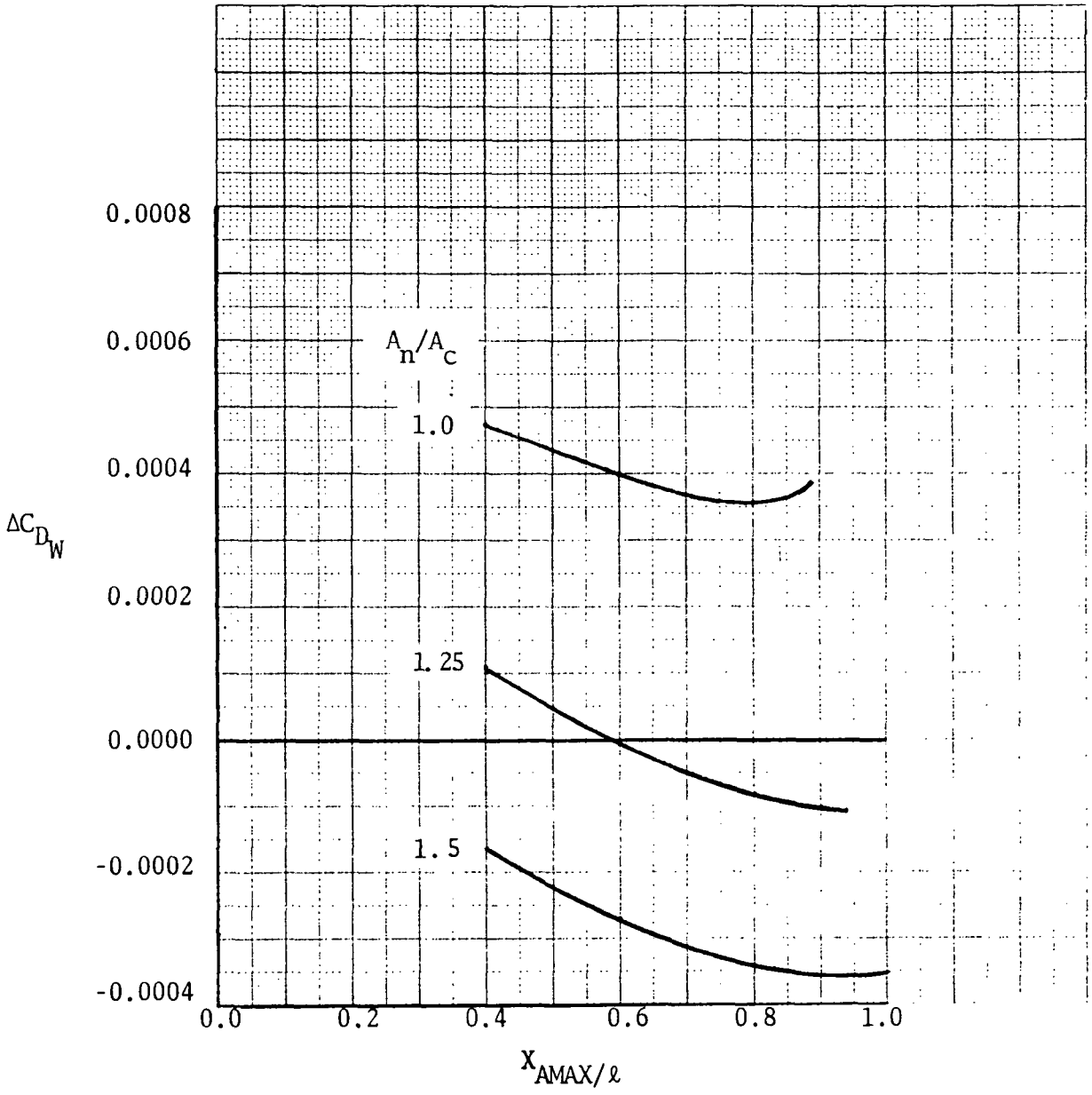

Figure 55.- Effect of geometry perturbations on nacelle incremental wave drag at $M_o = 2.32$

$A_c = 3.72$ sq. m. (40 sq. ft.) $\ell/d_c = 5.5$

$A_{MAX}/A_c = 1.5$

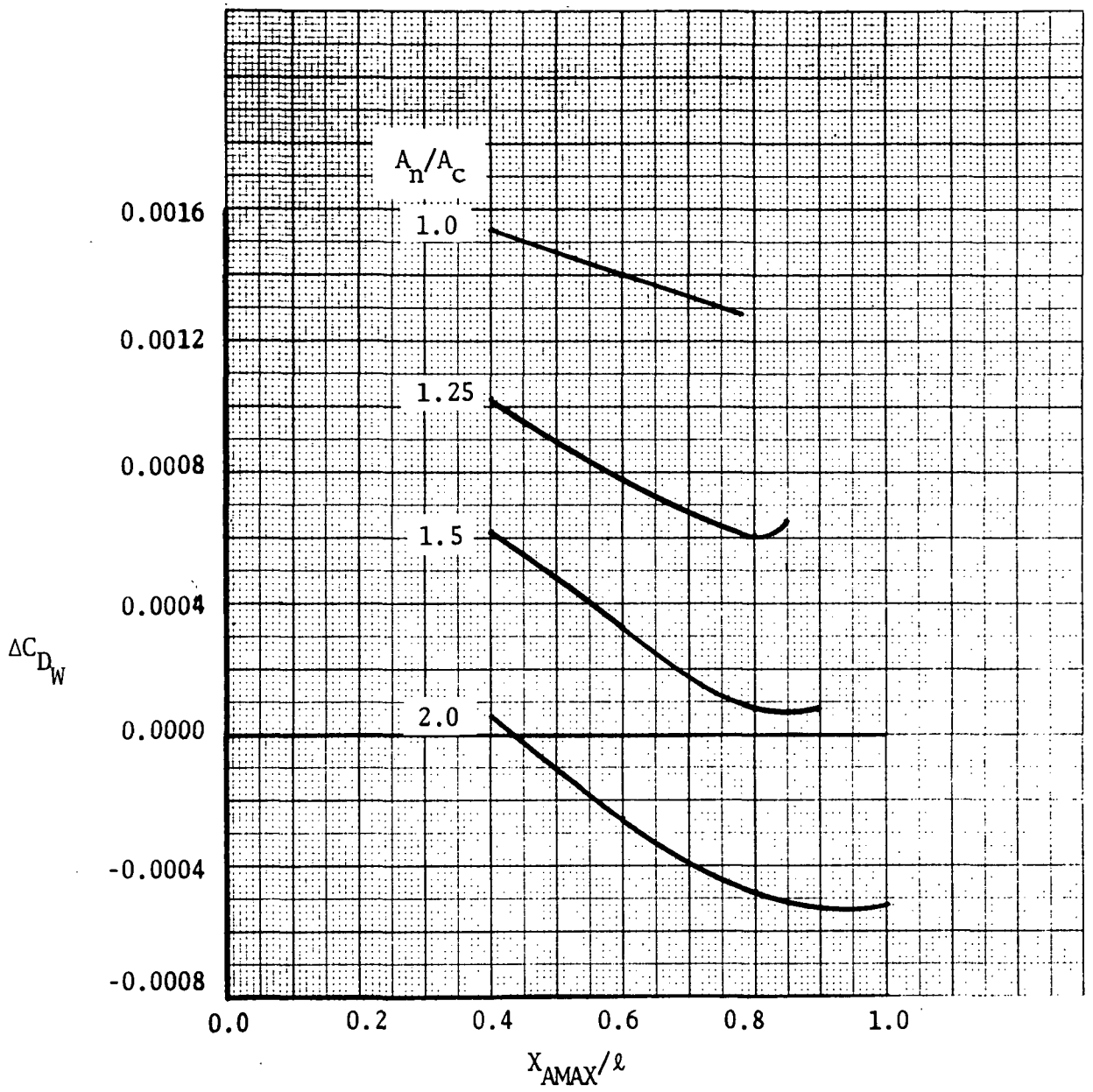

Figure 56.- Effect of geometry perturbations on nacelle incremental wave drag at $M_o = 2.32$

$A_c = 3.72$ sq. m. (40 sq. ft.) $\ell/d_c = 5.5$

$A_{MAX}/A_c = 2.0$

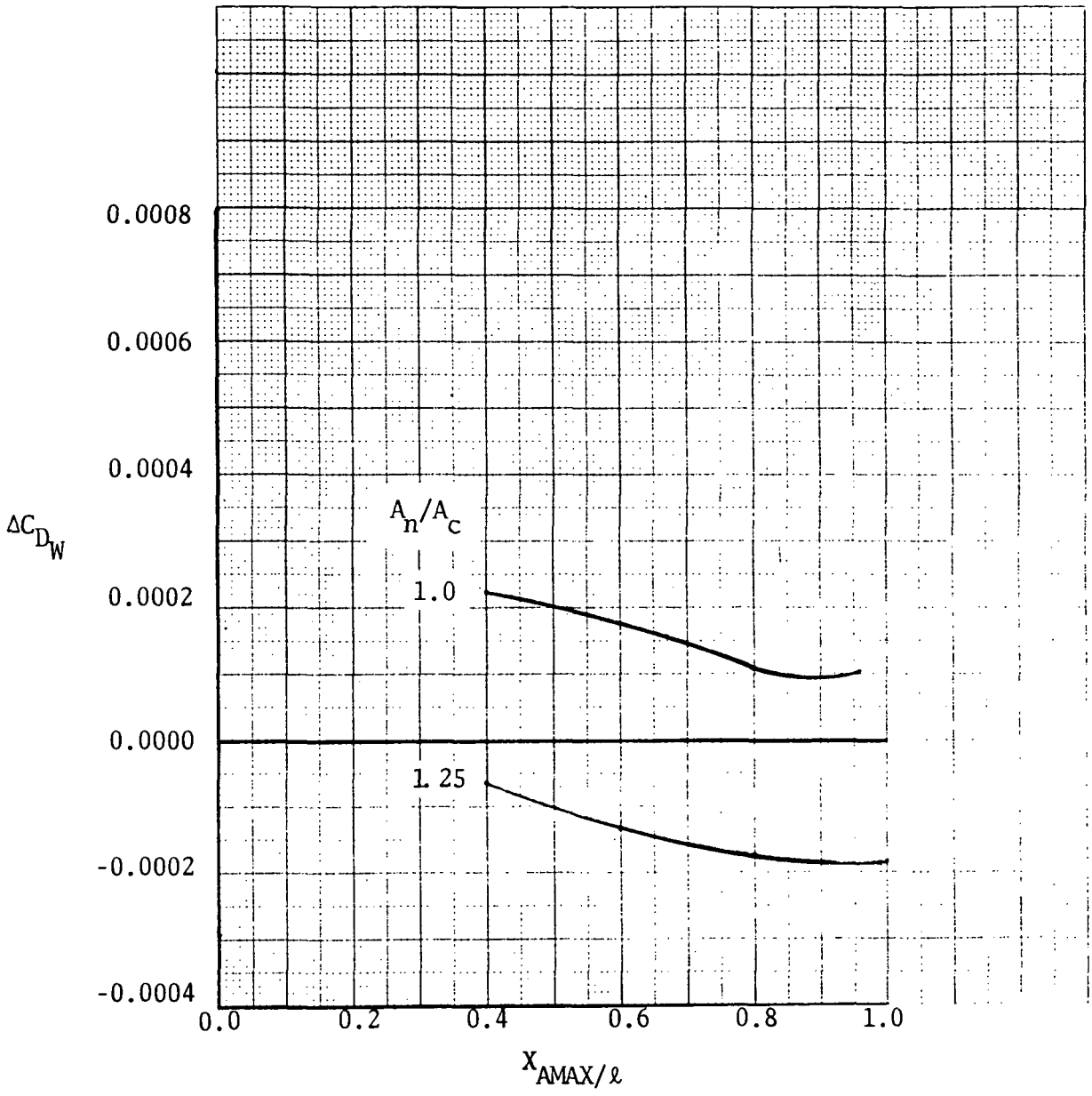

Figure 57.- Effect of geometry perturbations on nacelle incremental wave drag at $M_o = 2.32$

$A_c = 3.72$ sq. m. (40 sq. ft.) $\ell/d_c = 7.0$

$A_{MAX}/A_c = 1.25$

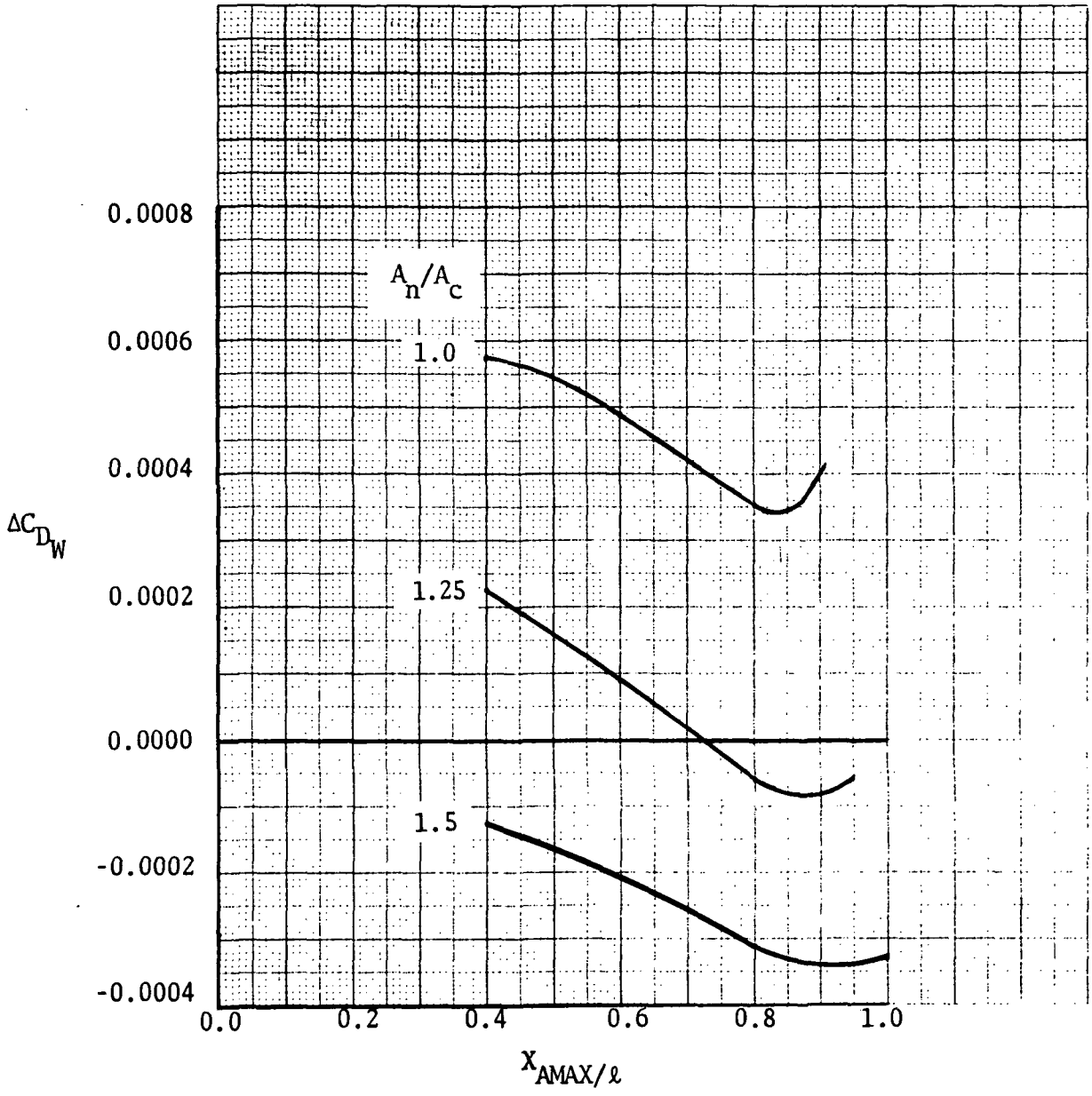

Figure 58.- Effect of geometry perturbations on nacelle incremental wave drag at $M_o = 2.32$

$A_c = 3.72$ sq. m. (40 sq. ft.) $\ell/d_c = 7.0$

$A_{MAX}/A_c = 1.5$

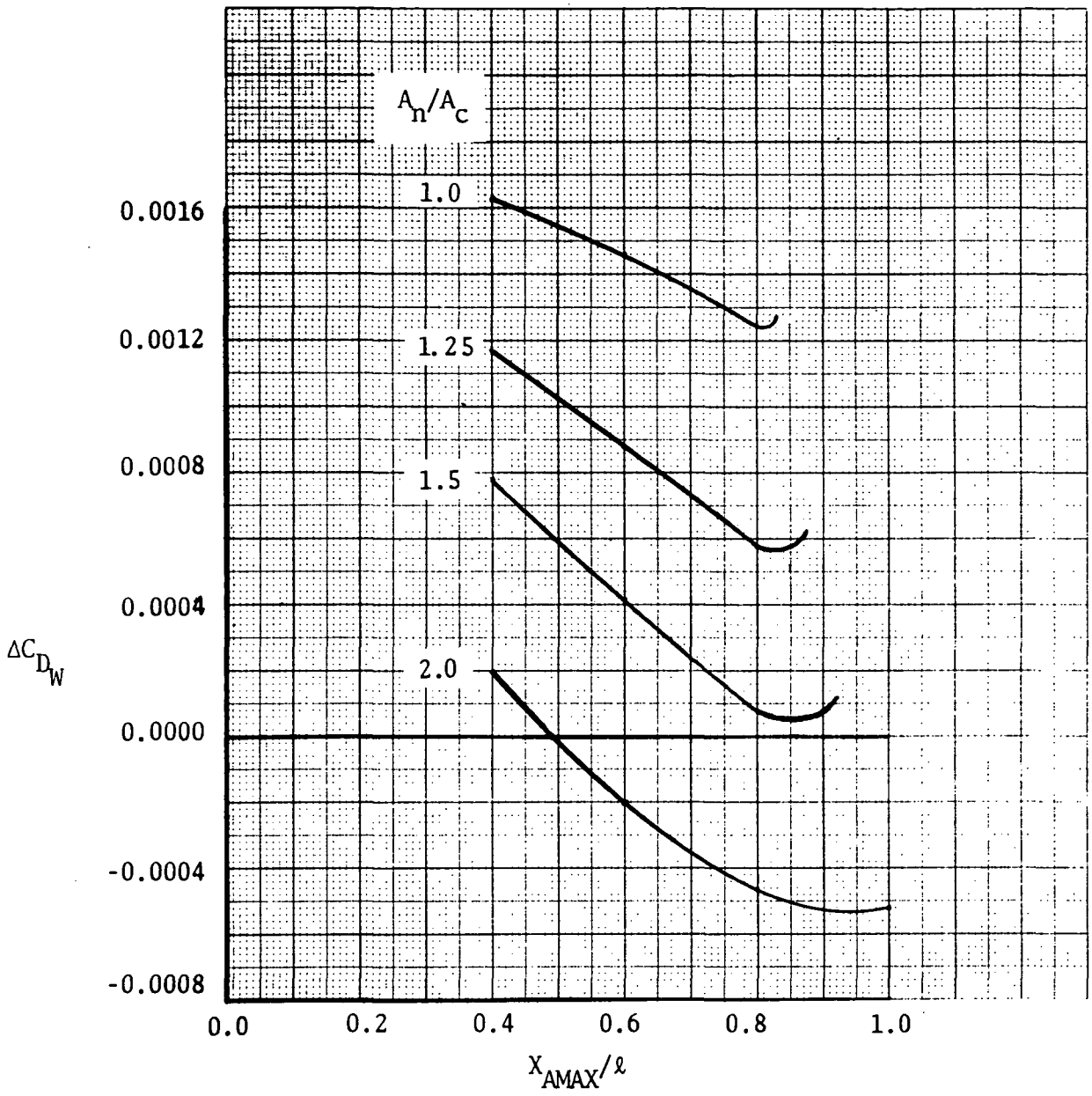

Figure 59.- Effect of geometry perturbations on nacelle incremental wave drag at $M_o = 2.32$

$A_c = 3.72$ sq. m. (40 sq. ft.) $\ell/d_c = 7.0$

$A_{MAX}/A_c = 2.0$

and the ratio of nozzle area to capture area A_n/A_c. In all cases, the maximum value of the former variable considered corresponds to a boattail angle of ten degrees. The results can be easily re-interpreted as total nacelle installation drag by a simple vertical shift of origin in accordance with table XI.

A discussion of the results is presented for a representative case of a medium size nacelle (A_c = 2.79 sq.m., 30 sq. ft.) for a fineness ratio of 5.5 at Mach 2.32 cruise condition. Examination of figures 42 through 44 indicates the incremental nacelle wave drag is a strong function of the ratio of maximum-to-capture cross-sectional area, A_{max}/A_c, boattail area, and to a somewhat lesser extent relative axial position of maximum cross-sectional area, X_{AMAX}/ℓ. The results for a circular cylinder correspond to the axis (i.e. $\Delta C_{DW} = 0$). The fact that nacelle shapes of less wave drag exist is a consequence of favorable total system thickness interferences associated with the location of growing nacelle cross-sectional area in a region of decreasing wing thickness.

The previously-cited nacelle geometric variable behavior and sensitivity are unchanged by Mach number, nacelle capture area, or nacelle fineness ratio. The incremental wave drag results are, in general, weak functions of the latter two variables for efficient installations (see figure 60).

Detailed nacelle wave drag variations with freestream Mach number are defined for a range of levels covering high-positive, zero, and negative installation increments. These characteristics correspond to nacelles with large maximum cross-sectional area relative to the capture and nozzle area, cylindrical, and near-truncated conical shapes, respectively. Figure 61 illustrates the Mach number difference for these extremes for the fineness ratio 5.5 medium size nacelle. Examination of the results indicate that weak to moderate Mach number variations are associated with small nacelle installation drags. Conversely, strong compressibility variations are exhibited for inefficient installations. The large benefit at transonic speeds is somewhat illusory as the thrust must be progressively penalized for nozzle contraction with decreasing Mach numbers.

Weight Sensitivity Analysis

To evaluate the effects of propulsion system variations on the airframe/engine system, the sensitivities of the airplane takeoff gross weight to variations of propulsion system parameters were determined. These sensitivity data were obtained by conducting design trades on the baseline airplane for variations of the following items:

- Incremental Nacelle Drag
- Propulsion System Weight
- Engine Specific Fuel Consumption
- Takeoff Thrust

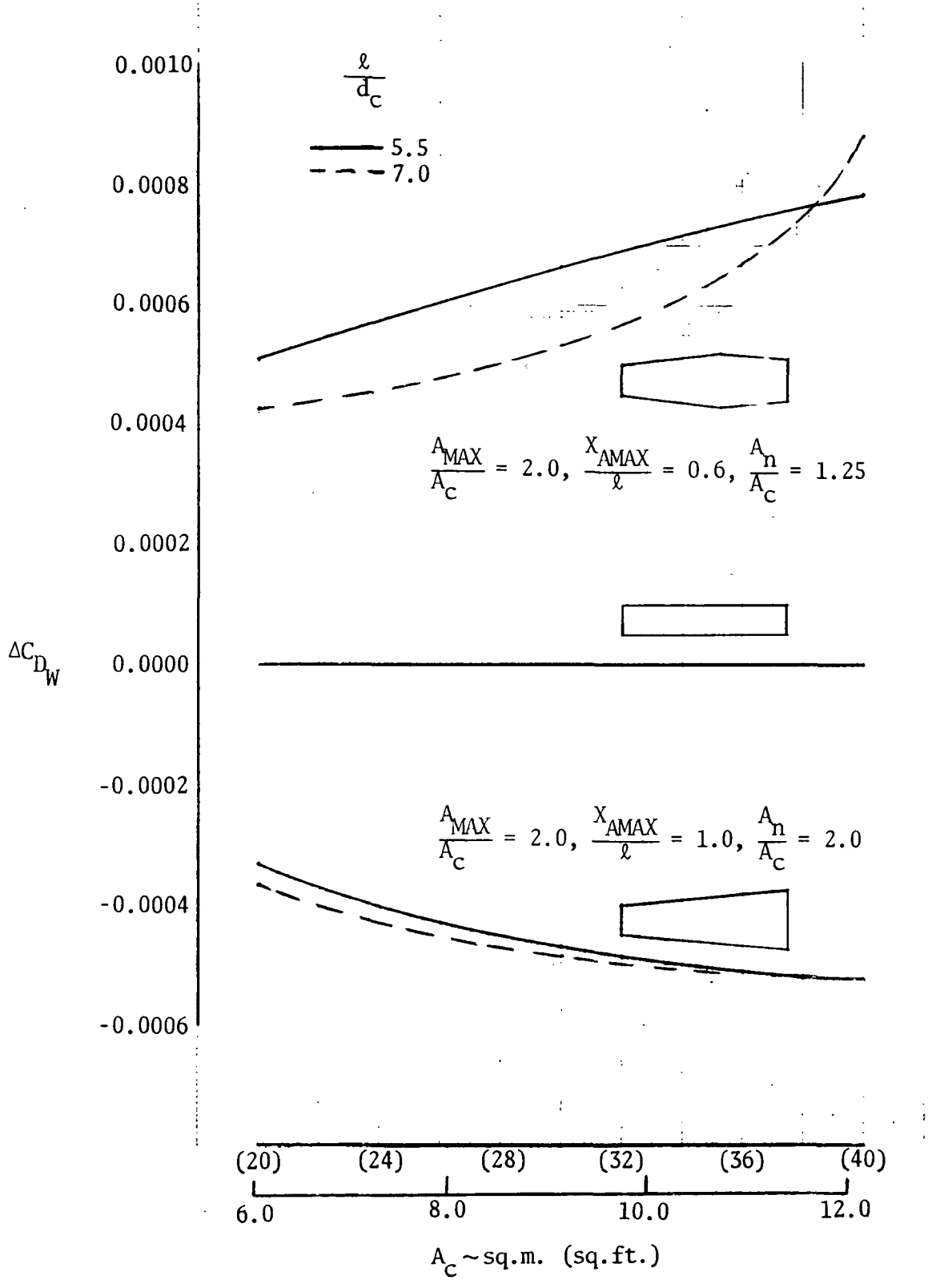

Figure 60.-Typical nacelle incremental wave drag variation with nacelle size at Mach 2.32

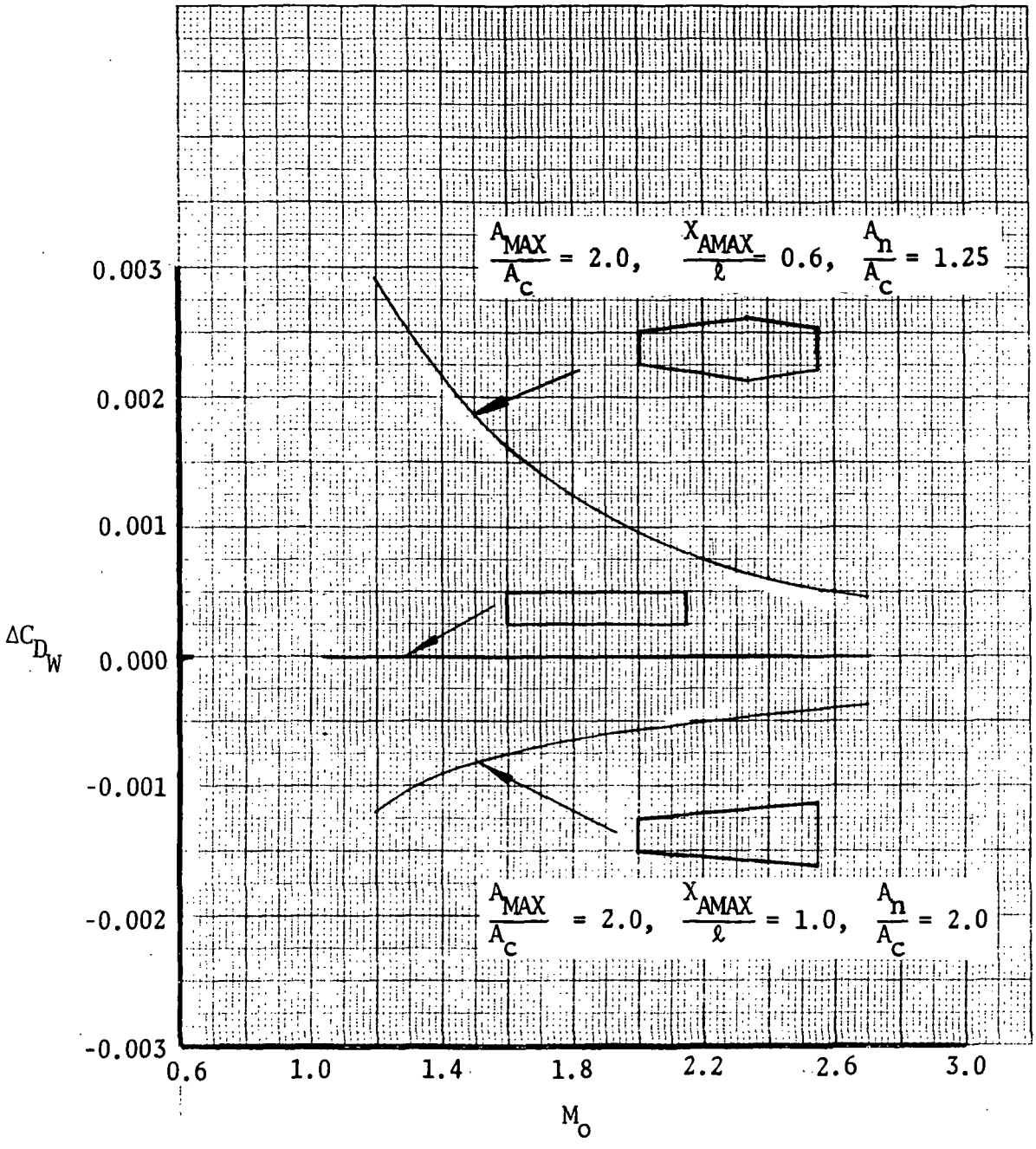

Figure 61. -Typical nacelle incremental wave drag variations with Mach number

A_c = 2.79 sq.m. (30 sq.ft.) ℓ/d_c = 5.5

In each case the parameter of interest was varied independently and the airplane resized to the design mission range of 7 408 km. (4 000 n.mi.) while maintaining thrust-to-weight and wing loading values equal to those for the baseline vehicle.

Incremental nacelle drag.-Several variations of nacelle drag were investigated. These were chosen as representative of the combined wave and friction drag variations as found in the nacelle shape analysis to allow use of the trade data for any nacelle geometry analyzed in this program.

The results of this trade are shown in figure 62 which shows relative TOGW versus nacelle drag at Mach 2.32 for several variations of the drag increment at 1.2 Mach. A typical curve of drag increment versus Mach number is depicted in figure 63.

Propulsion system weight trades.-Airplane takeoff gross weight was calculated for several propulsion system weight increments. Incremental propulsion weight, in this case, is defined as a percent of the sum of the engine, engine accessories, and nacelle weights. For the baseline airplane, having an engine airflow of 394 kg./sec. (869 lb./sec.), these total 31 522 kg. (69 439 lb.). The results of this trade are shown in figure 64 which plots relative TOGW versus propulsion weight increment.

Engine specific fuel consumption trades.-Four separate trades were performed with SFC increments applied independently to the following mission segments:

(1) maximum power climb legs only

(2) supersonic cruise legs only

(3) subsonic cruise and loiter legs only

(4) the entire mission.

The results of this trade are presented in figure 64 as relative takeoff gross weight versus percent change in SFC.

Takeoff thrust.-Figure 65 presents relative TOGW versus percent change in takeoff thrust. In this trade it is assumed that the thrust available during both ground roll and climbout portions of the takeoff vary without any change in propulsion characteristics at other flight conditions.

DISCUSSION OF RESULTS

Nacelle Drag

Following is a discussion of the parametric nacelle installation drag results at Mach 2.32 cruise conditions. The presentation of cuts through the basic data of figures 24 through 59 emphasize the low drag variable domain as it is necessarily the most interesting. In order to keep the results in proper perspective, it should be remembered that a typical supersonic cruise condition for the baseline configuration has a total drag

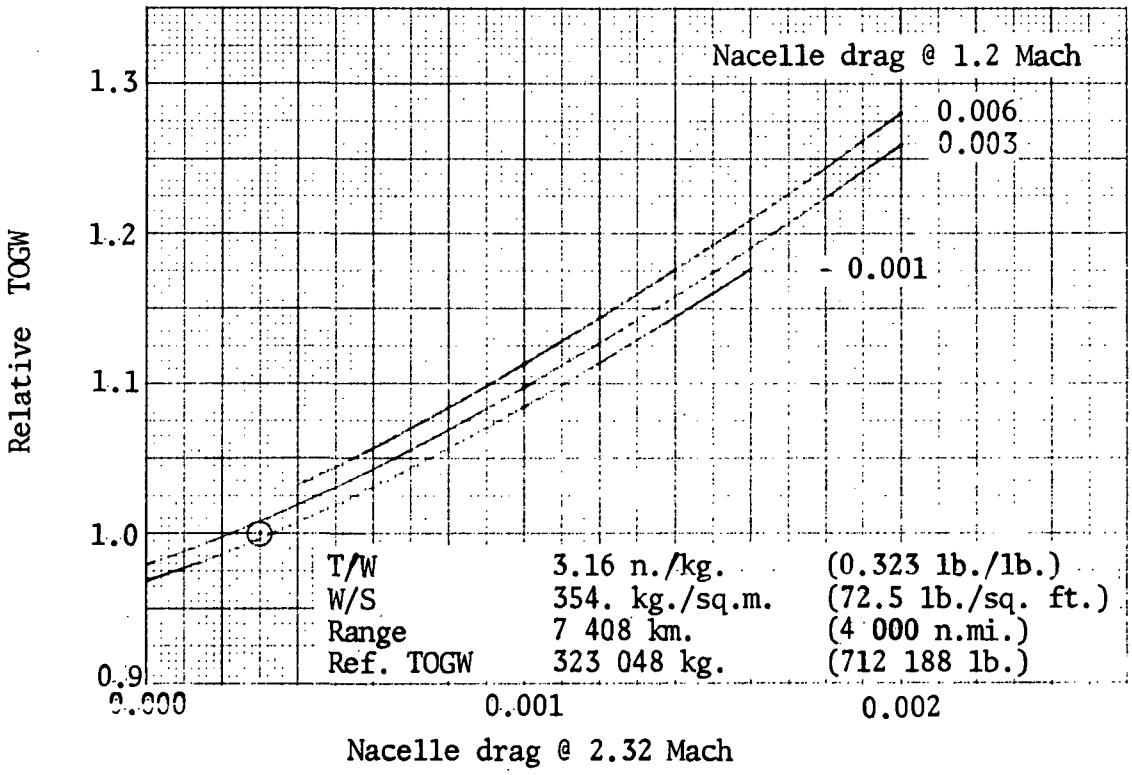

Figure 62.-Nacelle drag sensitivity trade

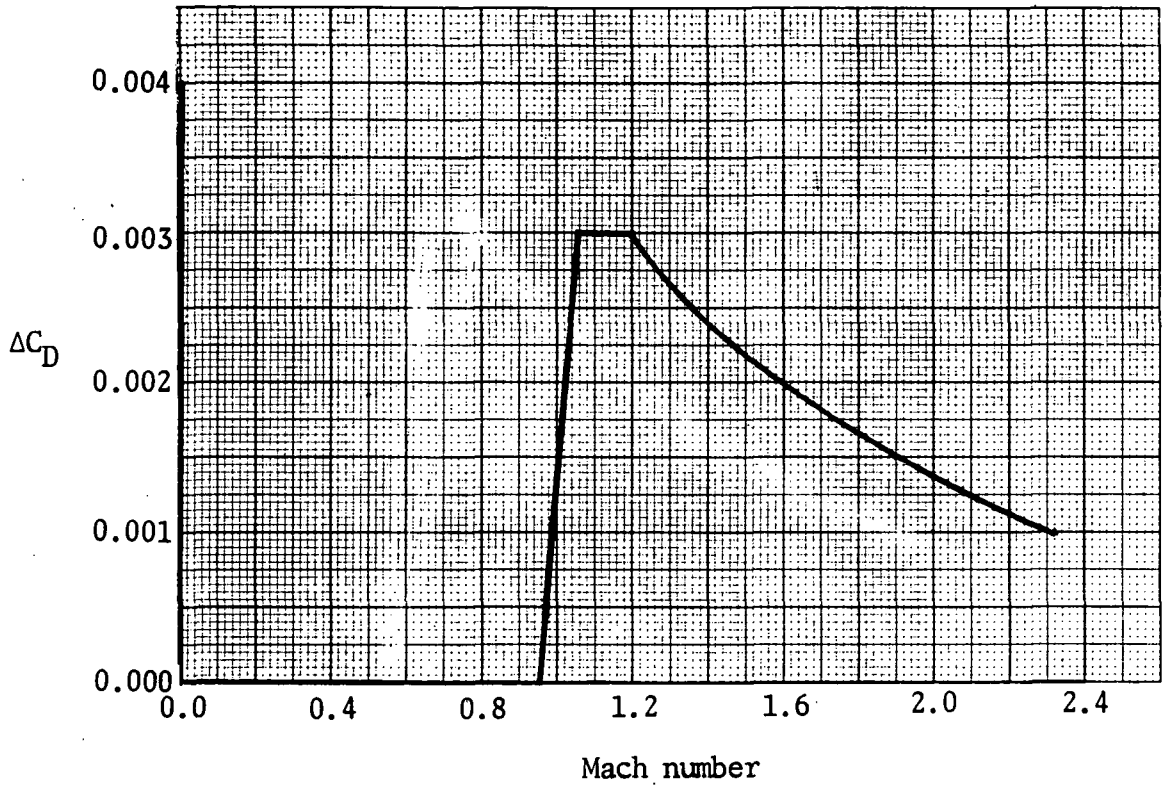

Figure 63.-Typical incremental nacelle drag variation

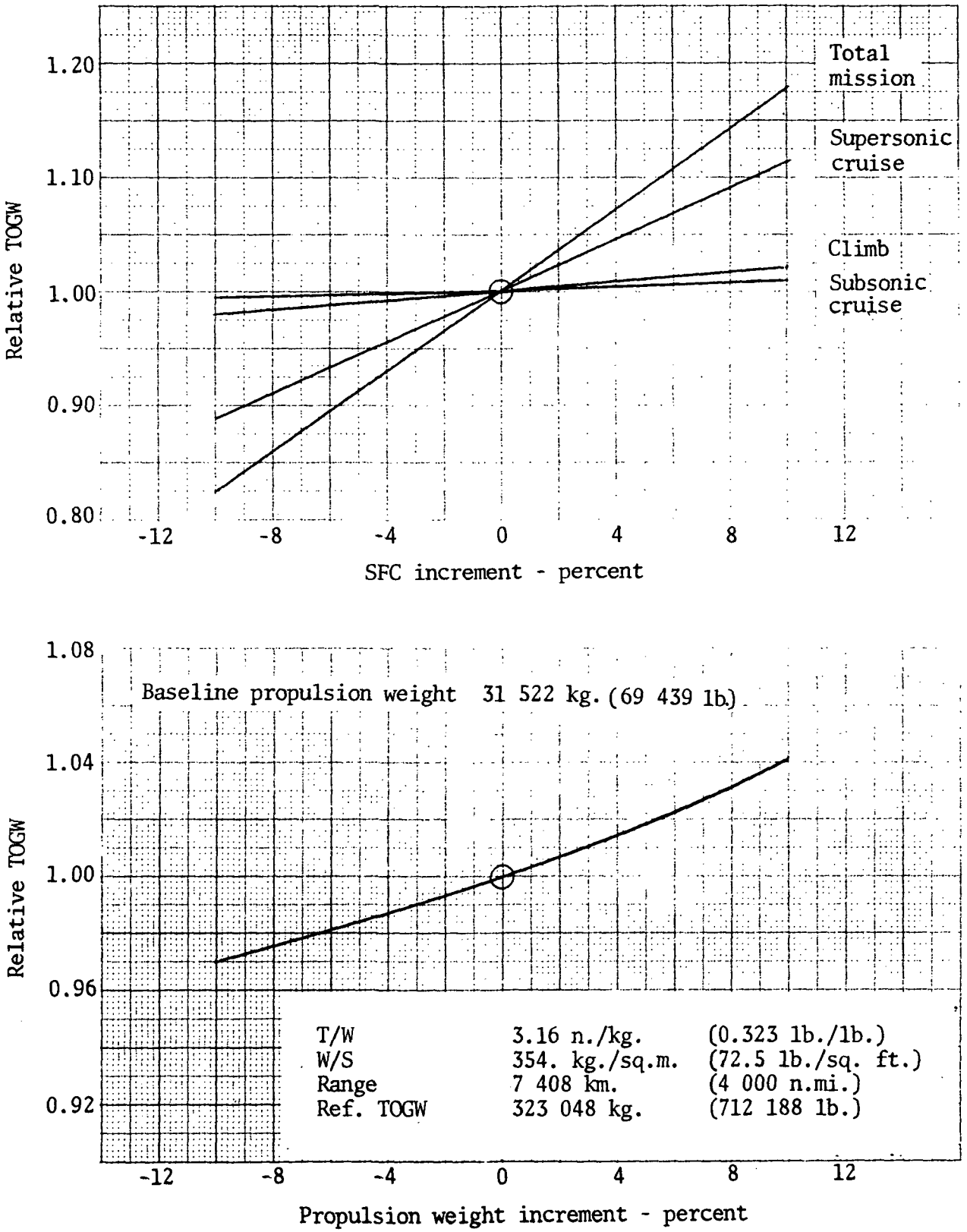

Figure 64.-Propulsion weight and SFC sensitivity trades

T/W	3.16 n./kg.	(0.323 lb./lb.)
W/S	354. kg./sq.m.	(72.5 lb./sq.ft.)
Range	7 408 km.	(4 000 n.mi.)
Ref. TOGW	323 048 kg.	(712 188 lb.)

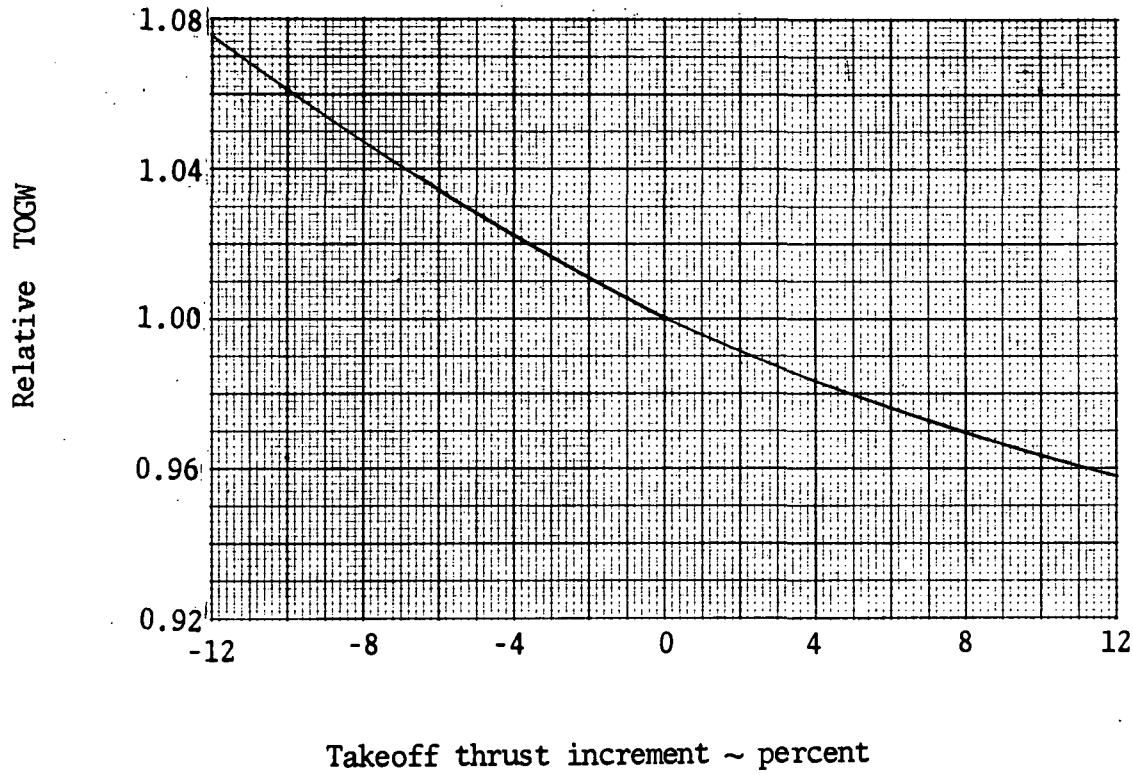

Figure 65.-Takeoff thrust sensitivity trade

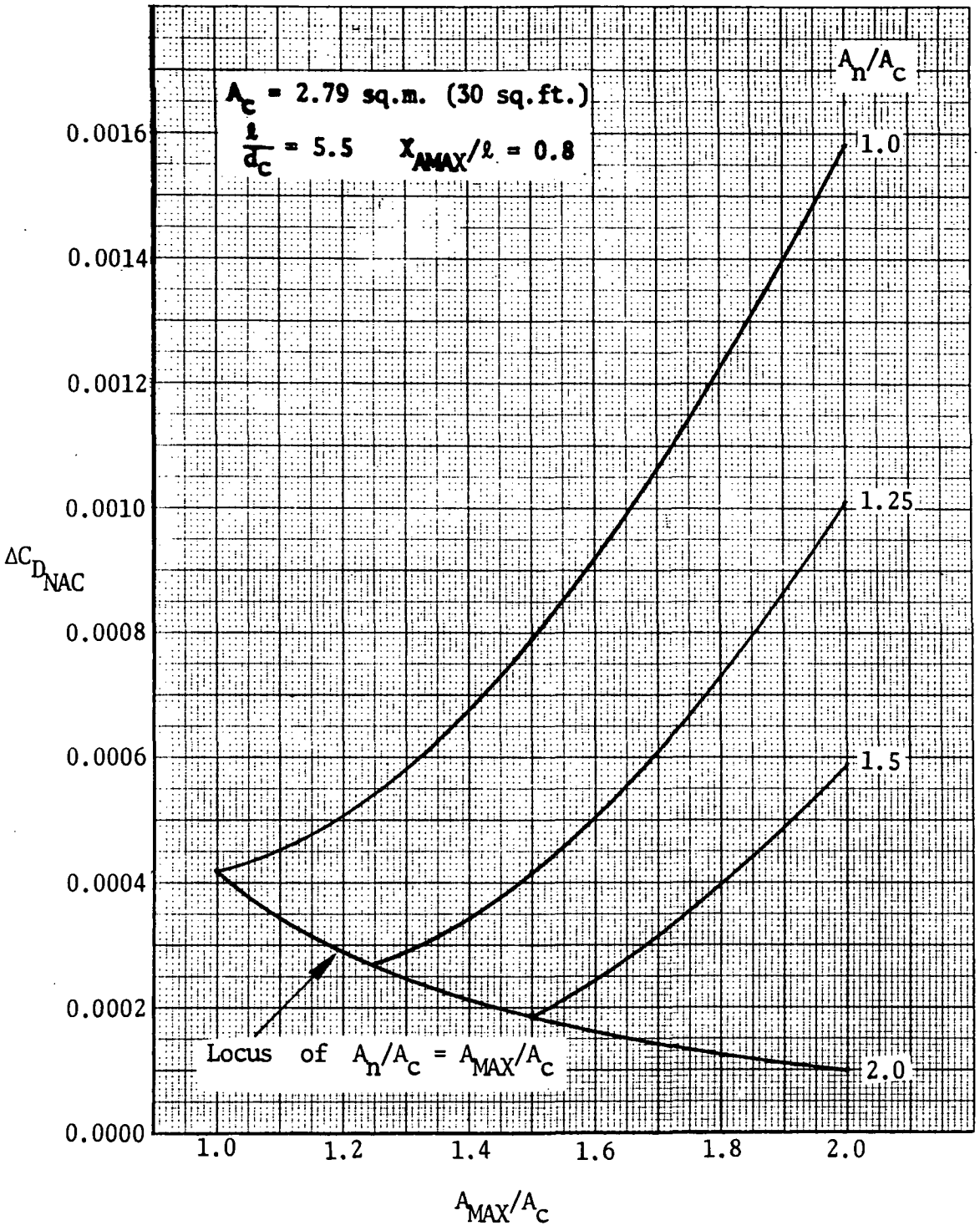

Figure 66.-Typical nacelle incremental drag variation with boattail area at M_o = 2.32

coefficient of approximately 0.0105 at a C_L of 0.1

Typical impact on installation drag of nacelle relative maximum cross-sectional area and nozzle area for a fixed axial location of maximum area is presented on figure 66. Clearly, both variables have a strong influence on the overall installation efficiency through the wave drag-due-to-thickness component.

The sensitivity of the nacelle drag to the axial position of maximum cross-sectional area is presented on figure 67. It is generally less important than either the maximum or nozzle area parameters although its proper selection can significantly aid in realizing a propulsion system installation goal of zero total drag.

The influence of the absolute size of the nacelle on installation drag is presented on figure 68. As would be expected, inclusion of friction drag results in more pronounced size dependence than observed previously for the wave drag component (figure 60). This range of nacelle sizes could represent a wide range of engine thrust and, therefore, vehicle thrust-to-weight ratios.

The parametric nacelle analysis has identified a family of quasi-conical nacelles $\left(\frac{X_{AMAX}}{\ell}\right.$ approaching 1, $\frac{A_n}{A_c}$ approaching $\left.\frac{A_{MAX}}{A_c}\right.$ approaching 2$\left.\right)$ which have a potential installation drag (wave plus friction) of zero at the supersonic cruise condition when modest allowances (ΔC_D of approximately -0.0002) are made for optimum meridial shaping refinements and the benefit of wing lift/nacelle thickness interference is accounted for. These propulsion system integrations effectively remove 200 to 400 sq.m. (2 000 - 4 000 sq.ft.), depending on nacelle size, of wetted area by use of favorable pressure drag interference.

Weight Sensitivity

Results of the weight sensitivity trades show that airplane gross weight is highly sensitive to both drag and engine specific fuel consumption (SFC) at the supersonic cruise condition of 2.32 Mach number just as expected. On the other hand changes in drag and engine SFC at other flight conditions and even propulsion system weight changes have a relatively minor effect on airplane gross weight. However, the baseline airplane has a relatively large thrust margin throughout the transonic acceleration. If that margin were reduced, gross weight would become more sensitive to drag variations at Mach 1.2 Variations in engine thrust at the takeoff condition have a significant impact on gross weight although not so great as that for drag and SFC at supersonic cruise conditions. Small thrust variations at conditions other than takeoff have only a minor impact on gross weight. Table XV compares the changes in parameters required to achieve a 4 540 kg. (10 000 lb.) reduction in takeoff gross weight. It can be seen from table XV that a one-drag count change at supersonic cruise results in a vehicle takeoff gross weight change approximately equal to that of a one percent SFC change at supersonic cruise.

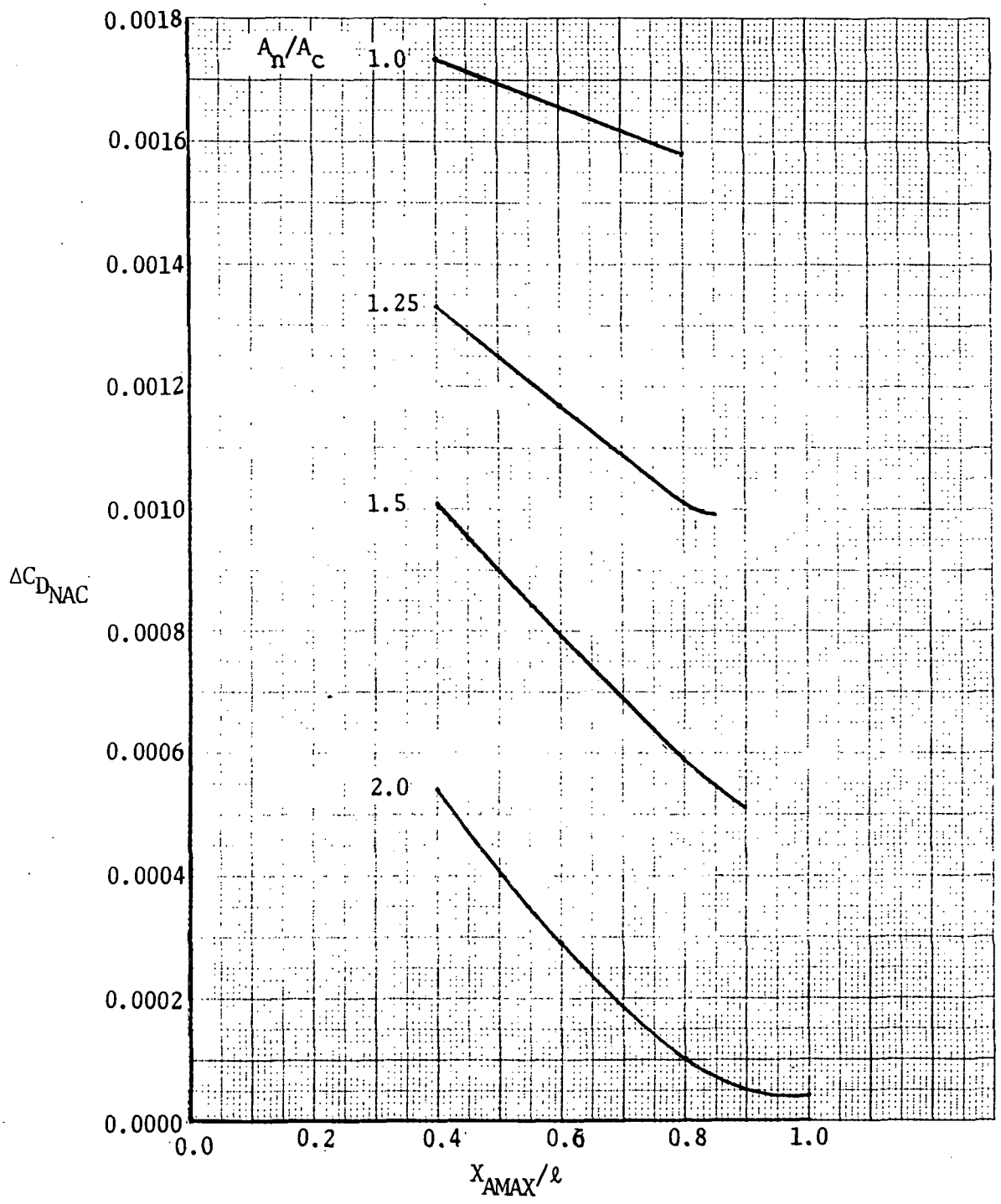

Figure 67.-Typical nacelle incremental drag variation vs. axial position of maximum area at M_o 2.32

A_c = 2.79 sq.m. (30 sq.ft.) $\frac{\ell}{d_c}$ = 5.5 A_{MAX}/A_c = 2.0

TABLE XV.-SENSITIVITY COMPARISON

Parameter	Change required to achieve a 1.4% reduction in vehicle takeoff gross weight
Supersonic cruise drag coefficient (C_D @ 1.2 Mo = baseline)	-0.00013 ($\sim$ 1.2%)
ΔSFC, %	
Supersonic cruise	-1.3
Total mission	-0.9
ΔPropulsion weight, %	-4.3
ΔTakeoff thrust, %	+3.3

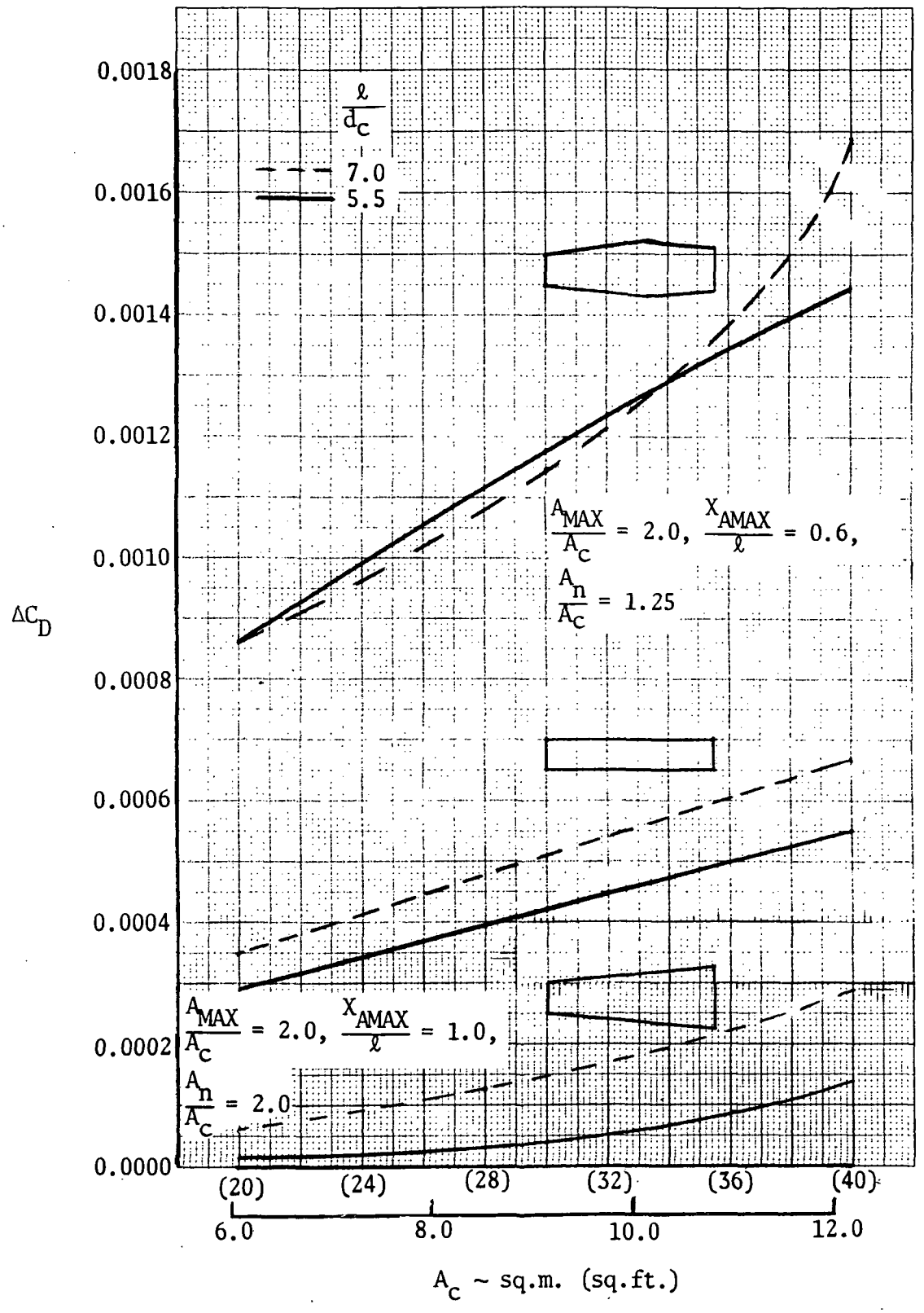

Figure 68.-Typical nacelle installation drag variation with nacelle size at Mach 2.32

RECOMMENDATIONS

It is recommended that the nacelle drag and vehicle sensitivity data generated in this program be used in future preliminary analyses of propulsion system trades.

It is further recommended that airframe/engine integration studies continue. In particular, investigations should include the following:

1) Close coordination between the engine companies and the airframe manufacturers is essential to achieve maximum benefit from all disciplines and technology advances.

2) Consideration should be given to vectorable, non-axisymmetric nozzles. These nozzles offer the potential advantages of reduced afterbody drag and vectored thrust with lift enhancement to reduce wing size (currently being set by takeoff requirements).

3) A study should be made to determine the angle at which exhaust nozzles should be canted. Theoretically, directing the nozzles downward relative to the freestream can produce sufficient lift (without excessively penalizing horizontal thrust) to significantly reduce wing size. However, this introduces a pitching moment; whether a canard is required remains to be determined.

REFERENCES

1. Bonner, E., et al, Influence of Propulsion System Size, Shape, and Location on Supersonic Aircraft Design, Rockwell International, NASA CR 132544, December 1974.

2. NASA CR-132374, Advanced Supersonic Technology Concept Study Reference Characteristics, Hampton Technical Center LTV Aerospace Corporation, 21 December, 1973.

3. Lockheed-California Company Report LR 26133, An Airline's View of Reserve Fuel Requirements for the Supersonic Transport, 19 September 1973.

4. Bushell, K. W., Measurement and Prediction of Jet Noise in Flight, AIAA Paper 75-461.

5. Crosthwait, E. L., Kennon, Jr., I.G., and Roland, H.L., et al, Preliminary Design Methodology for Air-Induction Systems, General Dynamics, Fort Worth Division, Technical Report SEG-TR-67-1, January 1967.

6. Schoenherr, K. E., Resistance of Flat Plates Moving Through a Fluid, Transactions of Society of Naval Architects and Marine Engineers, Vol 40, pp 279-313, 1932.

7. Sommer, S., and Short, B., Free Flight Measurements of Turbulent Boundary Skin Friction in the Presence of Severe Aerodynamic Heating at Mach Numbers from 2.8 to 7.0, NACA TN 3391, 1955.

8. Lomax, H., The Wave Drag of Arbitrary Configurations in Linearized Flow as Determined by Areas and Forces in Oblique Planes, NACA RM A55A18, 1955

9. Bonner, E., Theoretical Prediction of Supersonic Pressure Drag, Rockwell International Report NA-66-862, 1966.